SOME HYDRODYNAMIC CHARACTERISTICS OF BUBBLY MIXTURES FLOWING VERTICALLY UPWARD IN TUBES

Sewell C. Rose, Jr.
Peter Griffith

September, 1964

Technical Report No. 5003-30
Division of Sponsored Research
Massachusetts Institute
of Technology

Contract No. AT (30-1)-3301

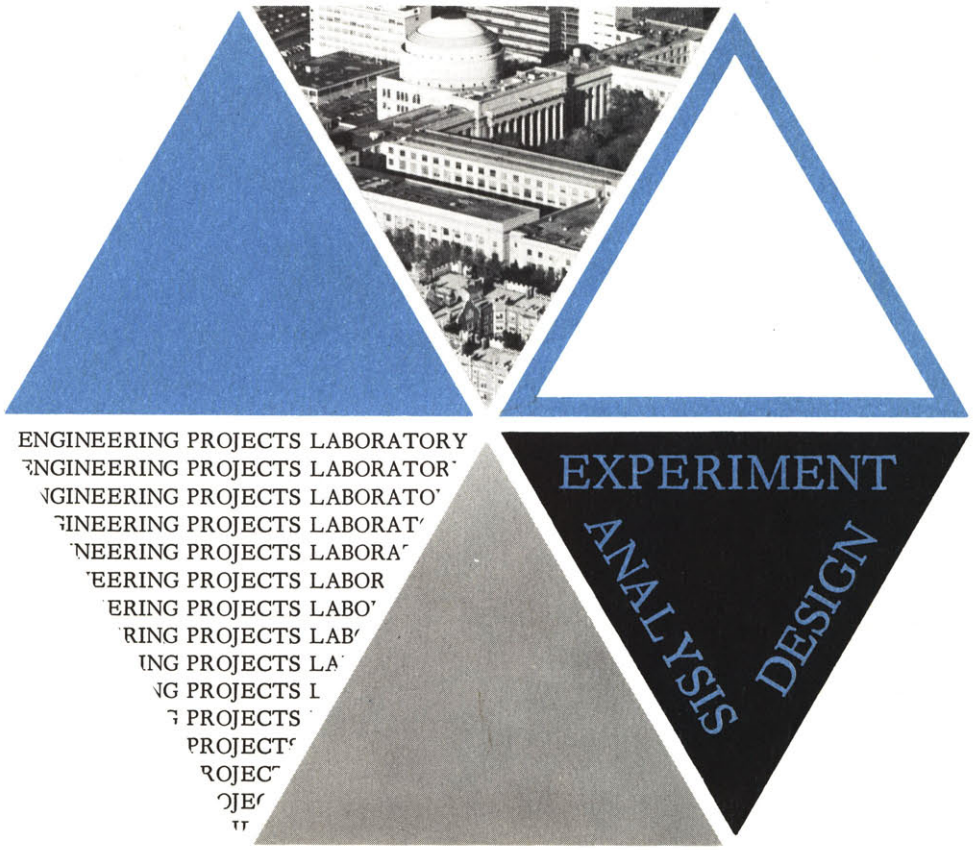

TECHNICAL REPORT NO. 5003-30

SOME HYDRODYNAMIC CHARACTERISTICS OF BUBBLY MIXTURES FLOWING VERTICALLY UPWARD IN TUBES

By

Sewell C. Rose, Jr.*
Peter Griffith**

Sponsored by the U. S. Atomic Energy Commission

Contract No. AT (30-1)-3301

DSR 5003

September, 1964

Division of Sponsored Research

Massachusetts Institute of Technology

Cambridge 39, Massachusetts

* Graduate Student, M.I.T., present address: Knolls Atomic Power Laboratory, Schenectady, New York

** Associate Professor of Mechanical Engineering, M.I.T.

ABSTRACT

An investigation of bubbly flow has been conducted in vertical plexiglass tubes using air and water at atmospheric pressure. The bubbly flow pattern is an entrance condition or a non-fully developed flow. A spontaneous changeover to slug or annular flow usually occurs if the channel is long enough. The experiments were performed in turbulent flow with superficial liquid velocities ranging from 5 to 30 ft/sec. The friction, hydrostatic, and momentum pressure drop have been separated and analyzed individually with the aid of two new experimental measurements. These measurements were of the wall shear force and the momentum flux. The validity of these measurements was verified with numerous single-phase tests. Several different air-water mixing methods, with the air always being introduced at the wall, had no affect on the results. Recommendations are presented for the use of these results when applied to steam-water mixtures.

ACKNOWLEDGMENTS

The authors wish to thank Professors James Daily and Warren Rohsenow for their many constructive comments.

TABLE OF CONTENTS

TABLE OF CONTENTS
(Continued)

LIST OF FIGURES

LIST OF FIGURES
(Continued)

LIST OF TABLES

NOMENCLATURE

a	Dimensionless coefficient, Equation (C7)
A	Flow area of tube
A_P	Solid cross-sectional area of the tube, Figure 1 (does not include the flow area)
b	Dimensionless coefficient, Equation (C7)
c	Dimensionless coefficient, Equation (C7)
C	Distance from fulcrum to the center of gravity of the lever assembly
C_1	Momentum flux ratio, Equation (37)
C_2	Momentum flux ratio, Equation (38)
C_3	Momentum flux ratio, Equation (39)
d	Dimensionless coefficient, Equation (C7)
D	Inside diameter of tube
f	Friction factor, Equation (14)
f_1	Two-phase friction factor, Equation (29)
f_2	Two-phase friction factor, Equation (25)
f_2'	Two-phase friction factor, Equation (43)
f_L	Single-phase friction factor by LVDT method, Equation (15)
f_M	Moody friction factor
f_P	Single-phase friction factor by manometer method, Equation (18)
F_1	Shear force in the pressure tap tubing
F_2	Shear force in the pressure tap tubing
F_3	Shear force in the pressure tap tubing
F_4	Force, Equation (4)
F_5	Effective force, Equation (21)
F_a	Shear force in the holding arm
F_E	Effective force, Equation (8)
F_L	Force transmitted to the holding arm by the lever
g	Acceleration of gravity

NOMENCLATURE
(Continued)

g_c	Gravitational constant
G	Total mass velocity
K	Distance from the fulcrum to the centerline of the tube
L	Tube length
L_1	Distance between top and bottom pressure tap
L_E	Length described in Appendix B
L_O	Length described in Appendix B
L_T	Length described in Appendix B
m	Dimensionless exponent, Equation (C6)
M	Two-phase momentum flux, Equation (C4)
M_1	Inlet momentum flux to the control volume of Figure 3
M_f	Single-phase momentum flux, Equation (A1)
M_H	Homogeneous model momentum flux, Equation (A14)
M_S	Separated model momentum flux, Equation (A23)
N_{Fr_m}	Mixture Froude number, Figure 29
P_1	Pressure at the tube inlet
P_2	Pressure at the tube exit
P_a	Absolute atmospheric pressure
P_A	Average gage tube pressure
P_B	Gage pressure at the bottom pressure tap
P_M	Gage pressure at the middle pressure tap
P_T	Gage pressure at the top pressure tap
ΔP_1	Single-phase hydrostatic pressure drop across the tube
ΔP_e	Hydrostatic pressure drop of two-phase mixture across the tube
ΔP_f	Friction pressure drop of two-phase mixture across the tube, Equation (40)
ΔP_T	Total measured pressure drop across the tube
$\Delta P'_T$	Total predicted pressure drop across the tube

NOMENCLATURE
(Continued)

ΔP_{f_1}	Friction pressure drop of two-phase mixture across the tube, Equation (41)
ΔP_m	Momentum pressure drop of two-phase mixture across the tube
ΔP_{m_2}	Momentum pressure drop of two-phase mixture calculated with homogeneous model
ΔP_{m_3}	Momentum pressure drop of two-phase mixture calculated with separated model
ΔP_{m_s}	Momentum pressure drop of two-phase mixture calculated with modified separated model, Equation (42)
ΔP_H^*	Hydrostatic pressure drop of liquid between bottom and top pressure taps
ΔP_f^*	Friction pressure drop of liquid between bottom and top pressure taps
ΔP_M^*	Momentum pressure drop of liquid
Q_f	Liquid volume flow rate
Q_g	Gas volume flow rate
R	Radius of tube
S	Dimensionless distance, Equation (A2)
t_w	Liquid temperature
T_1	Force in the top rubber connector
T_2	Force in the bottom rubber connector
U	Velocity of two-phase mixture with no local slip at distance Y from the wall
U_m	Velocity of two-phase mixture with no local slip at tube centerline
V_f	Velocity of liquid at distance Y from the wall
V_{f_c}	Velocity of liquid at tube centerline
$\overline{V}_f$	Average velocity of liquid, Equation (34) - Note, for the single-phase tests $\overline{V}_f = \frac{Q_f}{A}$
$\overline{V}_g$	Average velocity of gas, Equation (33)

NOMENCLATURE
(Continued)

V_m	Velocity of mixture, Equation (27)
V_H	Velocity of two-phase homogeneous mixture, Equation (A9)
W_1	Weight of the dry tube and apparatus in Figure 1
W_2	Weight of the lever assembly
W_3	Weight of the dry apparatus in the control volume of Figure 3
W_f	Liquid mass flow rate
W_g	Gas mass flow rate
W_p	Weight on the hook of the lever assembly
W_F	Weight of the fluid in the control volume of Figure 3
W_s	Average shear force exerted by the fluid on the tube
X	Weight quality
Y	Distance from the tube wall
α	Void fraction at distance Y from the wall
$\overline{\alpha}$	Average void fraction
α_c	Void fraction at the tube centerline
μ_f	Liquid viscosity
ρ	Mixture density
ρ_f	Liquid density
ρ_g	Gas density
τ_w	Wall shear stress

1. INTRODUCTION

During the past twenty years, the problems associated with two-phase flow have been the subject of numerous investigations. In recent years, progress on this subject has been achieved by concentrating analyses and experiments on particular flow patterns. Some of the most common flow patterns have been labeled bubbly, slug, annular, and mist[1*]. Early investigators recognized these flow patterns, but for the majority of cases, little or no attempt was made to limit the analyses and experiments to particular flow patterns. The result was usually poor agreement between the predicted and measured quantities.

This thesis concentrates on the bubbly flow pattern which has received relatively little attention. A bubbly flow is characterized by the gas phase being dispersed in the liquid phase in the form of small bubbles. In general, it does not represent a fully developed flow. The bubbly flow pattern usually changes spontaneously to a slug or annular flow if the channel is long enough. Bubbly flow in this thesis will include the case where the bubbles are not uniform in size or shape, but are small relative to the tube diameter. In this study, no distinction is made between the terms bubbly and frothy flow. Figures 25, 27, and 28 show photographs of typical bubbly flow patterns. This flow pattern has been observed in many practical applications, including those conditions associated with nuclear reactors[2][3].

The two-phase problem with a flow pattern approach consists of two parts. First; to predict in terms of known parameters when a certain flow pattern will exist, and

* Superscript numbers are referred to in the Bibliography.

second; to predict the characteristics of each particular flow pattern. This thesis is mainly concerned with the second part of the problem as applied to bubbly flows.

The chief objective has been to formulate a model to accurately predict the total pressure drop for a bubbly mixture flowing vertically upward in a tube. In doing this the frictional, hydrostatic, and momentum pressure drop have been analyzed and a procedure recommended to calculate them. This has required obtaining information on the related problems of void fraction, wall shear stress, and momentum flux.

The experimental program has used an air-water mixture at atmospheric pressure to generate the bubbly mixture. Tests have been conducted in three circular plexiglass tubes. The tubes were 5 feet in length with inside diameters of 1, 3/4, and 1/2 inch. Superficial liquid velocities from 5 to 30 ft/sec. were investigated. For each liquid flow rate, the air flow rate was increased until the flow pattern became unsteady at the tube exit. The unsteadiness was a result of bubble agglomeration and the onset of slug flow. The tests that have been performed were developed and dictated by the experimental information needed to properly answer the pressure drop question. In addition to the usual measurements, two new experimental measurements have been made that are unique to this author. The first measurement consists of a direct measurement of the wall shear force by suspending the test section with a stiff spring and measuring the deflection electronically. This procedure allows a direct calculation of the frictional pressure drop without making any assumptions about the momentum pressure drop. The second test procedure involves the direct measurement of the two-phase momentum flux. This is accomplished by passing the bubbly mixture through a tee where the vertical flow is

deflected 90°. The forces on the tee are again measured electronically and by the momentum equation can be related to the inlet momentum flux. The purpose of measuring the momentum flux has been to investigate the error associated with the one-dimensional momentum flux models. While both of these measurements are not needed, they were performed to investigate the relative ease and reliability of each measurement. In addition, the two measurements acted as a check on one another. The void fraction has been measured by suddenly trapping the flow with a pair of quick closing valves. Finally, the method in which the air and water is mixed has been varied over a significant range to investigate its affect on the measured quantities.

2. THEORY

2.1 Measuring the Wall Shear Force

An important, but difficult, problem associated with two-phase flow is the accurate prediction of the steady state total pressure drop. For the most general case, this problem involves the accurate prediction of the frictional, hydrostatic, and momentum pressure drop. The semiempirical nature of the analytical predictions requires that experimental data be obtained on each term.

Whenever the experimental pressure drop contains all three terms, the question arises as to what is the true frictional, hydrostatic, and momentum pressure drop? The frictional component is usually obtained by subtracting the hydrostatic and momentum terms from the total pressure drop. This differencing procedure is subject to error unless the hydrostatic and momentum terms are accurately calculated. If during the pressure drop test the average void fraction is measured, the hydrostatic term can be accurately determined. The momentum term, however, is a function of the velocity and void fraction profiles. Wallis and Griffith[4], Christiansen[5], and Petrick[6] have observed a strong two-dimensional behavior of the void fraction. Levy[7] has also analytically predicted significant two-dimensional velocity and void fraction profiles, while Bankoff[8] by assuming power law distribution for the velocity and void fraction, shows good agreement in certain regions between his predictions and the data. Therefore, if a one-dimensional model is used to predict the momentum term, an error will occur which is reflected on the frictional pressure drop. At present, the magnitude of this error is unknown. Consequently, before any correlation of the frictional

pressure drop is attempted, the friction data is already in error. To avoid this problem, a new technique was developed to measure the wall shear force directly.

A detailed discussion of the experimental equipment used to measure the wall shear force appears in Section 3.1. To continue this discussion a brief description of this equipment is necessary at this point. The basic technique consisted of joining the vertical tube at each end to the stationary supports with rubber hose connectors. The tube was then mechanically linked to a Linear Variable Differential Transformer (LVDT). Photographs of the equipment are shown in Figures 4, 6, and 7. When a vertical force was produced on the tube, the tube would deflect and the LVDT would produce a voltage signal. Through calibration, this voltage signal could be related to the total wall shear force acting on the tube. The following pages discuss this measurement technique in detail.

Consider a free body diagram of the vertical tube apparatus with a steady flow of air and water passing vertically upward through the tube. Figure 1 shows the free body diagram with the forces acting on it. A force balance in the vertical direction yields the following equation where the upward direction is considered positive:

$$F_a = W_s + (P_1 - P_2) A_P - T_1 - T_2 - W_1 + F_L \qquad (1)$$

$$- F_1 - F_2 - F_3$$

Next, consider a free body diagram of the lever shown in Figure 2. Photographs of the lever are also shown in Figures 6 and 7. Taking moments about the fulcrum where

clockwise is considered positive:

$$F_L = 3W_p + W_2 \frac{C}{K} \tag{2}$$

Substituting F_L from Eq. (2) into Eq. (1), the result is:

$$F_a = W_s + (P_1 - P_2) A_P - T_1 - T_2 - W_1 + 3W_P + W_2 \frac{C}{K} - F_1 - F_2 - F_3 \tag{3}$$

or letting:

$$F_4 = F_a + T_1 + T_2 + W_1 - W_2 \frac{C}{K} + F_1 + F_2 + F_3 \tag{4}$$

Therefore, Eq. (3) becomes:

$$F_4 = W_s + (P_1 - P_2) A_P + 3W_p \tag{5}$$

To relate F_4 to the LVDT voltage signal, the apparatus is calibrated. The best calibration procedure was determined after considerable experience was obtained with the equipment. A description of this procedure follows.

Consider the case where the tube is filled with water, but there is no flow and no weight on the hook of the lever. Under these conditions the LVDT is zeroed. At the zero point, the LVDT output voltage is set arbitrarily equal to 0.0100 volts. This is done by manually adjusting the movable core

of the LVDT by a screw mechanism. A rectifier in the circuit with a zero balance is also used as a fine control for zeroing the instrument. At the zero or reference voltage, the force F_4 is determined by Eq. (5), or:

$$F_4 = \Delta P_1 A_P \tag{6}$$

Where (ΔP_1) is constant and equal to the hydrostatic pressure drop of water across the tube. Next, known weights are placed on the hook and the LVDT voltage is recorded. During the calibration, Eq. (5) can be written in the form:

$$F_4 - \Delta P_1 A_P = 3W_p \tag{7}$$

or letting:

$$F_E = F_4 - \Delta P_1 A_P \tag{8}$$

Eq. (7) becomes:

$$F_E = 3W_p \tag{9}$$

The relation expressed by Eq. (9) is used to make a plot of F_E versus the LVDT voltage signal. With this plot and Eq. (5), the wall shear force can be determined for any single or two-phase flow.

Summarizing, the procedure to measure the wall shear force is as follows:

1. With the test section filled with water, but no flow and no weights on the hook, the LVDT is zeroed at 0.0100 volts.
2. The flow is turned on and the LVDT voltage and pressures recorded.
3. A linear extrapolation is used to obtain the total pressure drop from the measured pressure drop, or:

$$(P_1 - P_2) = (P_B - P_T) \frac{L}{L_1} \tag{10}$$

4. F_E is determined from the plot of F_E versus LVDT voltage.
5. The wall shear force is calculated by combining Eq. (5) where $W_p = 0$, and Eq. (8), or:

$$W_s = F_E - (P_1 - P_2) A_P + \Delta P_1 A_P \tag{11}$$

letting:

$$\Delta P_T = (P_1 - P_2) \tag{12}$$

Therefore, Eq. (11) can be written:

$$W_s = F_E - (\Delta P_T - \Delta P_1) A_P \tag{13}$$

Eq. (13) shall be referred to throughout this work as the equation which relates the wall shear force to the LVDT voltage signal.

The previous section has described how the LVDT voltage signal is related to (F_E) and how (F_E) is related to the wall shear force. The next section derives the equations that are needed for the single-phase tests. The purpose of these tests was to verify the LVDT concept by comparing the wall shear force measured by the LVDT method to that obtained from the measured pressure drop. Also, the single-phase tests allowed a comparison between the fully developed smooth Moody friction factor and the friction factor calculated from the measured pressure drop. For convenience, all comparisons were made on a friction factor basis. Expressing the wall shear force in terms of a friction factor:

$$W_s = \frac{fL\rho_f \bar{V}_f^2 \pi D}{8g_c} \tag{14}$$

Substituting W_s from Eq. (14) into Eq. (13) and solving for the friction factor:

$$f_L = [F_E - (\Delta P_T - \Delta P_1) A_P] \frac{8g_c}{L\rho_f \bar{V}_f^2 \pi D} \tag{15}$$

Note, f_L in Eq. (15) designates the value of the friction factor determined by the LVDT method.

In addition to f_L, the friction factor based on the measured pressure drop was calculated. Applying the momentum equation between the bottom and top pressure taps:

$$P_B - P_T = \Delta P_H^* + \Delta P_f^* + \Delta P_M^* \tag{16}$$

Combining $\Delta P_f^* + \Delta P_M^*$ and expressing the sum in friction factor form, Eq. (16) becomes:

$$P_B - P_T = \Delta P_H^* + f_P \frac{L_1 \rho_f \bar{V}_f^2}{2Dg_c} \tag{17}$$

or, solving Eq. (17) for f_P, the result is:

$$f_P = [(P_B - P_T) - \Delta P_H^*] \frac{2Dg_c}{L_1 \rho_f \bar{V}_f^2} \tag{18}$$

A close examination of f_L and f_P reveals the ratio f_L/f_P should not equal one unless the flow is fully developed. The flow entering the tube in this work may not be fully developed because of other necessities associated with the tests, like having the quick closing valves as near to the tube as possible. However, Deissler's[9] results indicate that for turbulent flow, f_P reaches its fully developed value in approximately ten diameters from the inlet. The wall shear stress on which f_L depends attains its fully developed value in approximately six diameters from the inlet. Thus, inlet affects should have little or no affect on the ratio f_L/f_P.

2.2 Measuring the Momentum Flux

The momentum pressure drop can be accurately calculated only if the momentum flux passing through a plane normal to the tube axis is known. Several models have been used to predict the two-phase momentum flux, but none have been verified by experimental data to this author's knowledge. The one-dimensional homogeneous and separated models, which are commonly used, cannot be correct if two-dimensional velocity and void fraction profiles are present. See Appendix A for a formulation of these models. The need for experimental data on the true momentum flux is necessary to evaluate the present one-dimensional models and to formulate a better model if the need arises.

This section derives the equations and explains the method used to measure the momentum flux of a two-phase bubbly mixture. A detailed discussion of the experimental equipment associated with the momentum flux measurement appears in Section 3.2.

Consider a control volume to include the tee and a portion of the holding arm as shown in Figure 3. Next, assume steady flow and that the exit flow is horizontal. Applying the momentum equation in the vertical direction and considering the upward direction as positive, the result is:

$$F_a + W_3 + W_F - F_L = M_1 \tag{19}$$

Note, the flow entering the control volume has a free surface and thus the pressure at the inlet is atmospheric. This results in no net pressure force acting on the control volume. Substituting F_L from Eq. (2) of Section 2.1 into Eq. (19):

$$F_a + W_3 + W_F - 3W_p - W_2 \frac{C}{K} = M_1 \tag{20}$$

combining terms, let:

$$F_5 = F_a + W_3 - W_2 \frac{C}{K} \tag{21}$$

or with F_5, Eq. (20) becomes:

$$F_5 + W_F - 3W_p = M_1 \tag{22}$$

Again, the apparatus is calibrated to relate F_5 to the LVDT voltage signal. Under the conditions of no flow and no weight on the hook, the LVDT is zeroed at 0.0100 volts. During the calibration, Eq. (22) becomes:

$$F_5 = 3W_p \tag{23}$$

With Eq. (23), a plot of F_5 versus the LVDT voltage is obtained. With this plot and Eq. (22), the momentum flux can be determined for any single or two-phase flow.

The only difference in the testing procedure from Section 2.1, is that the lever assembly was removed before the flow tests. The reason for this was that small vibrations during the testing would sometimes cause the contact point of the lever to become disengaged from the holding arm. If the application point of F_L varied from the centerline of the tee, a false voltage would be recorded. Removing the lever assembly before the flow tests has the effect of changing F_5 by a constant amount equal to $W_2 \frac{C}{K}$, but since the plot of F_5 versus the LVDT voltage is linear, this constant force can be zeroed out.

The weight of the fluid in the tee (W_F) was evaluated by assuming that the average velocity and density of the mixture in the tee was equal to the inlet values. This assumption fixed the volume occupied by the fluid in the control volume. The inlet density of the mixture was calculated with the use of the void fraction correlation obtained from the vertical tube data. The exact assumptions used to evaluate the weight of the fluid are relatively unimportant, as this force is very small compared to the force F_5 as shown in Appendices F and G.

Summarizing, the procedure to measure the momentum flux is as follows:

1. With no flow and the lever removed, the LVDT is zeroed at 0.0100 volts.
2. The flow is turned on and the LVDT voltage recorded.
3. F_5 is obtained from the plot of F_5 versus the LVDT voltage.
4. The weight of the mixture is calculated as previously described.
5. The inlet momentum flux is calculated from Eq. (22). Note, $W_p = 0$. The result is:

$$M_1 = F_5 + W_F \tag{24}$$

Again, before this concept was used to measure the two-phase momentum flux, single-phase tests were perfomed to check the validity of the method. The single-phase tests were performed with Reynolds numbers that varied from approximately 80,000 to 160,000. In this Reynolds number range, the single-phase momentum flux was calculated by assuming a fully developed turbulent velocity profile with a 1/7 power law distribution. The results of this work are presented in Appendix A.

3. EXPERIMENTAL EQUIPMENT

3.1 Vertical Tube Apparatus

A photograph of the apparatus used to measure the wall shear force is shown in Figure 4. Figure 5 is a schematic diagram of the same equipment, while Figures 6 and 7 are close-up photographs of the LVDT equipment. Referring to Figure 5, city water was introduced through a 1.5 inch copper pipe at the bottom and flowed through a Watts pressure regulator and a 1 inch globe valve. The pressure regulator maintained an almost constant downstream pressure, while the city water pressure varied $\pm$ 5 psi. about a mean pressure of 45 psig. The water then flowed vertically through the mixing chamber where shop air was introduced perpindicular to the flow through various hole patterns. Section 3.3 describes the mixing chambers in detail. The mixing chamber was located approximately 13 inches from the tube inlet. The two-phase mixture then passed through a 1 inch Crane cam operated quick closing gate valve. The gate valve was located approximately 5 inches before the tube. On the top side of the gate valve, brass adapters were machined to screw into the valve and mate with the inside and outside diameter of the different tubular test sections. Figure 8 shows a sketch of the adapters used for the 1, 3/4, and the 1/2 inch tubes. The diameters of the plexiglass tubes were all within $\pm$ 0.002 inches of the dimensions shown in Figure 8. Special effort was taken to insure a good alignment between the tube and adapters. The stationary equipment above and below the tube was fastened to the board with precision machined holders made of aluminum. The tube was separated from the adapter by a gap of approximately 1/16 inch. A piece of bicycle tire

tubing or 1/16 inch thick pure gum rubber tubing acted as a flexible connector. The rubber was fastened to the adapter and tube at the edge of the gap with radiator type clamps. The best results were obtained when the rubber was stretched and put in tension before clamping.

The mixture then flowed through the tube and a similar adapter and gate valve. It discharged through a 2 inch rubber hose which curved in a smooth 3 foot arc before dumping the flow into the weigh tank. In the weigh tank, the air and water separated and the liquid went to the drain.

The gate valves were connected with a piece of pipe and operated manually to measure the void fraction. Through the cam action, the valves could be closed in 60°. A scale mounted on the platform behind the tube was used to indicate the water level.

Referring to Figures 6 and 7, the tube was grasped by a fixture (referred to in the text as the holding arm) which is fastened to a pair of cantilever plates. By means of different split plexiglass adapters, the arm could hold the 1, 3/4, and 1/2 inch tubes. The deflection of these plates moved the core of a Sanborn Linear Variable Differential Transformer. A model 595DT-025 LVDT was used for the 1 inch vertical tube tests. At the end of these tests this model was replaced by a 590DT-025 LVDT because of a sudden erratic output signal from the former model. It would have been desirable to replace the 595DT-025 model with a similar model because of its high sensitivity. This possibility was ruled out because of a month delay in delivery by the manufacturer. The operating characteristics of these models are given in Reference (14).

The apparatus used to hold the LVDT was borrowed and modified for this work. It was originally designed and built

by Harrison[10] at M.I.T. for his Masters thesis. Subsequent refinements and improvements have been made by Rogers[11][12]. The oscillator and rectifier were also designed specifically for the LVDT apparatus. The LVDT output voltage was measured with a Hewlitt Packard d.c. vacuum tube voltmeter.

The static pressure was measured at three locations with 8 foot U-tube manometers. The pressure taps were located 2 inches from the tube inlet and exit and at the tube centerline. No. 3 Meriam fluid and mercury were used as manometer fluids. By means of a simple valve system, either fluid manometer could be used for a particular test.

The water flow rate was calculated by timing the accumulation of liquid in the weigh tank. The gas flow rate was measured with an A.S.M.E. square-edge orifice. The orifice pressure drop was measured with manometers whose sensitivity varied from 0.1 inches of water to 60 inches of mercury. The air flow rate was regulated by a needle and globe valve in parallel. An on-off valve was also located immediately before the mixing chamber. The gas temperature was measured with a thermometer upstream of the orifice and the liquid temperature was measured at the discharge to the weigh tank.

3.2 Momentum Apparatus

The equipment used to measure the momentum flux was built by modifying the vertical tube apparatus. Figure 9 is a photograph of the equipment, while Figure 10 is a schematic diagram of the equipment.

Referring to Figure 9, there was no change in the equipment up to the bottom gate valve. Then; the 5 foot tube, adapters, and gate valve connecting bar were removed.

A hole was then sawed in the mounting board. In place of the 5 foot tube, a 1 inch tube 31 inches long was secured with a rubber connector to the 1 inch momentum test adapter as shown in Figure 8. This tube extended up into the tee with a 1/8 inch clearance between the outside diameter of the tube and the inside diameter of the tee. Concentric with the 1 inch tube was a 3.5 inch tube approximately 2 feet long. This tube served a dual purpose. First; by being rigidly connected with plexiglass cement to the 1 inch tube at the bottom and top, it served to align the top of the 1 inch tube in the center of the tee. This was done with the top wooden clamp shown in Figure 9. A three prong spacer made of plexiglass also served to align the 1 inch tube in the 3.5 inch tube approximately 2 inches from the top. Secondly, at the bottom of the large tube two drain lines were provided to catch any back flow that occured when the flow was first turned on.

The tee was fabricated from two commercial 90°, 1.25 X 1 inch copper reducing elbows. The elbows were sawed and soldered together at the centerline. The two elbows were then soldered to a 6 inch long piece of 1.5 inch copper pipe which formed the tee. The tee, with the use of a split plexiglass bushing, was then clamped in the holding arm which was connected to the LVDT apparatus.

The flow discharged from each side of the tee into a 6 inch stove pipe. The stove pipe, using gravity flow, acted as a transport pipe from the tee to the weigh tank.

3.3 Mixing Chambers

Five different mixing chambers were built to investigate the affect of different air-water mixing methods on the measured data. Figure 11 is a cross-sectional sketch of a

typical mixing chamber. The common feature of all mixing chambers was that the air was introduced perpindicular to the water and at the periphery of the water.

The mixing chambers were constructed from two parts. First, various hole patterns were drilled in 1 inch brass nipples 4 inches long. Secondly, solid pieces of brass were machined as shown in Figure 13. The two parts were then soldered together to form the mixing chamber.

Four of the five mixing chambers had different hole patterns and were built as previously described. The fifth chamber was formed using a very fine mesh copper screen. The screen was cut 1 inch wide and wrapped tightly on a mandrel to give it the same inside and outside diameter as a 1 inch brass nipple. A 1 inch nipple was then sawed in half and each part soldered to the screen. This unit was then soldered into the brass chamber to complete the mixing chamber.

The different hole patterns are summarized in Table I.

TABLE I

Mixing Chamber Hole Patterns

Mixing Chamber	Hole Size (in.)	Rings of Holes	Holes Per Ring	Total No. Holes
1	0.040	1	33	33
2	0.040	2	33	66
3	0.040	3	33	99
4	0.120	1	11	11
5	Screen	---	---	---

When there was more than one ring of holes, the rings were spaced 1/4 inch apart. Each mixing chamber could be easily interchanged by simply unloosening the unions which appeared on both the water and air side as shown in Figure 9.

3.4 Photographic Apparatus

The photographs of the flow pattern were taken with a Poloroid Pathfinder Land Camera, model 110B. The film was type 47, 3000 speed. The best results were obtained with an aperature setting of f/45 and with a shutter speed of 1/300 second. All the photographs were taken approximately 6 inches from the tube with the use of close up lenses. The lighting was accomplished with a General Radio Co., type No. 1530-A microflash unit.

4. EXPERIMENTAL PROCEDURE

4.1 Vertical Tube Tests

4.1.1 Single-Phase Flow

The first step after the installation of a new tube was to obtain the relationship between F_E and the LVDT output voltage signal. Before the actual calibration started, the water would be turned on for approximately ten minutes. During this period the electronic equipment warmed up and the rubber connectors were wet, while their temperatures became close to test conditions. The water would then be shut off with the tube full of water for a delay period of ten minutes. The reason for the delay was to allow the rubber connectors, which displayed a slight hysterisis and sluggish behavior, to obtain their steady state position. The LVDT voltage would show a small change during this delay period. When there was no further change in the LVDT signal, the LVDT would be zeroed at 0.0100 volts with no weight on the hook. The actual zeroing was accomplished in two steps. The core of the LVDT was first adjusted with a screw mechanism to the approximate zero voltage. Then the zero balance on the rectifier was used for the fine adjustment.

A known weight was then placed on the hook at the end of the lever and the LVDT voltage recorded after a ten minute delay. After removing the weight, another ten minute delay was allowed for steady state conditions to take place. The entire procedure beginning with the zeroing process would then be repeated with a different weight. One pound increments or less were placed on the hook in obtaining the F_E versus voltage signal plot. The calibration procedure was slow, but the repeatibility of the data was excellent if performed in this deliberate manner. Spot checks of the calibration plot

were conducted throughout the entire testing period.

The single-phase tests were run consistent with the previous calibration procedure. With the tube full of water and no weight on the hook, the LVDT would be zeroed at 0.0100 volts. The word zeroed always implies a sufficient delay period has taken place to allow steady state conditions to exist. The water was then turned on and the flow rate controlled by the pressure regulator and globe valve. After ten minutes of operation, the necessary data was recorded. The water was then turned off at the main supply and the procedure repeated. For all single and two-phase tests, two complete and independent tests with the same flow rate were conducted. The average values of the raw data were used in the data reduction process.

Two advantages result from zeroing the LVDT when the tube is full of water rather than being empty. First, the tests can be run much more quickly without having to drain the apparatus each time the LVDT is zeroed. Secondly, the rubber is closer to actual test conditions if it is wet during the calibration.

4.1.2 Two-Phase Flow

The two-phase test procedure was very similar to that previously described and only the important differences and additions will be mentioned. Before each test, the manometer lines were flushed of any trapped air. Opening a valve to the atmosphere in the system used to select the mercury or meriam fluid manometer accomplished this task. The same procedure was used to establish a given water flow rate and then the air would be introduced by opening the valve before the mixing chamber. After a ten minute delay, the raw data would be

recorded. The manometers would then be isolated by closing the valves at the pressure taps. Next, the gate valves would be suddenly closed. Immediately, the on-off valve used to introduce the air would be closed to prevent any water from flowing back into the air line. The water was then shut off at the main supply and the pressure reduced on the upstream side of the gate valve by opening a relief valve.

After allowing the air and water to separate, the liquid level on the scale behind the tube was recorded. The gate valves were then opened and the tube filled with water. After flushing the manometer lines, the LVDT would be zeroed and the procedure repeated.

To expedite the two-phase tests, a predetermined water flow rate would be set and the air flow rate increased for several tests with no attempt being made to maintain a constant water flow rate. Then the water flow rate would be changed and the procedure repeated. Before each new group of two-phase tests were performed with a particular water flow rate, a single-phase test would be conducted to keep a running check on the apparatus.

4.2 Momentum Flux Tests

The momentum tests were much easier and quicker to perform than the vertical tube tests. The principal reason was the absence of the rubber connectors and the necessary delay periods.

A calibration procedure similar to that previously described was used to relate F_5 to the LVDT output voltage.

The single and two-phase test procedures were very similar. In each case, the LVDT would be zeroed with the lever having been removed. The water would then be turned on

and after a few minutes operation the raw data recorded. During the two-phase tests, the air would again be increased with no attempt being made to hold a constant water flow rate.

4.3 Accuracy of Measurements

The accuracy of all tests was increased by conducting two independent tests at the same liquid and gas flow rate. The measured values of each test were then averaged and used in the data reduction process. The recorded data in the Appendices represents the averaged values. All calculations were performed with a slide rule.

The average liquid flow rate was determined very precisely with a calibrated platform scale and a stopwatch. For the majority of tests, the liquid flow rate was known to be better than $\pm$ 1/2 %. At the largest flow rates, where the precision decreased, the error was still less than $\pm$ 2 %.

The gas flow rate was calculated to within $\pm$ 1% with the A.S.M.E. square-edge orifices. According to Leary and Tsai[27], the careful use and installation of these orifices will give results within $\pm$ 1/2 % when the appropriate corrections are made. Considering the errors from the slide rule calculations, the gas flow rate should be accurate to within $\pm$ 1%. In addition, Haberstroh[28] performed tests with the same orifice apparatus, and reports several independent checks to support a gas flow rate accuracy of within $\pm$ 1 %.

The accuracy of the void fraction depended on the absolute measured value. At low void fractions, i.e., less than 20%, the errors in the measured liquid level were magnified, but still resulted in a reported void fraction accurate to within $\pm$ 5%. At the larger void fractions, this error was reduced to less than $\pm$ 2% of the reported value. The repeatibility

of the void fraction measurements was excellent.

The pressures during the bubbly flow tests were very steady and accurate to within $\pm$ 1 %. As the flow pattern became unsteady due to bubble agglomerations, the pressures showed some oscillations. By partly closing the pressure tap valves, the flucuations in the liquid level of the manometers lines were damped. Maximum excursions of the liquid level (for the most unsteady tests) were $\pm$ 2 inches. An estimate of the maximum error in the unsteady pressures would be $\pm$ 10 %. For the majority of the unsteady tests, this error was probably a lot less.

The largest error in this study was associated with the LVDT output voltage. The estimated accuracy of the recorded voltage was $\pm$ .001 volt. The resulting error in the calculated upward force, i.e., F_E or F_5, depended on which LVDT was used and the absolute value of the mean voltage. The maximum error was estimated to $\pm$ 10 % of the upward force at the lowest recorded voltage.

5. RESULTS

5.1 LVDT Calibration

The results of the four LVDT calibrations are shown in Figure 12. In each case, the LVDT output voltage was a linear function of the upward force, i.e., F_E or F_5. Spot checks of the individual calibrations were also conducted during the testing period, and the repeatibility of the LVDT response was excellent. The maximum deviation was only $\pm$ 0.0005 volts from any of the lines in Figure 12. For data reduction purposes, the linear equation representing each calibration was used to relate the LVDT voltage to the upward force.

The line designated D = 1.000" applies to the 595DT-025 model. Its greater sensitivity produced a larger voltage response than the 590DT-025 model. The slight difference in the 3/4 and 1/2 inch tube calibrations was a result of different elastic properties of the rubber connectors. The 3/4 inch tube used bicycle tire tubing while the 1/2 inch tube used pure gum rubber hose for the flexible connectors. The momentum tests, which had no rubber connectors, exhibited a slightly larger response than the 1/2 or 3/4 inch tube. From the results of Figure 12 and the LVDT specification[14], the maximum tube or LVDT core deflection was calculated to be only a few thousandths of an inch.

5.2 Vertical Tube Tests

5.2.1 Wall Shear Force

5.2.1.1 Single-Phase Flow

In Section 2.1, the theory and equations are developed

to measure the wall shear force. This Section presents the results of numerous single-phase tests which were performed to check the validity of the method proposed in Section 2.1.

Figure 13 shows the results of the friction factor obtained by the LVDT procedure (Eq. 15) and the manometer method (Eq. 18). For values of F_E greater than 2.5, the agreement between f_L and f_P is very good. The majority of the data points fall within $\pm$ 5 % of the 1.0 line. At the low values of F_E, the larger scatter is attributed to the errors associated with very small measured quantities. This does not cause a great concern, for the forces involved in the two-phase tests are much larger and thus fall in the region where the agreement is very good. The results of Figure 13 place a lower limit on the two-phase wall shear force capable of being accurately measured with this particular LVDT apparatus.

Figure 14 shows the results of the friction factor calculated from the measured pressure drop and the smooth Moody[15] curve. The scatter of the data is typical of that for fully developed turbulent flow in circular tubes as indicated in Reference (16). Hence, the inlet flow is nearly fully developed and any momentum pressure drop associated with the velocity profile development is small. In Figure 14, the 3/4 inch tube acted as being slightly rough with the measured friction factor approximately 5% higher than the smooth Moody value. The data supporting these single-phase tests is tabulated in Appendix D.

5.2.1.2 Two-Phase Flow

The two-phase tests were initiated after numerous single-phase tests verified the LVDT method of measuring the wall

shear force. For the two-phase tests, the wall shear force was calculated by Eq. (13).

Numerous methods have been proposed in the literature to correlate the two-phase wall shear force or frictional pressure drop. Reference (22) is an excellent source for reviewing and comparing the many existing correlations for predicting the frictional pressure drop. The results of Reference (22) clearly indicate the need for better frictional pressure drop correlations.

In this work, the wall shear force data has been correlated by using the friction factor method of single-phase turbulent flow. With this method, the problem still exists as to what density, diameter, velocity, and viscosity should be used in defining the friction factor and Reynolds number. Several different definitions were considered, but the best correlation resulted from the following definitions:

$$f_2 = \frac{8\tau_w g_c}{\rho V_m^2} \tag{25}$$

where the density and velocity are defined as:

$$\rho = \bar{\alpha}\,\rho_g + (1 - \bar{\alpha})\,\rho_f \tag{26}$$

$$V_m = \frac{Q_g + Q_f}{A} \tag{27}$$

and the Reynolds number is defined as:

$$N_{Re_2} = \frac{V_m\,\rho D}{\mu_f} \tag{28}$$

The quantities τ_w, $\bar{\alpha}$, and ρ_g are the average values in the tube. The density of the air was evaluated from the ideal gas law, where the air and water temperature were assumed equal. Except for a few of the highest flow rate tests, the pressure drop remained practically linear.

Figure 15 shows the friction factor correlation with these definitions for the 1 inch tube with the No. 3 mixing chamber. The dark points indicate an unsteady exit flow pattern. The unsteadiness occurred because of bubble agglomeration and the resulting non-fully developed slug flow pattern. For a large variation in superficial liquid velocities (10 to 20 ft/sec.) and average void fractions from 0 to 0.6, the data shows relatively little scatter. It is a coincidence that the data lies so close to the smooth Moody curve. Figure 16 shows the 3/4 and 1/2 inch tube data, along with the 1 inch data. The 3/4 inch data is slightly higher than the 1/2 and 1 inch data. The rough behavior of the 3/4 inch tube indicated by the single-phase tests would account for some of this deviation. A further discussion of this data will occur in Section 6 after the momentum data has been measured and evaluated.

Figure 17 is a plot of the same data, only now the total mass velocity is used in defining the friction factor and Reynolds number. That is:

$$f_1 = \frac{8\tau_w \rho g_c}{G^2} \tag{29}$$

and:

$$N_{Re_1} = \frac{GD}{\mu_f} \tag{30}$$

A comparison of Figures 17 and 15 shows a much larger scatter in the data resulting from the use of the mass velocity. The friction factor and Reynolds number defined by Eq. (29) and Eq. (30) are equivalent to Eq. (25) and Eq. (28) only for the case of no slip. Figure 18 is a plot of all the data points with the No. 3 mixing chamber on the f_1 versus N_{Re_1} coordinate system. Again, there is more scatter than Figure 16. Several other correlating parameters were considered, including those of Reference (22), but none had the success of Figure 16. The use of the true density, i.e., Eq. (26), in the best correlation emphasizes the necessity to know the void fraction.

The question of the proper viscosity for a two-phase flow is open to discussion. The models proposed by Eirich[17] and Zuber[18] for evaluating the apparent two-phase viscosity do not apply to turbulent flow. The justification for using the liquid viscosity in the Reynolds number is the satisfactory correlation that results from this procedure. In this study, the liquid viscosity was obtained from Reference (32).

Figure 19 shows no change in the best correlation as a result of different air-water mixing methods. The two-phase data for the vertical tube tests is tabulated in Appendix E.

5.2.2 Void Fraction

The average void fraction was correlated as a function of the volumetric flow concentration, i.e., $\frac{Q_g}{Q_g + Q_f}$. Correlating the bubbly void fraction in this manner was suggested by several previous investigations. Armand[19] successfully correlated his void fraction data for both air-water and steam-water mixtures in vertical tubes in this way. For values of the volumetric flow concentration less than 0.9, the void fraction was a linear function of the volumetric flow

concentration. Isbin[23] also reported a good agreement between the Minnesota steam-water data and the Armand correlation. Bankoff's[8] model for bubbly flow indicates that the void fraction is simply a coefficient times the volumetric flow concentration. The coefficient is a function of the velocity and void fraction profiles. When Bankoff assumed a constant value for the coefficient equal to 0.89, the agreement in Reference (8) between the steam-water data (assumed to be bubbly flow) and his model was quite good.

Figure 20 shows the correlation for the 1 inch tube data with the No. 3 mixing chamber. The homogeneous line represents the case of no slip. The slug flow line is taken from the work of Reference (20). The results of this Reference showed that the void fraction for upward vertical fully developed slug flow could be expressed as:

$$\bar{\alpha} = \frac{Q_g/A}{1.2\left(\frac{Q_g + Q_f}{A}\right) + 0.35\,(gD)^{1/2}} \qquad (31)$$

For the test conditions in this study, the second term in the denominator is much less than the first, or a very good approximation is:

$$\bar{\alpha} = 0.83\left(\frac{Q_g}{Q_g + Q_f}\right) \qquad (32)$$

Eq. (32) is also the result that Armand found empirically.

The unsteady points in Figure 20 lie very close to the slug flow line. At first this result was quite surprising, as photographs of the flow indicated no fully developed slug flow. Yet, Griffith[24] with a modification of the fully developed slug flow theory, successfully predicted the void fraction for some heated channel steam-water data that was

certainly not fully developed slug flow. The interesting point is that Griffith's modification for entrance and heating affects was to the second term in the denominator of Eq. (31), but for the tests in this work, that term is negligible. Thus, the agreement of the unsteady data and the fully developed slug flow line is not so unusual.

The slip ratios accompanying the data of Figure 20 vary from approximately 0.8 to 1.7. Slip ratios less than one pertain to the data above the homogeneous line in Figure 23. This is easily shown by applying the continuity equation to the gas and liquid phase. That is:

$$Q_g = \overline{V}_g \, \alpha \, A \tag{33}$$

$$Q_f = \overline{V}_f \, (1-\overline{\alpha}) \, A \tag{34}$$

Combining Eq. (33) and (34) and solving for $\overline{\alpha}$:

$$\overline{\alpha} = \frac{Q_g}{Q_g + \left(\frac{\overline{V}_g}{\overline{V}_f}\right) Q_f} \tag{35}$$

or when:

$$\overline{\alpha} > \frac{Q_g}{Q_g + Q_f} \qquad \left(\frac{\overline{V}_g}{\overline{V}_f}\right) < 1 \tag{36}$$

Referring again to Figure 20, for values of the volumetric flow concentration up to 0.25, the slip ratio is less than one.

This results from a two-dimensional velocity profile and

the air being mainly located in the low velocity region, i.e., near the wall. It is not attributed to a local difference in the gas and liquid velocity. Reference (25) shows that the individual rise velocity of single bubbles is less than 0.8 ft/sec. and that for many bubbles is closer to 0.4 ft/sec. according to Reference (31). This fact in conjunction with the gas and liquid velocities of Figure 20, which ranged from 10 to 60 ft/sec., supports a model based on no local slip. Slip ratios less than one have also been measured for steam-water mixtures by Haywood et al[26] for low quality conditions. If the bubbles which are generated at the wall remain close to the wall, the slip ratio will be less than 1.0.

Figure 21 shows the 3/4 inch tube data, while Figure 22 is for the 1/2 inch tube. Figure 23 shows all the data points with the No. 3 mixing chamber. Figure 24 again shows no affect due to the air-water mixing method.

A more detailed investigation of the void fraction must be based on a two-dimensional model. To mathematically obtain a slip ratio less than one, where there is little or no local slip, the void fraction profile must peak at a position other than the centerline. Bankoff's[8] model does not do this and will not predict slip ratios less than one. Appendix C formulates a set of equations which can be solved numerically to investigate the two-dimensional velocity and void fraction profiles of bubbly flow.

5.2.3 Flow Patterns

For each test, the flow was classified bubbly or unsteady. This distinction was based on visual and photographic observations. Undoubtedly, there is a gray region in which the

data could be placed in either category. This is especially true at the higher velocities (50 ft/sec.) of this study. The reason for classifying the flow pattern was to limit the investigation to bubbly flows.

To help describe and clarify the flow pattern, many still photographs were taken. Several high speed movies at 4000 pps were also taken, but were not fast enough to illustrate the fine detail of the flow pattern. They did indicate that the bubbly flow pattern was very steady. Of special interest was the affect on the flow pattern of different mixing chambers for the same gas and liquid flow rates. To answer this question, still photographs of nine different gas and liquid flow rates were taken with the No. 1, No. 2, and No. 3 mixing chambers on the 1 inch tube. These nine cases correspond to tests where data was taken and referenced in Appendix E. The main result was no apparent difference in the flow pattern for different mixing chambers with the same gas and liquid flow rate. This observation coincides with the previous results of no difference in the measured data. Figure 25 shows a typical photograph of the bubbly flow pattern. The dash 1, 2, and 3 after test 102 signifies the No. 1, No. 2, and No. 3 mixing chambers. The photographs in Figures 25, 26, 27, and 28 were all taken at the center of the tube. In Figure 26, the bubbles have started to agglomerate and the flow pattern was unsteady. Figures 27 and 28 show bubbly flow patterns with larger velocities. The average bubble size appeared inversely proportional to the superficial liquid velocity.

The visual observations of the flow patterns indicated a liquid core at the tube entrance for low air flow rates. As the flow passed through the tube, the bubbles showed little tendency to penetrate the liquid core by turbulent mixing.

The void faction measurements support this observation and show that up to volumetric flow concentrations of 0.30, the slip ratio is less than 1.0.

Table II summarizes the approximate range of air velocities through the holes of the mixing chamber for the tests on the 1 inch tube.

TABLE II

Mixing Chamber Air Velocities

Mixing Chamber	Max. Air Velocity ft/sec.	Min. Air Velocity ft/sec.
1	615	35
2	308	17
3	205	11

It is surprising that variations in the air velocity by a factor of 3 produced no net effect on the measured or observed data. No detailed analysis of the bubble size was attempted, nor was it felt warrented. A close look at the photographs indicates a wide variation in the bubble sizes and shapes. Yet, for the bubbly flow pattern, the data appears insensitive to the individual bubbles.

Figures 29 and 30 are flow regime maps showing the area where the data was taken. Figure 29 does a better job at separating the bubbly and unsteady regions.

5.3 Momentum Flux

5.3.1 Single-Phase Flow

The purpose of running the single-phase momentum tests was to check out the method proposed in Section 2.2. Originally, tests were planned for the 1, 3/4, and 1/2 inch tubes. This plan was changed when a check showed that only the 1 inch tube produced large enough forces, within the allowable velocity range, to warrant testing. The single-phase momentum flux as well as the one-dimensional two-phase homogeneous and separated models are developed in Appendix A.

Figure 31 shows the single-phase momentum flux for the three tubes as a function of liquid velocity. For comparison purposes, the predicted and measured momentum flux is expressed as a ratio, or:

$$C_1 = \frac{M_f}{M_1} \tag{37}$$

Figure 32, represents the results of the single-phase check out tests. The measured momentum flux was slightly larger than the predicted value for all tests. As the measured force (F_5) increased, C_1 approached 1.0. Above an LVDT force of 2.5, the agreement is very good. The majority of the two-phase tests were for values of F_5 greater than 2.5. This check out procedure is slightly different than the wall shear force verification. In this case, the measured value is being compared to an assumed flow condition. That condition is a fully developed velocity profile with a 1/7 power law distribution. For the Reynolds number range and inlet condition of these tests, this assumption is very good. The data for the single-phase momentum tests is tabulated in Appendix F.

5.3.2 Two-Phase Flow

In analyzing the two-phase data, the measured momentum flux was compared to the one-dimensional homogeneous and separated models. These models, while not correct, should approximate the actual momentum flux. The separated model was evaluated by using the void fraction correlation obtained in Section 5.2.2., i.e., Figure 20. Expressing the momentum fluxes in the form of ratios:

$$C_2 = \frac{M_H}{M_1} \tag{38}$$

$$C_3 = \frac{M_S}{M_1} \tag{39}$$

Figure 33 shows the value of C_2 versus the volumetric flow concentration. At low values of the volumetric flow concentration, i.e., less than 0.475, the homogeneous model underpredicts the true momentum flux. The reason is that the liquid is mainly located near the centerline of the tube or in the high velocity region, and the homogeneous model forces the liquid to assume a velocity which is smaller than the actual liquid velocity.

At the larger values of the volumetric flow concentrations, i.e., greater than 0.475, the homogeneous model overpredicts the momentum flux. Now the liquid is located near the wall or in the lower velocity region, but the homogeneous model forces it to assume a larger than actual velocity. As the gas flow rate goes to zero, C_2 will equal 0.98 for a velocity profile with a 1/7 power law distribution. No data was taken above a volumetric flow concentration of 0.8, because the flow pattern was not bubbly. For those conditions near 0.8 at the high liquid flow rates, where

flow was classified bubbly, further increases in the volumetric flow concentration were not possible because of limitations on the maximum liquid flow rate. One concludes, however, that the ratio must reach a maximum before returning to 0.98 as the liquid flow rate goes to zero. The effect of four different mixing chambers was negligible.

Figure 34 illustrates the momentum flux ratio as a function of the slip ratio. The important feature to notice is that a slip ratio of one is no reason that the homogeneous model should accurately predict the momentum flux. This results from the momentum flux being an integral function of the velocity squared while the slip ratio is an integral function of the velocity to the first power.

Figure 35 is a comparison of the separated model and the measured momentum flux. The separated model, because of its one-dimensional nature, always underpredicts the actual momentum flux. This plot again shows a successful correlation of the momentum ratio as simply a function of the volumetric flow concentration. Figure 36 shows C_3 plotted versus the slip ratio. Appendix G is a tabulation of all the two-phase momentum flux data. Note in Appendix G, the small value of the liquid weight in the tee compared to the measured force F_5.

In addition to the mixing chambers used on the vertical tube tests, two new mixing chambers were investigated in the momentum tests. The No. 4 and No. 5 mixing chambers were used to investigate the effect of different size holes where the air was introduced into the liquid. Again, different mixing methods had no affect on the measured data. Photographs of the flow pattern also indicated no change among any of the mixing chambers.

With the success of the momentum flux measurements and correlations, one can now go back and compare the wall shear force and momentum measurements. In addition, the magnitude

of the momentum pressure drop can be established.

In the wall shear force tests, the frictional pressure drop was:

$$\Delta P_f = \frac{W_s}{A} \tag{40}$$

where W_s was calculated from Eq. (13). With a momentum flux model that has been tested, the frictional pressure drop can now be calculated from a differencing procedure, or:

$$\Delta P_{f_1} = \Delta P_T - (\Delta P_e + \Delta P_{m_s}) \tag{41}$$

where:

$$\Delta P_{m_S} = \frac{1}{A^2 g_c}\left\{ \frac{1}{C_3}\left[\frac{W_f Q_f}{(1-\bar{\alpha})} + \frac{W_g Q_g}{\bar{\alpha}} \right]_{\text{Exit}} - \frac{1}{C_3}\left[\frac{W_f Q_f}{(1-\bar{\alpha})} + \frac{W_g Q_g}{\bar{\alpha}} \right]_{\text{Inlet}} \right\} \tag{42}$$

The modified separated model as opposed to the modified homogeneous model is recommended to calculate the momentum pressure drop. This is because C_3 reflects only the two-dimensional affects, while C_2 in addition is based on a fictious no slip model.

Figure 37 shows the results of the friction pressure drop calculated by the LVDT method, i.e., Eq. (40), and the differencing procedure, i.e., Eq. (41). The difference in

the two procedures is a result of errors in each method. Overall, the agreement is quite good. A discussion on the recommended procedure to obtain the frictional pressure drop appears in Section 6. A close look at Figure 37 reveals that the majority of the 3/4 inch data was slightly higher than the 1 and 1/2 inch data. This coincides with the friction factor plots where the 3/4 inch data appeared slightly high.

Assuming C_3 in Figure 35 is valid for all three tubes and only a function of the local volumetric flow concentration, the momentum pressure drop was calculated by Eq. (42). Figure 38 shows the results of this calculation. The maxiumum momentum pressure drop was approximately 28 % of the total pressure drop. In Appendix E, the one-dimensional homogeneous and separated momentum pressure drops have been calculated for comparison with the modified separated model. In addition, the momentum pressure drop (ΔP_m) obtained by a differencing procedure, where the friction pressure drop was calculated from Eq. (40), is tabulated.

6. DISCUSSION OF RESULTS

The experimental errors associated with the wall shear force and momentum flux measurements have resulted in two different friction pressure drops. While neither method is exactly correct, the recommended procedure is to use the differencing method, i.e., Eq. (41), to obtain the friction pressure drop. This recommendation is based on the small momentum pressure drop for the majority of tests, and the relative errors associated with each method. With the use of Eq. (41) to predict the friction pressure drop, the friction factor was recalculated for all the test points. That is:

$$f_2' = f_2 \left(\frac{\Delta P_{f_1}}{\Delta P_f} \right) \tag{43}$$

In calculating (ΔP_{f_1}), the void fraction was obtained from the best fit line of Figure 23. Figure 39 shows the friction factor (f_2') and the best fit line for all the data points. The 3/4 inch tube data has been reduced by 5% to factor out the single-phase roughness effect. The scatter is much less than Figure 16. Finally, using (f_2'), the total pressure drop was calculated for all the bubbly flow tests and compared with the measured data. Figure 40 shows the results of this calculation. The agreement between the predicted and measured total pressure drop is excellent.

The application of these results is recommended for bubbly flows where the superficial liquid velocity is greater than 5 ft/sec. and the gas phase is introduced at the wall. They should also apply to horizontal pipes, especially for larger velocities, where the inertia forces completely

outweigh the gravity or stratification affects. Small deviations from the bubbly flow pattern should not cause serious errors. The average void fraction appears to be the most sensitive quantity with regard to the flow pattern.

If a visual observation of the flow pattern is not possible, the flow regime maps in Figures 32 and 33 are the recommended regions where the flow regime should be bubbly. Because bubbly flow is an entrance condition and not a fully developed flow, these maps can only be recommended to indicate bubbly flow for applications similar to those of this study. References (33) and (34) have attempted to determine the bubbly flow regime boundaries, but no specific criteria of a general nature was obtained to solve this problem. Their results did show that large diameters, small initial bubble sizes, large velocities, relatively unpure liquid (tap water), and short pipes all favor bubbly flow. Additional studies are needed to determine the flow regime boundaries of bubbly flow.

Radically different mixing chambers, such as an ordinary tee, will affect these results depending on the resultant initial bubble size and bubble location in the tube. If the bubbles are large to begin with, the change-over to slug flow will occur sooner or at a lower average void fraction. Unless the gas phase is introduced at the wall, it is doubtful that slip ratios less than one will be obtained. For bubbly flows where the gas is not introduced at the wall, the recommended procedure for calculating the void fraction is to assume a homogeneous model up to a volumetric flow concentration of 0.3. Above this value, the best fit line of Figure 23 is still recommended. The friction factor (f'_2) and the momentum multiplier (C_3) should not change appreciably as long as the flow is bubbly.

In the case of a heated tube, these results should apply for bubbly flow if the bubbles detach from the wall and maintain their identity as they are swept into the main flow. If the bubbles collapse on or remain close to the surface, as is the case for highly subcooled boiling, the pressure drop characteristics will probably change. The introduction of the air at the periphery of the water in these tests was done to help simulate the nucleate boiling case. In the case of heated high pressure systems, very little flow regime mapping has been done. Based on the results of Tippet's[2] and Hosler's[3] observations, bubbly flow in steam-water mixtures for heated high pressure systems is most likely to occur up to volumetric flow concentrations of 0.6. Figure 41 illustrates this region in terms of pressure and quality.

7. CONCLUSIONS

The conclusions are summarized as follows:

1. The direct measurement of the wall shear force and momentum flux has demonstrated two new experimental methods that can be used to investigate two-phase flow.
2. The recommended procedure for determining the frictional pressure drop is to use the differencing procedure with the momentum flux calculated from the modified separated model.
3. The wall shear stress, void fraction, and momentum flux have been successfully correlated for bubbly flow.
4. The terms in the total pressure drop equation show a smooth transition with the change from an ideal bubbly to a non-fully developed slug flow pattern.
5. At high liquid flow rates, the bubbly flow pattern persisted up to void fractions of 0.6.
6. The use of five different air-water mixing methods, with the air always being introduced at the tube wall, had no affect on the results.

BIBLIOGRAPHY

1. Martinelli, R.C., L.M.K. Boelter, T.H.M. Taylor, E.G. Thomsen, E.H. Morrin, "Isothermal Pressure Drop for Two-Phase Two-Component Flow in a Horizontal Pipe", Trans. ASME, Vol. 66, 139, 1944.
2. Tippets, F.E., "Critical Heat Fluxes and Flow Patterns in High-Pressure Boiling Water Flows", Journal of Heat Transfer, Trans. ASME, Series C, Vol. 86, p. 12, February, 1964.
3. Hosler, E.R., "Visual Study of Boiling at High Pressure", A.I.Ch.E. Preprint No.10, 6th National Heat Transfer Conference, Boston, Mass.
4. Wallis, G.B.and P. Griffith, "Liquid and Gas Distributions in a Two-Phase Boiling Analogy", M.I.T. Tech. Report No. 13, December, 1958.
5. Christiansen, H., "Power to Void Transfer Functions", Ph.D. Thesis, Nuclear Engineering, M.I.T., September, 1961.
6. Petrick, M., "Two-Phase Air-Water Flow Phenomena", Argonne Nat. Lab. Report, ANL 5787, March, 1958.
7. Levy, S., "Prediction of Two-Phase Pressure Drop and Density Distribution From Mixing Length Theory", ASME Paper No. 62-HT-6.
8. Bankoff, S.G., "A Variable Density Single-Fluid Model for Two-Phase Flow With Particular Reference to Steam Water Flow", Journal of Heat Transfer, Trans. ASME, Series C, Vol. 82, p. 265, November, 1960.
9. Deissler, R.G., NACA TN 3016, 1953.
10. Harrison, T.D., "The Design of a Micro Rocket Test Stand", S.M. Thesis, Mechanical Engineering, M.I.T., May, 1959.
11. Rogers, E.J., "Recent Improvements in Design and Reconstruction of the Micro Rocket Test Stand", D.A.C.L. Memorandum No. M-7845-2, November, 1959.

BIBLIOGRAPHY
(Continued)

12. Rogers, E.J., "Adaption of the Micro Rocket Test Stand to L.V.D.T. Transducers", D.A.C.L. Memorandum No. M-8543-4, April, 1961.
13. Rogers, E.J., "Summary Description of the Micro Rocket Test Stand", D.A.C.L. Memorandum No. M-8543-5, April, 1961.
14. Sanborn Linearsyn Differential Transformers, Instruction Manual, IM-575DT-5, Sanborn Co., Waltham, Mass.
15. Moody, L.F., Trans. ASME, Vol. 66, p. 671, 1944.
16. Hartnett, H.P., J.C.Y. Koh, and S.T. McComas, "A Comparison of Predicted and Measured Friction Factors for Turbulent Flow Through Rectangular Ducts", Journal of Heat Transfer, Trans. ASME, Series C., Vol. 84, p. 82, February, 1962.
17. Eirich, F.R., "Rheology", Academic Press, Inc., New York, 1956.
18. Zuber, N., "On the Dispersed Two-Phase Flow in the Laminar Flow Regime", Adv. Tech. Labs., Report No. 63GL50, General Electric Co., Schenectady, New York, 1963.
19. Armand, A.A. and G.G. Treschev, "Investigation of the Resistance During the Movement of Vapor-Water Mixtures in Heated Pipes at High Pressure", Izv. Vsesou. Teplotek. Inst., No. 4, 1-5, AERE Lib/Trans. 816.
20. Nicklin, D.J., J.O. Wilkes, and J.F. Davidson, "Two-Phase Flow in Vertical Tubes", Trans. Inst. of Chem. Eng., Vol. 40, p. 61, 1962.
21. Zuber, N., "On the Variable-Density Single-Fluid Model for Two-Phase Flow", Journal of Heat Transfer, Trans. ASME, Series C, Vol. 82, p. 255, August, 1960.

BIBLIOGRAPHY
(Continued)

22. Dukler, A.E., M. Wicks, and R.G. Cleveland, "Frictional Pressure Drop in Two-Phase Flow", A. A Comparison of Existing Correlations for Pressure Loss and Holdup, B. An Approach Through Similarity Analysis. Univ. of Houston, Houston, Texas, 1963.

23. Isbin, H.S., H. Rodriguez, H. Larson and B. Pattie, "Void Fractions in Two-Phase Flow", A.I.Ch.E. Journal, Vol. 5, No. 4, p. 427, December, 1959.

24. Griffith, P., "The Prediction of Low Quality Boiling Voids", ASME Paper, 63-HT-20, August, 1963.

25. Haberman, W.L. and R.K. Morton, "An Experimental Investigation of the Drag and Shape of Air Bubbles Rising in Various Liquids", David W. Taylor Model Basin, Report No. 802, NS715-102, September, 1953.

26. Haywood, R.W., G.A. Knight, M.A. Middleton, and J.R.S. Thom, "Experimental Study of the Flow Conditions and Pressure Drop of Steam-Water Mixtures at High Pressure in Heated and Unheated Tubes", Presented at the Institution of Mechanical Engineers, London, England, p. 26 and p. 36, March, 1961.

27. Leary, W.A. and D.H. Tsai, "Metering of Gases by Means of the ASME Square-Edged Orifice with Flange Taps", Sloan Laboratory, M.I.T., July, 1951.

28. Haberstroh, R.D., "Transition Between Annular and Semi-annular Regimes in Two-Phase Flow", Sc.D. Thesis, Mech. Eng., M.I.T., June, 1964.

29. James, W. and E. Silberman, "Two-Phase Flow Studies in Horizontal Pipes with Special Reference to Bubbly Mixtures", Saint Anthony Falls Hydraulic Lab., Tech. Paper No. 26, Series B, September, 1958.

BIBLIOGRAPHY
(Continued)

30. Schlichting, H., "Boundary Layer Theory", McGraw Hill Book Co., 1960.
31. Wallis, G.B., "Some Hydrodynamic Aspects of Two-Phase Flow and Boiling", Intern. Heat Transfer Conference, Boulder, Colorado, 1961.
32. Chemical Engineering Handbook, McGraw Hill Book Co., 3rd Ed., p. 374.
33. Radovcich, N., and R. Moissis, "The Transition Flow From Two Phase Bubble Flow to Slug Flow", Technical Report No. 7-7673-22, Division of Sponsored Research, M.I.T., June, 1962.
34. Snyder, G., and P. Griffith, "The Bubbly-Slug Transition In a High Velocity Two Phase Flow", Technical Report No. 5003-29, Division of Sponsored Research, M.I.T., July, 1964.

APPENDIX A

Momentum Flux Models

1. Single-Phase

The following notes relate the single-phase momentum flux to the tube diameter and the average liquid velocity. Consider the steady flow of water through a circular tube. The momentum flux through a plane perpendicular to the tube axis is:

$$M_f = \frac{2\pi\rho_f R^2}{g_c} \int_0^1 V_f^2 \,(1-S)ds \qquad (A1)$$

where:

$$S = \frac{Y}{R} \qquad (A2)$$

According to Schlichting[30], a fully developed turbulent velocity profile is represented very well by a 1/7 power law distribution at a Reynolds number of 1.1×10^5. A look at the single-phase data in Appendix F indicates that the average Reynolds number is very close to 1.1×10^5. Therefore, the local velocity is represented as:

$$\frac{V_f}{V_{f_c}} = S^{1/7} \qquad (A3)$$

From the continuity equation, the average velocity can be related to the centerline velocity with the use of Eq. (A3). The result is:

$$\overline{V}_f = 0.817\, V_{f_c} \qquad (A4)$$

Combining Eqs. (A4), (A3), and (A1), the final expression for the momentum flux is:

$$M_f = \frac{1.02\ \pi R^2 \rho_f \overline{V}_f^{\,2}}{g_c} \qquad (A5)$$

With a 1/7 power law distribution, the actual momentum flux is 1.02 times the one-dimensional case. The momentum flux calculated with Eq. (A5) is shown as a function of the tube diameter and average velocity in Figure 31.

2. Two-Phase Flow

2.1 Homogeneous Model

The homogeneous model implies the following assumptions:

1) One-dimensional velocity and void fraction profiles.

2) No slip, i.e., $\left(\overline{V_g/V_f}\right) = 1.0$

With steady flow and assumptions (1) and (2), the homogeneous momentum flux is:

$$M_H = \frac{1}{g_c} \left[W_f\ \overline{V}_f + W_g\ \overline{V}_g\right] \qquad (A6)$$

Since there is no slip:

$$V_H = \overline{V}_f = \overline{V}_g \qquad (A7)$$

or Eq. (A6) can now be written as:

$$M_H = \frac{W_T\ V_H}{g_c} \qquad (A8)$$

Using the continuity equation on the flow, one can write:

$$V_H = \frac{W_T}{\rho_H A} \tag{A9}$$

where (ρ_H) is the homogeneous density and is expressed as:

$$\frac{1}{\rho_H} = \frac{X}{\rho_g} + \frac{1-X}{\rho_f} \tag{A10}$$

Combining Eqs. (A8), (A9), and (A10), the result is:

$$M_H = \frac{W_T^2}{Ag_c} \left[\frac{X}{\rho_g} + \frac{1-X}{\rho_f} \right] \tag{A11}$$

A slightly different form of Eq. (A11), which is more suitable for calculation purposes, results from using the volume flow rates. From continuity we can write:

$$Q_g = \frac{X\ W_T}{\rho_g} \tag{A12}$$

$$Q_f = \frac{(1-X)\ W_T}{\rho_f} \tag{A13}$$

Substituting Eqs. (A12) and (A13) into Eq. (A11), the result is:

$$M_H = \frac{W_T}{Ag_c} (Q_g + Q_f) \tag{A14}$$

2.2 Separated Model

The separated flow model implies the following assumptions:

1) One-dimensional velocity and void fraction profiles.

2) Slip allowed, i.e., $\left(\overline{V_g/V_f}\right) \neq 1.0$

Again, assuming steady flow, the separated momentum flux is:

$$M_S = \frac{1}{g_c} \left[W_f \overline{V}_f + W_g \overline{V}_g\right] \tag{A15}$$

by definition:

$$W_f = (1-X)\, W_T \tag{A16}$$

$$W_g = X\, W_T \tag{A17}$$

$$A_f = (1-\overline{\alpha})\, A \tag{A18}$$

$$A_g = \overline{\alpha}\, A \tag{A19}$$

Applying the continuity equation to each phase, one can write:

$$\overline{V}_f = \frac{W_f}{A_f\, \rho_f} \tag{A20}$$

$$\overline{V}_g = \frac{W_g}{A_g\, \rho_g} \tag{A21}$$

Combining Eqs. (A15) through (A21), the result is:

$$M_S = \frac{W_T^2}{Ag_c} \left[\frac{(1-X)^2}{(1-\bar{\alpha})\ \rho_f} + \frac{X^2}{\bar{\alpha}\ \rho_g} \right] \tag{A22}$$

or making use of Eqs. (A12) and (A13), the final desired form is:

$$M_S = \frac{1}{Ag_c} \left[\frac{W_f\ Q_f}{(1-\bar{\alpha})} + \frac{W_g\ Q_g}{\bar{\alpha}} \right] \tag{A23}$$

APPENDIX B

Void Fraction Calibration

The purpose of this calibration was to determine the volume from the gate valve to the bottom of the tube. This value was needed to relate the measured liquid level to the average void fraction.

The calibration procedure consisted of pouring a known volume of water into the tube with the bottom gate valve closed and then recording the liquid level on the scale. An example will best explain the procedure. Suppose 305 ml. was poured into the 1 inch tube and the scale reading was 19.06 inches. Note, one liter equals 61.03 $in.^3$ and the cross-sectional area of a 1 inch tube is 0.785 $in.^2$. The equivalent length of a 1 inch tube representing the volume of water is:

$$L_0 = \frac{(.305)(61.03)}{(.785)} = 23.70 \text{ in.} \qquad \text{(B1)}$$

The length of tube representing the volume from the gate valve to the bottom of the tube is therefore:

$$L_E = 23.70 - 19.06 = 4.64 \text{ in.} \qquad \text{(B2)}$$

The results of several tests gave an average value for L_E of 4.87 inches. If the value of L_E is assumed equal for the bottom and top gate valves, the length of tube equal to the volume between the gate valves is:

$$L_T = 60 + 2\ (4.87) = 69.74 \text{ in.} \qquad \text{(B3)}$$

By knowing the length of tube expressed by Eq. (B3), the average void fraction can now be calculated directly from the measured liquid level, or:

$$\bar{\alpha} = \frac{L_T - (\text{Scale Reading} + L_E)}{L_T} \qquad (B4)$$

for the 1 inch tube:

$$\bar{\alpha} = 1 - \frac{(\text{Scale Reading} + 4.87)}{69.74} \qquad (B5)$$

Using a similar procedure, the results for the 3/4 and 1/2 inch tubes were respectively:

$$\bar{\alpha} = 1 - \frac{(\text{Scale Reading} + 6.86)}{73.72} \qquad (B6)$$

$$\bar{\alpha} = 1 - \frac{(\text{Scale Reading} + 11.76)}{83.52} \qquad (B7)$$

APPENDIX C

Velocity and Void Fraction Profiles

The results of this investigation indicate that a more fundamental understanding of two-phase flow must consider the two-dimensional velocity and void fraction profiles. The following notes develop a set of equations that can be solved numerically to study this aspect of two-phase bubbly flow.

The basic model assumes no local slip between the gas and liquid phase, and in this respect is identical to Bankoff's[8] model. This is a good assumption for bubbly flow and is even better as the superficial liquid velocity increases. The equations in this Appendix are written for a circular tube, but can be adapted to other geometries if the required experimental data is available.

Consider the steady flow of a bubbly mixture in a circular tube. Applying the continuity equation to each phase, the result is:

$$W_f = 2\pi\rho_f R^2 \int_0^1 U\,(1-\alpha)(1-S)\,dS \qquad (C1)$$

$$W_g = 2\pi\rho_g R^2 \int_0^1 U\,\alpha\,(1-S)\,dS \qquad (C2)$$

where: $S = Y/R$

A third equation expresses the average void fraction in terms of the local quantity, or:

$$\bar{\alpha} = 2 \int_0^1 \alpha\,(1-S)\,dS \qquad (C3)$$

A fourth equation relating the variables is the expression for the momentum flux, or:

$$M = \frac{2\pi\rho_f R^2}{g_c} \int_0^1 U^2 (1-\alpha)(1-S)\, dS + \frac{2\pi\rho_g R^2}{g_c} \int_0^1 U^2 \alpha (1-S)\, dS \qquad (C4)$$

for the case where $\left(\rho_f/\rho_g\right) \gg 1$, Eq. (C4) becomes:

$$M = \frac{2\pi\rho_f R^2}{g_c} \int_0^1 U^2 (1-\alpha)(1-S)\, dS \qquad (C5)$$

So far, the only assumption has been the idea of no local slip and the introduction of one velocity, namely (U). Next, a power law distribution is assumed for the velocity. This assumption is again similar to Bankoff's[8] model and in addition is supported by the work of Reference (29). In Reference (29), the velocity profile of a bubbly mixture was measured with a pitot tube and a power law distribution fit the data very well. Therefore, we let:

$$\frac{U}{U_m} = (S)^{\frac{1}{m}} \qquad (C6)$$

Finally, the void fraction can be expressed in terms of a power series with four undetermined coefficients, or:

$$\alpha = a + bS + cS^2 + dS^3 \qquad (C7)$$

Where the boundary conditions are:

$$\text{at } S = 0: \qquad \alpha = 0 \tag{C8}$$

$$\text{at } S = 1: \qquad \alpha = \alpha_c \tag{C9}$$

$$\text{at } S = 1: \qquad \frac{\partial \alpha}{\partial S} = 0 \tag{C10}$$

In this analysis, the wall is assumed to be wetted by the liquid so that the void fraction at the wall is zero. For the case of a heated tube, where vapor is generated at the wall, this assumption is no longer valid. In contrast to Bankoff's[8] model, which will not predict slip ratios less than one, Eq. (C7) allows the void fraction to peak off center and represent the observed data. This procedure of assuming an arbitrary profile and making use of the boundary conditions to help determine its shape, is similar to single-phase boundary layer theory. Combining the boundary conditions and Eq. (C7), the result is:

$$a = 0 \tag{C11}$$

$$b = 2\alpha_c + d \tag{C12}$$

$$c = -\alpha_c - 2d \tag{C13}$$

$$\alpha = (2\alpha_c + d)S - (\alpha_c + 2d)S^2 + dS^3 \tag{C14}$$

A check shows that there are now enough independent equations to solve for the unknowns. The required known quantities are: W_f, W_g, $\bar{\alpha}$. and M. Unfortunately, a solution of these equations for one set of known quantities will not provide the final answer to the velocity and void fraction profile question. The reason is because the profiles change for different bubbly flows. But, if the unknown coefficients, b, c, and d along with the exponent m, can be correlated as simple functions of the flow parameters, then a two-dimensional

analysis may prove very beneficial. The solution of the simultaneous equations is now carried to the point where a numerical solution is needed. The procedure is to first eliminate the velocity (U) expressed by Eq. (C6) by substituting it into Eqs. (C1), (C2), and (C5). Then, the void fraction (α) expressed by Eq. (C14) is substituted into Eqs. (C1), (C2), (C3), and (C5). The integrations are then performed and the result is:

$$W_f = 2\pi\rho_f R^2 U_m \left[\frac{m}{m+1} - \frac{(1+2\alpha_c+d)\,m}{2m+1} + \frac{(3\alpha_c+3d)\,m}{3m+1} - \frac{(\alpha_c+3d)\,m}{4m+1} + \frac{dm}{5m+1}\right] \tag{C15}$$

$$W_g = 2\pi\rho_g R^2 U_m \left[\frac{(2\alpha_c+d)\,m}{2m+1} - \frac{(3\alpha_c+3d)\,m}{3m+1} + \frac{(\alpha_c+3d)\,m}{4m+1} - \frac{dm}{5m+1}\right] \tag{C16}$$

$$\bar{\alpha} = \frac{d}{10} + \frac{\alpha_c}{2} \tag{C17}$$

$$M = \frac{2\pi\rho_f R^2 U_m^{\,2}}{g_c}\left[\frac{m}{2+m} - \frac{(1+2\alpha_c+d)\,m}{2m+2} + \frac{(3\alpha_c+3d)\,m}{3m+2} - \frac{(\alpha_c+3d)\,m}{4m+2} + \frac{dm}{5m+2}\right] \tag{C18}$$

The problem now reduces to the numerical solution of Eqs. (C15) to (C18) for the unknowns U_m, α_c, d, and m. Note, if the exponent m was determined by pitot tube measurements, the analysis could be extended to the heated tube as the boundary condition expressed by Eq. (C8) could be treated as an unknown.

APPENDIX D

SINGLE-PHASE TEST DATA - VERTICAL TUBES

1" Tube

Test No.	Water Temp. °F.	$\bar{V}_f$ ft/sec.	P_B-P_M psi.	P_M-P_T psi.	P_B-P_T psi.	N_{Re_f}	F_E lb_f	f_M	f_P	f_L	f_P/f_M	f_L/f_P	f_L/f_M
73	48	10.1	1.41	1.37	2.78	58,000	1.42	0.0200	0.0198	0.0195	0.99	0.98	0.97
74	48	14.0	1.74	1.63	3.37	80,000	2.52	0.0187	0.0182	0.0179	0.98	0.98	0.96
75	48	17.7	2.15	1.95	4.10	101,000	3.90	0.0179	0.0176	0.0173	0.98	0.98	0.97
76	48	20.4	2.46	2.18	4.64	117,000	5.07	0.0175	0.0167	0.0176	0.95	1.05	1.00
77	47	10.0	1.44	1.38	2.82	56,000	1.68	0.0201	0.0212	0.0258	1.05	1.22	1.28
78	47	14.1	1.85	1.57	3.42	79,500	2.65	0.0187	0.0187	0.0187	1.00	1.00	1.00
79	47	17.9	2.14	1.96	4.10	101,000	3.91	0.0179	0.0172	0.0170	0.96	0.99	0.95
80	47	20.0	2.46	2.19	4.65	113,000	4.89	0.0176	0.0174	0.0167	0.99	0.96	0.95
81	47	16.6	2.01	1.84	3.85	93,600	3.45	0.0180	0.0176	0.0175	0.98	1.00	0.98
82	47	13.3	1.69	1.58	3.27	75,500	2.41	0.0190	0.0187	0.0194	0.99	1.04	1.02
83	47	9.4	1.39	1.33	2.72	53,000	1.20	0.0205	0.0209	0.0167	1.02	0.82	0.80
84	46	10.2	1.44	1.38	2.82	56,500	1.68	0.0201	0.0204	0.0257	1.01	1.26	1.28
85	46	14.5	1.77	1.67	3.44	80,000	2.74	0.0188	0.0179	0.0188	0.95	1.05	1.00
86	46	17.5	2.11	1.94	4.05	97,000	3.91	0.0180	0.0176	0.0183	0.98	1.04	1.01
87	46	19.6	2.43	2.12	4.55	109,000	4.83	0.0175	0.0175	0.0170	1.00	0.97	0.97
88	46	17.7	2.16	1.96	4.12	98,000	3.97	0.0180	0.0178	0.0178	0.99	1.00	0.99

APPENDIX D

SINGLE-PHASE TEST DATA - VERTICAL TUBES

1" Tube

Test No.	Water Temp. °F	$\overline{V}_f$ ft/sec.	P_B-P_M psi.	P_M-P_T psi.	P_B-P_T psi.	N_{Re_f}	F_E lb_f	f_M	f_P	f_L	f_P/f_M	f_L/f_P	f_L/f_M
89	46	14.7	1.85	1.69	3.54	81,500	2.88	0.0187	0.0186	0.0188	1.00	1.01	1.00
90	46	10.9	1.46	1.42	2.88	60,000	1.72	0.0199	0.0192	0.0197	0.97	1.02	0.99
95	42	9.6	1.38	1.33	2.71	49,600	1.26	0.0207	0.0199	0.0185	0.98	0.93	0.90
99	39	9.7	1.39	1.36	2.75	47,900	1.47	0.0210	0.0205	0.0235	0.98	1.14	1.12
101	39	12.1	1.60	1.52	3.12	59,700	2.01	0.0199	0.0199	0.0184	1.00	0.93	0.93
106	39	14.7	1.84	1.74	3.58	72,500	2.91	0.0190	0.0191	0.0187	1.00	0.98	0.98
113	39	18.2	2.23	2.06	4.29	89,400	4.20	0.0183	0.0181	0.0172	0.99	0.95	0.94
119	39	15.9	2.01	1.82	3.83	78,500	3.42	0.0189	0.0189	0.0188	1.00	1.00	1.00
126	39	20.3	2.58	2.29	4.87	100,000	5.28	0.0179	0.0183	0.0174	1.02	0.95	0.97
131	39	12.2	1.62	1.52	3.14	60,000	2.04	0.0199	0.0199	0 0183	1.00	0.92	0.92
135	38	20.0	2.46	2.23	4.69	97,500	4.98	0.0180	0.0177	0.0172	0.98	0.97	0.96
143	39	18.3	2.23	2.05	4.28	90,400	4.05	0.0182	0.0178	0.0155	0.98	0.87	0.85
151	39	16.2	1.99	1.87	3.86	79,700	3.45	0.0188	0.0186	0.0183	0.99	0.99	0.97
157	39	14.0	1.82	1.67	3.49	69,000	2.70	0.0193	0.0198	0.0187	1.02	0.95	0.97
162	38	12.2	1.62	1.54	3.16	59,000	2.31	0.0200	0.0203	0.0240	1.01	1.18	1.20
167	38	10.1	1.49	1.41	2.90	48,900	1.56	0.0208	0.0228	0.0198	1.09	0.87	0.95
101-2	38	12.1	1.63	1.52	3.15	59,000	1.89	0.0200	0.0204	0.0154	1.02	0.75	0.77

APPENDIX D

SINGLE-PHASE TEST DATA - VERTICAL TUBES

1" Tube

Test No.	Water Temp. °F.	$\bar{V}_f$ ft/sec.	P_B-P_M psi.	P_M-P_T psi.	P_B-P_T psi.	N_{Re_f}	F_E lb_f	f_M	f_P	f_L	f_P/f_M	f_L/f_P	f_L/f_M
119-2	38	15.9	1.98	1.86	3.84	77,000	3.15	0.0189	0.0189	0.0154	1.00	0.81	0.81
135-2	38	20.2	2.51	2.29	4.80	97,500	5.00	0.0180	0.0180	0.0161	1.00	0.90	0.90
101-2'	38	12.1	1.61	1.54	3.15	58,500	2.12	0.0200	0.0204	0.0202	1.02	0.99	1.01
119-2'	38	15.9	1.99	1.86	3.85	77,000	3.38	0.0189	0.0189	0.0181	1.00	0.96	0.96
135-2'	38	19.8	2.40	2.22	4.62	97,000	4.94	0.0180	0.0176	0.0179	0.98	0.99	1.01
101-1	38	12.2	1.62	1.55	3.17	58,800	2.04	0.0200	0.0206	0.0179	1.03	0.87	0.90
119-1	38	16.1	1.98	1.86	3.84	78,500	3.50	0.0189	0.0187	0.0189	0.99	1.01	1.00
135-1	38	20.2	2.47	2.31	4.78	97,500	5.22	0.0180	0.0179	0.0180	1.00	1.00	1.00

3/4" Tube

226	42	20.3	3.12	2.96	6.08	79,000	3.57	0.0188	0.0196	0.0212	1.04	1.08	1.13
227	42	25.2	4.13	3.84	7.97	98,000	5.22	0.0180	0.0187	0.0198	1.04	1.06	1.10
236	42	29.6	5.20	4.83	10.03	115,000	7.02	0.0175	0.0182	0.0196	1.04	1.08	1.12
241	43	15.2	2.26	2.20	4.46	60,000	2.16	0.0200	0.0209	0.0229	1.04	1.09	1.14
245	44	10.2	1.65	1.60	3.25	41,000	--	0.0217	0.0234	--	1.08	--	--
249	44	5.3	1.22	1.18	2.40	21,200	--	0.0255	0.0269	--	1.05	--	--

APPENDIX D

SINGLE-PHASE TEST DATA - VERTICAL TUBES

3/4" Tube

Test No.	Water Temp. °F.	$\overline{V}_f$ ft/sec.	P_B-P_M psi.	P_M-P_T psi.	P_B-P_T psi.	N_{Re_f}	F_E lb_f	f_M	f_P	f_L	f_P/f_M	f_L/f_P	f_L/f_M
253	44	15.4	2.27	2.20	4.47	61,700	--	0.0198	0.0205	--	1.04	--	--
257	44	19.8	3.00	2.79	5.79	79,500	3.03	0.0189	0.0191	0.0176	1.01	0.92	0.93
260	45	30.0	5.19	4.86	10.05	123,000	6.65	0.0172	0.0178	0.0172	1.03	0.97	1.00
266	46	25.0	3.94	3.79	7.73	104,000	4.68	0.0179	0.0182	0.0173	1.02	0.95	0.97
271	47	20.3	3.08	2.96	6.04	86,000	3.36	0.0184	0.0194	0.0192	1.05	0.99	1.04

1/2" Tube

300	50	19.9	3.88	3.98	7.86	59,000	1.75	0.0200	0.0195	0.0180	0.98	0.92	0.90
301	50	29.6	6.67	7.05	13.72	87,900	3.53	0.0183	0.0177	0.0164	0.97	0.93	0.90
302	50	39.2	10.43	10.84	21.27	116,000	5.75	0.0175	0.0166	0.0152	0.95	0.92	0.87
303	51	20.4	4.16	4.11	8.27	61,000	1.95	0.0198	0.0199	0.0194	1.00	0.98	0.98
308	51	10.2	1.95	1.91	3.86	30,600	--	0.0230	0.0234	--	1.02	--	--
313	51	5.0	1.29	1.28	2.57	15,000	--	0.0276	0.0290	--	1.05	--	--
318	51	30.2	6.95	7.39	14.34	90,700	3.66	0.0181	0.0179	0.0163	0.99	0.91	0.90

APPENDIX E

TWO-PHASE DATA - VERTICAL TUBES

1" Tube No.3 Mixing Chamber

Test No.	Flow Pattern	t_w °F.	P_a psia.	W_f lbm/min.	W_g lbm/min.	X	P_B psig.	P_M psig.	P_T psig.	P_A psig.	$\bar{\alpha}$	$\frac{Q_g}{Q_g + Q_f}$	$\left(\frac{\overline{V_g}}{V_f}\right)$
91	Bubbly	44	14.50	195	0.126	0.000647	3.39	2.06	0.70	2.05	0.272	0.312	1.22
92	Unsteady	44	14.50	196	0.190	0.000970	3.84	2.35	0.94	2.37	0.345	0.401	1.26
93	Unsteady	44	14.50	194	0.270	0.00139	4.03	2.49	0.97	2.49	0.408	0.488	1.38
94	Bubbly	42	14.73	193	0.061	0.000316	3.58	2.27	1.00	3.04	0.190	0.171	0.88
96	Bubbly	42	14.62	196	0.061	0.000312	3.61	2.27	1.00	3.05	0.190	0.169	0.86
97	Bubbly	42	14.62	195	0.136	0.000695	3.36	1.99	0.61	1.99	0.294	0.326	1.16
98	Unsteady	42	14.62	193	0.235	0.00121	3.89	2.40	0.91	2.40	0.382	0.456	1.36

Test No.	F_E lb_f	ΔP_T psi.	ΔP_f psi.	ΔP_e psi.	ΔP_m psi.	ΔP_{m_s} psi.	ΔP_{m_2} psi.	ΔP_{m_3} psi.	f_1	N_{Re_1}	f_2	N_{Re_2}	N_{Fr_m}
91	1.56	2.88	1.10	1.58	0.20	0.08	0.10	0.07	0.0216	51,300	0.0193	54,000	72
92	2.10	3.11	1.50	1.42	0.19	0.14	0.15	0.12	0.0263	51,500	0.0221	56,100	96
93	2.49	3.28	1.78	1.28	0.22	0.21	0.23	0.13	0.0286	51,000	0.0216	58,700	129
94	1.32	2.76	0.94	1.75	0.07	0.05	0.04	0.04	0.0210	49,000	0.0219	48,000	49
96	1.38	2.80	0.98	1.75	0.07	0.05	0.04	0.04	0.0211	50,000	0.0222	48,500	50
97	1.71	2.94	1.21	1.53	0.20	0.09	0.11	0.09	0.0230	49,700	0.0208	52,100	76
98	2.28	3.20	1.61	1.34	0.25	0.06	0.19	0.10	0.0273	49,100	0.0212	55,500	113

APPENDIX E

TWO-PHASE DATA - VERTICAL TUBES

1" Tube No.3 Mixing Chamber

Test No.	Flow Pattern	t_w °F.	P_a psia.	W_f lbm/min.	W_g lbm/min.	X	P_B psig.	P_M psig.	P_T psig.	P_A psig	$\bar{\alpha}$	$\frac{Q_g}{Q_g + Q_f}$	$\left(\frac{\overline{V_g}}{V_f}\right)$
100	Unsteady	39	14.81	179	0.305	0.00170	3.90	2.42	0.99	2.43	0.437	0.532	1.47
102	Bubbly	39	14.81	239	0.062	0.00026	2.66	1.13	-0.34	1.14	0.174	0.158	0.89
103	Bubbly	39	14.81	226	0.1375	0.000608	3.41	1.95	0.43	1.94	0.272	0.296	1.12
104	Unsteady	39	14.81	220	0.237	0.00108	4.27	2.56	0.92	2.58	0.367	0.417	1.23
105	Unsteady	39	14.81	217	0.326	0.00150	4.68	2.89	1.06	2.88	0.410	0.495	1.41
107	Bubbly	39	14.55	288	0.0616	0.000214	2.68	0.84	-0.90	0.86	0.156	0.138	0.87
108	Bubbly	39	14.55	275	0.1375	0.00050	3.98	2.12	0.34	2.14	0.251	0.257	1.03

Test No.	F_E lb_f	ΔP_T psi.	ΔP_f psi.	ΔP_e psi.	ΔP_m psi.	ΔP_{m_s} psi.	ΔP_{m_2} psi.	ΔP_{m_3} psi.	f_1	N_{Re_1}	f_2	N_{Re_2}	N_{Fr_m}
100	2.37	3.12	1.83	1.22	0.07	0.18	0.22	0.13	0.0328	43,400	0.0228	52,100	132
102	2.16	3.22	1.44	1.79	-0.01	0.07	0.07	0.07	0.0213	57,900	0.0222	56,700	72
103	2.13	3.19	1.43	1.57	0.19	0.15	0.14	0.10	0.0209	54,800	0.0197	56,200	92
104	2.82	3.59	1.82	1.37	0.40	0.22	0.23	0.14	0.0244	53,300	0.0208	57,700	127
105	3.36	3.88	2.15	1.28	0.45	0.29	0.33	0.23	0.0276	52,500	0.0204	61,000	165
107	3.06	3.94	1.81	1.83	0.30	0.13	0.11	0.09	0.0189	69,800	0.0197	68,200	100
108	3.18	3.90	1.89	1.62	0.39	0.22	0.20	0.13	0.0192	66,500	0.0191	66,700	122

APPENDIX E

TWO-PHASE DATA - VERTICAL TUBES

1" Tube No.3 Mixing Chamber

Test No.	Flow Pattern	t_w $^oF.$	P_a psia.	W_f $\frac{lbm}{min.}$	W_g $\frac{lbm}{min.}$	X	P_B psig.	P_M psig.	P_T psig.	P_A psig.	$\bar{\alpha}$	$\frac{Q_g}{Q_g + Q_f}$	$\left(\frac{\overline{V_g}}{\overline{V_f}}\right)$
109	Bubbly	39	14.55	257	0.273	0.00106	5.06	3.04	1.05	3.05	0.390	0.411	1.09
110	Bubbly	39	14.55	248	0.416	0.00168	5.59	3.44	1.26	3.43	0.457	0.519	1.28
111	Unsteady	39	14.55	243	0.613	0.00252	6.21	3.97	1.41	3.89	0.519	0.555	1.44
112	Unsteady	39	14.55	232	0.870	0.00373	7.01	4.64	1.67	4.49	0.593	0.694	1.58
114	Bubbly	39	14.62	358	0.0632	0.00018	3.64	1.31	-0.85	1.35	0.125	0.113	0.89
115	Bubbly	39	14.62	347	0.1407	0.00041	4.56	2.19	-0.06	2.22	0.217	0.216	1.00
116	Bubbly	39	14.62	339	0.282	0.00083	6.34	3.71	1.10	3.71	0.320	0.343	1.11

Test No.	F_E lb_f	ΔP_T psi.	ΔP_f psi.	ΔP_e psi.	ΔP_m psi.	ΔP_{m_s} psi.	ΔP_{m_2} psi.	ΔP_{m_3} psi	f_1	N_{Re_1}	f_2	N_{Re_2}	N_{Fr_m}
109	3.78	4.30	2.15	1.32	0.83	0.34	0.37	0.18	0.0204	62,300	0.0191	64,200	171
110	4.56	4.64	2.73	1.17	0.74	0.48	0.56	0.39	0.0248	60,000	0.0194	67,600	238
111	5.44	5.15	3.21	1.04	0.90	0.67	0.87	0.46	0.0269	58,800	0.0175	72,800	352
112	6.45	5.72	3.76	0.88	1.08	0.70	1.24	0.49	0.0289	56,500	0.0165	74,600	515
114	4.71	4.82	2.69	1.89	0.24	0.21	0.16	0.17	0.0189	86,500	0.0194	85,200	146
115	5.04	4.95	2.96	1.69	0.30	0.31	0.32	0.26	0.0198	83,800	0.0197	84,000	177
116	6.15	5.61	3.54	1.47	0.60	0.59	0.61	0.48	0.0216	82,000	0.0201	84,600	238

APPENDIX E

TWO-PHASE DATA - VERTICAL TUBES

1" Tube No.3 Mixing Chamber

Test No.	Flow Pattern	t_w °F.	P_a psia.	W_f lbm/min.	W_g lbm/min.	X	P_B psig.	P_M psig.	P_T psig.	P_A psig.	$\bar{\alpha}$	$\frac{Q_g}{Q_g + Q_f}$	$\left(\frac{\overline{V_g}}{V_f}\right)$
117	Bubbly	39	14.62	325	0.403	0.00124	7.33	4.44	1.64	4.46	0.390	0.428	1.17
118	Bubbly	39	14.62	312	0.710	0.00265	8.70	5.52	2.08	5.45	0.506	0.568	1.28
120	Bubbly	39	15.11	309	0.0636	0.000206	3.85	1.88	0.04	1.91	0.140	0.122	0.85
121	Bubbly	39	15.11	300	0.1415	0.000471	4.32	2.27	0.35	2.30	0.237	0.238	1.00
122	Bubbly	39	15.11	288	0.281	0.000976	5.45	3.22	1.04	3.23	0.344	0.379	1.17
123	Bubbly	39	15.10	276	0.430	0.00156	6.28	3.81	1.40	3.82	0.431	0.486	1.25
124	Unsteady	39	15.10	258	0.750	0.00289	7.16	4.56	1.67	4.49	0.531	0.630	1.51

Test No.	F_E lb_f	ΔP_T psi.	ΔP_f psi.	ΔP_e psi.	ΔP_m psi.	ΔP_{m_s} psi.	ΔP_{m_2} psi.	ΔP_{m_3} psi.	f_1	N_{Re_1}	f_2	N_{Re_2}	N_{Fr_m}
117	6.90	6.10	3.87	1.32	0.91	0.74	0.84	0.43	0.0230	78,500	0.0202	83,700	300
118	8.70	7.10	4.94	1.07	1.09	1.20	1.53	1.02	0.0256	75,500	0.0198	86,000	466
120	3.45	4.08	2.01	1.86	0.21	0.16	0.10	0.11	0.0186	74,600	0.0193	73,200	112
121	3.84	4.25	2.29	1.65	0.31	0.24	0.23	0.16	0.0200	72,500	0.0200	72,500	139
122	4.71	4.72	2.80	1.42	0.50	0.37	0.43	0.25	0.0228	69,500	0.0202	74,000	194
123	5.55	5.22	3.25	1.23	0.74	0.54	0.66	0.36	0.0250	66,600	0.0202	74,000	260
124	6.60	5.87	3.77	1.01	1.09	0.85	1.15	0.50	0.0270	62,500	0.0168	79,400	442

APPENDIX E

TWO-PHASE DATA - VERTICAL TUBES

1" Tube No.3 Mixing Chamber

Test No.	Flow Pattern	t_w °F	P_a psia.	W_f lbm/min.	W_g lbm/min.	X	P_B psig.	P_M psig.	P_T psig.	P_A psig.	$\bar{\alpha}$	$\frac{Q_g}{Q_g + Q_f}$	$\left(\frac{\overline{V_g}}{V_f}\right)$
125	Unsteady	39	15.10	241	1.37	0.00567	8.55	5.99	2.31	5.72	0.650	0.756	1.69
127	Bubbly	39	14.50	410	0.0633	0.00015	4.32	1.61	-0.92	1.66	0.114	0.098	0.84
128	Bubbly	39	14.50	415	0.140	0.00034	5.42	2.45	-0.30	2.50	0.199	0.183	0.91
129	Bubbly	39	14.50	400	0.279	0.00070	7.29	4.26	0.94	4.19	0.293	0.297	1.02
130	Bubbly	39	14.50	390	0.380	0.00098	8.58	5.19	1.87	5.22	0.336	0.349	1.10
132	Bubbly	39	14.52	226	0.0633	0.00028	3.22	1.69	0.27	1.72	0.177	0.166	0.92
133	Bubbly	39	14.52	219	0.140	0.00064	3.52	1.97	0.48	1.98	0.281	0.310	1.14

Test No.	F_E lb_f	ΔP_T psi.	ΔP_f psi.	ΔP_e psi.	ΔP_m psi.	ΔP_{m_s} psi.	ΔP_{m_2} psi.	ΔP_{m_3} psi.	f_1	N_{Re_1}	f_2	N_{Re_2}	N_{Fr_m}
125	8.10	6.68	4.69	0.76	1.23	1.00	2.05	0.72	0.0288	58,500	0.0138	84,500	895
127	6.18	5.61	3.57	1.92	0.12	0.27	0.21	0.17	0.0194	99,000	0.0200	97,400	188
128	7.32	6.13	4.37	1.73	0.03	0.56	0.47	0.34	0.0209	100,000	0.0217	98,400	231
129	8.31	6.80	4.78	1.53	0.49	0.78	0.84	0.56	0.0217	96,500	0.0215	97,300	290
130	9.06	7.20	5.26	1.44	0.50	1.04	1.06	0.78	0.0236	94,000	0.0221	97,500	332
132	1.89	3.16	1.17	1.78	0.21	0.10	0.12	0.06	0.0194	54,500	0.0198	54,000	66
133	2.28	3.26	1.54	1.56	0.16	0.15	0.14	0.10	0.0237	52,900	0.0219	55,000	90

APPENDIX E

TWO-PHASE DATA - VERTICAL TUBES

1" Tube No.3 Mixing Chamber

Test No.	Flow Pattern	t_w °F.	P_a psia.	W_f lbm/min.	W_g lbm/min.	X	P_B psig.	P_M psig.	P_T psig.	P_A psig.	$\bar{\alpha}$	$\frac{Q_g}{Q_g + Q_f}$	$\left(\frac{\overline{V_g}}{V_f}\right)$
134	Unsteady	39	14.52	207	0.279	0.00135	4.24	2.57	0.95	2.58	0.386	0.477	1.44
136	Bubbly	38	14.85	391	0.0635	0.00016	4.06	1.48	-0.91	1.53	0.115	0.103	0.88
137	Bubbly	38	14.85	387	0.141	0.00036	4.88	2.19	-0.36	2.22	0.206	0.198	0.94
138	Bubbly	38	14.85	379	0.281	0.00074	6.90	3.88	0.98	3.91	0.305	0.313	1.04
139	Bubbly	38	14.85	373	0.415	0.00111	8.46	5.26	2.02	5.25	0.367	0.389	1.10
140	Bubbly	38	14.85	357	0.741	0.00207	10.31	6.82	2.80	6.68	0.482	0.527	1.20
141	Bubbly	39	14.65	350	0.930	0.00265	11.45	7.63	3.24	7.50	0.525	0.580	1.25

Test No.	F_E lb_f	ΔP_T psi.	ΔP_f psi.	ΔP_e psi.	ΔP_m psi.	ΔP_{m_s} psi.	ΔP_{m_2} psi.	ΔP_{m_3} psi.	f_1	N_{Re_1}	f_2	N_{Re_2}	N_{Fr_m}
134	2.73	3.52	1.78	1.33	0.41	0.21	0.26	0.16	0.0263	50,000	0.0190	58,700	140
136	5.46	5.33	3.01	1.92	0.40	0.40	0.19	0.32	0.0179	93,600	0.0184	92,500	171
137	6.12	5.61	3.49	1.72	0.40	0.79	0.40	0.32	0.0190	92,700	0.0194	91,900	210
138	7.32	6.35	4.10	1.51	0.74	0.80	0.74	0.52	0.0204	90,800	0.0198	92,100	274
139	8.43	6.90	4.84	1.37	0.69	0.94	1.01	0.71	0.0226	89,500	0.0210	93,000	336
140	10.23	8.05	5.68	1.12	1.25	1.49	1.81	1.27	0.0236	85,800	0.0198	93,600	511
141	11.07	8.80	5.80	1.03	1.97	1.74	2.33	1.29	0.0230	84,800	0.0181	95,500	625

APPENDIX E

TWO-PHASE DATA - VERTICAL TUBES

1" Tube No.3 Mixing Chamber

Test No.	Flow Pattern	t_w °F.	P_a psia.	W_f lbm/min.	W_g lbm/min.	X	P_B psig.	P_M psig.	P_T psig.	P_A psig.	$\bar{\alpha}$	$\frac{Q_g}{Q_g + Q_f}$	$\left(\frac{\overline{V_g}}{\overline{V_f}}\right)$
142	Bubbly	39	14.65	344	1.152	0.00334	12.33	8.34	3.68	8.17	0.570	0.628	1.27
144	Bubbly	39	14.60	360	0.0632	0.000175	3.51	1.19	-0.98	1.23	0.129	0.114	0.86
145	Bubbly	39	14.60	357	0.141	0.000395	4.56	2.16	-0.16	2.18	0.222	0.214	0.95
146	Bubbly	39	14.60	331	0.280	0.000845	6.41	3.81	1.29	3.83	0.319	0.345	1.13
147	Bubbly	39	14.60	316	0.435	0.00138	7.31	4.61	1.92	4.61	0.409	0.452	1.19
148	Bubbly	39	14.60	304	0.740	0.00242	8.71	5.62	2.23	5.54	0.528	0.582	1.25
149	Bubbly	39	14.60	296	0.941	0.00316	9.35	6.17	2.52	6.05	0.572	0.638	1.31

Test No.	F_E lb_f	ΔP_T psi.	ΔP_f psi.	ΔP_e psi.	ΔP_m psi.	ΔP_{m_s} psi.	ΔP_{m_2} psi.	ΔP_{m_3} psi.	f_1	N_{Re_1}	f_2	N_{Re_2}	N_{Fr_m}
142	12.06	9.26	6.49	0.93	1.84	2.00	2.82	1.34	0.0241	83,400	0.0181	96,100	768
144	4.44	4.81	2.34	1.89	0.58	0.21	0.17	0.20	0.0162	87,000	0.0167	85,500	147
145	5.22	5.15	3.05	1.68	0.42	0.38	0.35	0.28	0.0191	86,300	0.0195	85,500	186
146	5.73	5.49	3.13	1.47	0.89	0.57	0.57	0.43	0.0201	80,000	0.0185	83,500	229
147	7.11	5.77	3.55	1.28	0.94	0.68	0.82	0.51	0.0216	76,500	0.0186	82,400	298
148	8.43	6.95	4.78	1.02	1.15	1.17	1.50	0.93	0.0249	73,600	0.0196	82,900	475
149	9.42	7.31	5.56	0.93	0.82	1.27	1.89	1.04	0.0276	71,600	0.0198	85,000	606

APPENDIX E

TWO-PHASE DATA - VERTICAL TUBES

1" Tube No.3 Mixing Chamber

Test No.	Flow Pattern	t_w °F.	P_a psia.	W_f lbm/min.	W_g lbm/min.	X	P_B psig.	P_M psig.	P_T psig.	P_A psig.	$\bar{\alpha}$	$\frac{Q_g}{Q_g + Q_f}$	$\left(\frac{\bar{V_g}}{V_f}\right)$
150	Bubbly	39	14.60	292	1.171	0.00400	10.06	6.92	2.83	6.68	0.606	0.684	1.41
152	Bubbly	39	14.61	320	0.0635	0.000198	3.04	0.98	-0.95	1.01	0.146	0.128	0.85
153	Bubbly	39	14.61	318	0.141	0.000444	4.30	2.22	0.22	2.22	0.239	0.233	1.00
154	Bubbly	39	14.61	291	0.280	0.000961	5.67	3.46	1.26	3.46	0.340	0.381	1.19
155	Unsteady	39	14.61	279	0.435	0.00156	6.41	4.05	1.58	4.02	0.436	0.491	1.25
156	Unsteady	39	14.61	267	0.740	0.00276	7.45	4.79	1.88	4.73	0.539	0.623	1.41
158	Bubbly	39	14.71	269	0.0641	0.000238	3.53	1.79	0.11	1.81	0.160	0.143	0.87

Test No.	F_E lb_f	ΔP_T psi.	ΔP_f psi.	ΔP_e psi.	ΔP_m psi.	ΔP_{m_s} psi.	ΔP_{m_2} psi.	ΔP_{m_3} psi.	f_1	N_{Re_1}	f_2	N_{Re_2}	N_{Fr_m}
150	10.32	7.75	6.18	0.85	0.72	1.32	2.32	1.02	0.0292	70,800	0.0187	88,500	773
152	3.78	4.28	2.18	1.85	0.25	0.14	0.13	0.16	0.0187	77,200	0.0195	75,500	120
153	3.99	4.37	2.34	1.65	0.38	0.26	0.26	0.19	0.0181	76,800	0.0184	76,200	154
154	4.68	4.72	2.76	1.43	0.53	0.41	0.45	0.26	0.0221	70,300	0.0195	75,000	197
155	5.64	5.17	3.44	1.22	0.51	0.55	0.70	0.46	0.0266	67,400	0.0208	74,800	270
156	6.84	5.97	3.97	1.00	1.00	0.92	1.23	0.69	0.0262	64,700	0.0177	78,000	449
158	2.70	3.66	1.57	1.82	0.27	0.12	0.09	0.08	0.0187	65,000	0.0194	63,900	89

APPENDIX E

TWO-PHASE DATA - VERTICAL TUBES

1" Tube No.3 Mixing Chamber

Test No.	Flow Pattern	t_w °F.	P_a psia.	W_f lbm/min.	W_g lbm/min.	X	P_B psig.	P_M psig.	P_T psig.	P_A psig.	$\bar{\alpha}$	$\frac{Q_g}{Q_g + Q_f}$	$\left(\frac{\overline{V_g}}{V_f}\right)$
159	Bubbly	39	14.71	262	0.141	0.000538	3.89	2.09	0.40	2.12	0.259	0.268	1.05
160	Unsteady	39	14.71	251	0.280	0.00111	4.83	3.05	1.13	3.01	0.365	0.420	1.26
161	Unsteady	39	14.71	239	0.435	0.00182	5.54	3.47	1.38	3.46	0.455	0.535	1.29

Test No.	F_E lb_f	ΔP_T psi.	ΔP_f psi.	ΔP_e psi.	ΔP_m psi.	ΔP_{m_s} psi.	ΔP_{m_2} psi.	ΔP_{m_3} psi.	f_1	N_{Re_1}	f_1	N_{Re_2}	N_{Fr_m}
159	3.03	3.74	1.90	1.60	0.24	0.19	0.18	0.10	0.0212	63,300	0.0205	64,000	115
160	3.69	3.96	2.46	1.37	0.13	0.37	0.34	0.23	0.0255	60,600	0.0213	66,300	169
161	4.32	4.45	2.65	1.18	0.62	0.40	0.54	0.33	0.0260	57,700	0.0187	68,000	238

APPENDIX E

TWO-PHASE DATA - VERTICAL TUBES

1" Tube No.2 Mixing Chamber

Test No.	Flow Pattern	t_w $^oF.$	P_a psia.	W_f $\frac{lbm}{min.}$	W_g $\frac{lbm}{min.}$	X	P_B psig.	P_M psig.	P_T psig.	P_A psig.	$\bar{\alpha}$	$\frac{Q_g}{Q_g + Q_f}$	$\left(\frac{\overline{V_g}}{V_f}\right)$
102-2	Bubbly	38	14.51	239	0.0628	0.000262	3.30	1.74	0.25	1.76	0.172	0.156	0.90
103-2	Bubbly	38	14.51	227	0.1395	0.000615	3.57	2.02	0.50	2.03	0.285	0.299	1.07
104-2	Unsteady	38	14.51	220	0.241	0.00109	4.41	2.71	1.04	2.72	0.362	0.422	1.29
120-2	Bubbly	38	14.51	309	0.0635	0.000206	3.02	1.03	-0.86	1.05	0.145	0.131	0.89
121-2	Bubbly	38	14.51	296	0.1405	0.000475	4.22	2.22	0.32	2.25	0.244	0.246	1.01
123-2	Bubbly	38	14.51	275	0.428	0.00156	6.43	4.03	1.61	4.02	0.432	0.491	1.27
136-2	Bubbly	38	14.51	391	0.0626	0.000160	4.02	1.52	-0.87	1.55	0.115	0.103	0.88

Test No.	F_E lb_f	ΔP_T psi.	ΔP_f psi.	ΔP_e psi.	ΔP_m psi.	ΔP_{m_s} psi.	ΔP_{m_2} psi.	ΔP_{m_3} psi.	f_1	N_{Re_1}	f_2	N_{Re_2}	N_{Fr_m}
102-2	2.03	3.27	1.21	1.79	0.27	0.07	0.07	0.07	0.0180	57,000	0.0187	56,000	72
103-2	2.19	3.30	1.39	1.55	0.36	0.15	0.14	0.08	0.0198	53,800	0.0190	55,000	94
104-2	2.59	3.62	1.50	1.38	0.74	0.22	0.24	0.16	0.0203	52,100	0.0166	57,600	131
120-2	3.50	4.16	1.97	1.85	0.34	0.16	0.13	0.13	0.0182	73,300	0.0186	72,500	114
121-2	3.78	4.18	2.31	1.64	0.23	0.24	0.23	0.14	0.0205	70,100	0.0203	70,500	139
123-2	5.44	5.16	3.18	1.23	0.75	0.54	0.67	0.38	0.0246	65,200	0.0197	72,600	262
136-2	5.47	5.25	3.12	1.91	0.22	0.40	0.19	0.26	0.0186	92,700	0.0190	91,500	171

APPENDIX E

TWO-PHASE DATA - VERTICAL TUBES

1" Tube No.2 Mixing Chamber

Test No.	Flow Pattern	t_w $^oF.$	P_a psia.	W_f $\frac{lbm}{min.}$	W_g $\frac{lbm}{min.}$	X	P_B psig.	P_M psig.	P_T psig.	P_A psig.	$\bar{\alpha}$	$\frac{Q_g}{Q_g+Q_f}$	$\left(\frac{\overline{V_g}}{\overline{V_f}}\right)$
138-2	Bubbly	38	14.51	377	0.280	0.000743	7.25	4.28	1.39	4.30	0.300	0.312	1.06
140-2	Bubbly	38	14.51	359	0.740	0.00206	10.60	7.00	3.04	6.91	0.479	0.525	1.20
102-2'	Bubbly	38	14.62	239	0.0626	0.000262	3.27	1.71	0.21	1.72	0.176	0.156	0.86
103-2'	Bubbly	38	14.62	227	0.1397	0.000615	3.58	2.01	0.47	2.02	0.280	0.298	1.09
104-2'	Unsteady	38	14.62	220	0.242	0.00110	4.39	2.70	1.02	2.70	0.360	0.422	1.30
120-2'	Bubbly	38	14.55	309	0.0633	0.000205	3.00	1.02	-0.87	1.04	0.150	0.139	0.92
121-2'	Bubbly	38	14.55	295	0.1402	0.000476	4.26	2.29	0.41	2.31	0.246	0.244	0.99

Test No.	F_E lb_f	ΔP_T psi.	ΔP_f psi.	ΔP_e psi.	ΔP_m psi.	ΔP_{m_s} psi.	ΔP_{m_2} psi.	ΔP_{m_3} psi.	f_1	N_{Re_1}	f_2	N_{Re_2}	N_{Fr_m}
138-2	7.29	6.30	4.15	1.52	0.63	0.80	0.72	0.55	0.0210	89,500	0.0202	91,000	270
140-2	10.52	8.11	5.99	1.13	0.99	1.49	1.85	1.34	0.0247	85,500	0.0205	93,700	515
102-2'	2.25	3.28	1.48	1.78	0.02	0.08	0.07	0.08	0.0219	56,700	0.0230	55,300	72
103-2'	2.39	3.33	1.59	1.56	0.18	0.15	0.14	0.10	0.0229	53,800	0.0217	55,300	94
104-2'	3.03	3.61	2.28	1.39	-0.06	0.22	0.24	0.14	0.0311	52,100	0.0251	58,000	131
120-2'	3.75	4.15	2.31	1.84	0.0	0.17	0.13	0.13	0.0211	73,300	0.0217	72,400	115
121-2'	3.78	4.13	2.37	1.63	0.13	0.23	0.23	0.14	0.0211	70,000	0.0212	69,800	137

APPENDIX E

TWO-PHASE DATA - VERTICAL TUBES

1" Tube No.2 Mixing Chamber

Test No.	Flow Pattern	t_w °F.	P_a psia.	W_f lbm/min.	W_g lbm/min.	X	P_B psig.	P_M psig.	P_T psig.	P_A psig.	$\bar{\alpha}$	$\frac{Q_g}{Q_g + Q_f}$	$\left(\frac{\overline{V_g}}{V_g}\right)$
123-2'	Bubbly	38	14.55	276	0.428	0.00155	6.48	4.03	1.61	4.03	0.436	0.490	1.24
136-2'	Bubbly	38	14.71	391	0.0635	0.000162	4.03	1.51	-0.86	1.55	0.116	0.103	0.88
138-2'	Bubbly	38	14.71	375	0.280	0.000746	7.11	4.14	1.33	4.18	0.303	0.312	1.05

Test No.	F_E lb_f	ΔP_T psi.	ΔP_f psi.	ΔP_e psi.	ΔP_m psi.	ΔP_{m_s} psi.	ΔP_{m_2} psi.	ΔP_{m_3} psi.	f_1	N_{Re_1}	f_2	N_{Re_2}	N_{Fr_m}
123-2'	5.97	5.22	3.80	1.23	0.19	0.53	0.68	0.49	0.0290	65,500	0.0237	72,300	262
136-2'	5.66	5.24	3.36	1.91	-0.03	0.40	0.19	0.28	0.0200	92,700	0.0206	91,500	171
138-2'	7.25	6.20	4.20	1.51	0.49	0.80	0.69	0.51	0.0214	89,000	0.0209	90,000	266

APPENDIX E

TWO-PHASE DATA - VERTICAL TUBES

1" Tube No.1 Mixing Chamber

Test No.	Flow Pattern	t_w °F.	P_a psia.	W_f lbm/min.	W_g lbm/min.	X	P_B psig.	P_M psig.	P_T psig.	P_A psig.	$\bar{\alpha}$	$\frac{Q_g}{Q_g+Q_f}$	$\left(\frac{\overline{V_g}}{V_f}\right)$
102-1	Bubbly	38	14.62	242	0.0626	0.000259	3.28	1.69	0.15	1.70	0.169	0.155	0.89
103-1	Bubbly	38	14.62	227	0.140	0.000617	3.69	2.09	0.50	2.09	0.267	0.297	1.16
104-1	Unsteady	38	14.62	219	0.241	0.00110	4.39	2.69	1.01	2.69	0.366	0.421	1.26
120-1	Bubbly	38	14.74	309	0.0635	0.000205	2.99	1.02	-0.88	1.03	0.148	0.130	0.86
121-1	Bubbly	38	14.74	302	0.141	0.000467	4.29	2.25	0.25	2.26	0.230	0.240	1.06
123-1	Unsteady	38	14.74	275	0.430	0.00156	6.34	4.05	1.62	4.01	0.429	0.477	1.21
136-1	Bubbly	38	14.74	391	0.0635	0.000162	4.00	1.49	-0.88	1.52	0.114	0.103	0.90
138-1	Bubbly	38	14.74	377	0.280	0.000743	6.94	4.00	1.12	4.01	0.294	0.302	1.04
140-1	Bubbly	38	14.74	352	0.740	0.00210	10.30	6.85	3.00	6.75	0.477	0.529	1.23

Test No.	F_E lb_f	ΔP_T psi.	ΔP_f psi.	ΔP_e psi.	ΔP_m psi.	ΔP_{m_s} psi.	ΔP_{m_2} psi.	ΔP_{m_3} psi.	f_1	N_{Re_1}	f_2	N_{Re_2}	N_{Fr_m}
102-1	2.09	3.35	1.18	1.80	0.37	0.08	0.07	0.10	0.0173	57,500	0.0178	56,500	74
103-1	2.44	3.42	1.55	1.59	0.28	0.15	0.13	0.12	0.0226	53,900	0.0208	56,000	93
104-1	2.78	3.62	1.73	1.37	0.52	0.22	0.24	0.18	0.0236	52,000	0.0195	57,000	129
120-1	3.63	4.15	2.15	1.84	0.16	0.17	0.12	0.11	0.0198	74,000	0.0205	72,600	113
121-1	3.94	4.32	2.32	1.67	0.33	0.24	0.24	0.21	0.0202	72,000	0.0196	73,000	142
123-1	5.50	5.05	3.40	1.23	0.42	0.54	0.64	0.41	0.0264	65,200	0.0221	71,200	248
136-1	5.63	5.23	3.35	1.92	-0.04	0.40	0.19	0.26	0.0200	92,600	0.0204	91,600	170
138-1	7.40	6.24	4.35	1.53	0.36	0.80	0.72	0.55	0.0223	89,500	0.0216	90,600	262
140-1	10.28	7.81	6.05	1.13	0.63	1.49	1.57	1.02	0.0261	83,600	0.0223	90,500	479

APPENDIX E

TWO-PHASE DATA - VERTICAL TUBES

3/4" Tube No.3 Mixing Chamber

Test No.	Flow Pattern	t_w $^oF.$	P_a psia.	W_f $\frac{lbm}{min.}$	W_g $\frac{lbm}{min.}$	X	P_B psig.	P_M psig.	P_T psig.	P_A psig.	$\bar{\alpha}$	$\frac{Q_g}{Q_g + Q_f}$	$\left(\frac{\overline{V_g}}{\overline{V_f}}\right)$
227	Bubbly	42	14.62	216	0.067	0.00031	5.15	1.79	-1.56	1.79	0.200	0.180	0.88
228	Bubbly	42	14.62	210	0.115	0.00055	6.13	2.41	-1.36	2.40	0.283	0.272	0.95
232	Bubbly	42	14.80	266	0.0665	0.00025	6.10	1.68	-2.84	1.65	0.175	0.149	0.83
233	Bubbly	42	14.80	254	0.115	0.00045	7.17	2.51	-2.40	2.45	0.251	0.234	0.91
234	Bubbly	42	14.80	240	0.211	0.00088	9.00	3.85	-1.91	3.70	0.359	0.355	0.98
235	Bubbly	42	14.80	232	0.297	0.00128	10.51	5.03	-1.37	4.80	0.419	0.432	1.05
237	Bubbly	42	14.81	317	0.067	0.00021	7.27	1.69	-4.25	1.60	0.150	0.130	0.84

Test No.	F_E lb_f	ΔP_T psi.	ΔP_f psi.	ΔP_e psi.	ΔP_m psi.	ΔP_{m_s} psi.	ΔP_{m_2} psi.	ΔP_{m_3} psi.	f_1	N_{Re_1}	f_2	N_{Re_2}	N_{Fr_m}
227	4.03	7.20	5.28	1.73	0.19	0.57	0.48	0.50	0.0220	73,200	0.0231	71,400	263
228	4.50	8.01	5.65	1.55	0.81	0.95	0.85	0.78	0.0224	71,000	0.0230	70,000	316
232	5.74	9.57	7.25	1.79	0.53	0.94	0.82	0.63	0.0207	90,000	0.0216	88,000	374
233	6.41	10.25	8.25	1.62	0.38	1.39	1.33	1.25	0.0234	86,000	0.0243	84,000	418
234	7.16	11.70	8.81	1.39	1.50	2.36	2.35	1.83	0.0240	81,200	0.0240	81,000	529
235	7.91	12.70	9.72	1.26	1.72	2.92	3.15	1.90	0.0255	78,500	0.0245	80,000	631
237	7.98	12.35	10.15	1.84	0.36	1.65	1.38	1.22	0.0210	107,000	0.0218	105,000	500

APPENDIX E

TWO-PHASE DATA - VERTICAL TUBES

3/4" Tube No.3 Mixing Chamber

Test No.	Flow Pattern	t_w $^oF.$	P_a psia.	W_f $\frac{lbm}{min.}$	W_g $\frac{lbm}{min.}$	X	P_B psig.	P_M psig.	P_T psig.	P_A psig.	$\bar{\alpha}$	$\frac{Q_g}{Q_g + Q_f}$	$\left(\frac{\overline{V_g}}{V_f}\right)$
238	Bubbly	42	14.81	300	0.150	0.00050	9.49	3.51	-3.81	3.18	0.265	0.253	0.94
239	Bubbly	42	14.81	282	0.258	0.00091	12.00	5.43	-3.00	4.96	0.360	0.350	0.96
242	Bubbly	43	14.65	160	0.474	0.000295	4.57	2.30	0.08	2.31	0.182	0.168	0.91
243	Bubbly	43	14.65	156	0.082	0.000525	4.98	2.51	0.10	2.52	0.252	0.262	1.05
246	Bubbly	44	14.52	102	0.0368	0.00036	3.75	2.20	0.73	2.22	0.200	0.200	1.00
247	Unsteady	44	14.52	101	0.0668	0.00066	3.77	2.18	0.67	2.20	0.280	0.314	1.18
248	Unsteady	44	14.52	101	0.115	0.00114	3.92	2.21	0.57	2.23	0.386	0.441	1.26

Test No.	F_E lb_f	ΔP_T psi.	ΔP_f psi.	ΔP_e psi.	ΔP_m psi.	ΔP_{m_s} psi.	ΔP_{m_2} psi.	ΔP_{m_3} psi.	f_1	N_{Re_1}	f_2	N_{Re_2}	N_{Fr_m}
238	8.91	14.25	10.80	1.59	1.86	3.05	2.97	2.82	0.0214	101,500	0.0222	100,000	613
239	10.27	16.10	12.45	1.39	2.26	4.50	4.58	3.63	0.0244	95,500	0.0252	94,000	711
242	2.25	4.80	3.04	1.77	-0.01	--	0.15	--	0.0235	55,500	0.0242	54,700	142
243	2.55	5.23	3.38	1.62	0.23	--	0.28	--	0.0254	54,000	0.0245	54,800	170
246	--	3.02	1.35	1.62	--	--	0.05	--	0.0272	35,700	0.0268	35,800	62
247	--	3.10	1.56	1.45	--	--	0.09	--	0.0289	35,400	0.0260	37,000	82
248	--	3.35	1.94	1.24	--	--	0.17	--	0.0308	35,400	0.0251	38,900	124

APPENDIX E

TWO-PHASE DATA - VERTICAL TUBES

3/4" Tube No.3 Mixing Chamber

Test No.	Flow Pattern	t_w °F.	P_a psia.	W_f lbm/min.	W_g lbm/min.	X	P_B psig.	P_M psig.	P_T psig.	P_A psig.	$\bar{\alpha}$	$\frac{Q_g}{Q_g + Q_f}$	$\left(\frac{\bar{V}_g}{\bar{V}_f}\right)$
250	Bubbly	44	14.52	60.2	0.0213	0.000354	3.23	2.11	1.03	2.12	0.207	0.198	0.94
251	Bubbly	44	14.52	60.2	0.0474	0.000789	3.04	1.96	0.89	1.96	0.306	0.358	1.26
252	Unsteady	44	14.52	62.2	0.0668	0.00107	3.01	1.88	0.82	1.90	0.363	0.431	1.34
254	Bubbly	44	14.70	160	0.0368	0.000229	4.53	2.29	0.16	2.32	0.156	0.135	0.85
255	Bubbly	44	14.70	159	0.0670	0.000420	4.78	2.41	0.09	2.42	0.229	0.222	0.96
256	Bubbly	44	14.70	155	0.116	0.000749	5.23	2.66	0.09	2.66	0.319	0.334	1.07
261	Bubbly	45	14.95	317	0.0673	0.000212	7.07	1.66	-4.22	1.54	0.153	0.130	0.83

Test No.	F_E lb_f	ΔP_T psi.	ΔP_f psi.	ΔP_e psi.	ΔP_m psi.	ΔP_{m_s} psi.	ΔP_{m_2} psi.	ΔP_{m_3} psi.	f_1	N_{Re_1}	f_2	N_{Re_2}	N_{Fr_m}
250	--	2.20	0.59	1.60	--	--	0.01	--	0.0340	21,100	0.0338	21,000	22
251	--	2.15	0.72	1.40	--	--	0.03	--	0.0361	21,100	0.0304	22,900	34
252	--	2.19	0.86	1.29	--	--	0.04	--	0.0372	21,800	0.0291	24,500	46
254	--	4.37	2.56	1.70	--	--	0.11	--	0.0220	56,200	0.0230	54,800	130
255	--	4.69	2.92	1.56	--	--	0.21	--	0.0232	55,800	0.0234	55,400	159
256	--	5.14	3.39	1.38	--	--	0.37	--	0.0253	54,200	0.0238	55,700	207
261	7.26	12.10	8.73	1.84	1.53	1.65	1.34	1.45	0.0180	113,000	0.0189	110,000	504

APPENDIX E

TWO-PHASE DATA - VERTICAL TUBES

3/4" Tube No.3 Mixing Chamber

Test No.	Flow Pattern	t_w °F.	P_a psia.	W_f lbm/min.	W_g lbm/min.	X	P_B psig.	P_M psig.	P_T psig.	P_A psig.	$\bar{\alpha}$	$\frac{Q_g}{Q_g + Q_f}$	$\left(\frac{\overline{V_g}}{V_f}\right)$
262	Bubbly	45	14.95	298	0.150	0.000503	9.39	3.42	-3.77	3.11	0.264	0.245	0.91
263	Bubbly	45	14.95	281	0.258	0.000918	12.22	5.46	-3.15	5.00	0.352	0.350	0.99
265	Bubbly	45	14.95	276	0.332	0.00120	13.88	6.90	-2.25	6.36	0.394	0.400	1.02
267	Bubbly	46	14.72	263	0.067	0.000255	5.89	1.67	-2.73	1.62	0.178	0.154	0.84
268	Bubbly	46	14.72	256	0.116	0.000436	7.16	2.52	-2.48	2.43	0.255	0.236	0.90
269	Bubbly	46	14.72	243	0.211	0.000869	8.96	3.92	-2.01	3.70	0.359	0.356	0.98
270	Bubbly	46	14.72	232	0.297	0.00128	10.48	5.11	-1.28	4.86	0.414	0.434	1.09

Test No.	F_E lb_f	ΔP_T psi.	ΔP_f psi.	ΔP_e psi.	ΔP_m psi.	ΔP_{m_s} psi.	ΔP_{m_2} psi.	ΔP_{m_3} psi.	f_1	N_{Re_1}	f_2	N_{Re_2}	N_{Fr_m}
262	8.51	14.11	10.00	1.60	2.51	3.00	2.88	2.84	0.0204	106,000	0.0211	104,000	592
263	9.83	16.49	11.14	1.40	3.95	4.38	4.68	3.81	0.0224	100,000	0.0224	100,000	710
265	10.19	17.30	11.31	1.31	4.70	4.85	5.52	4.04	0.0221	100,000	0.0214	101,000	805
267	5.33	9.25	6.57	1.78	0.90	0.99	0.80	0.80	0.0192	95,200	0.0200	93,000	368
268	5.81	10.33	6.83	1.61	1.89	1.48	1.41	1.35	0.0191	92,700	0.0198	90,800	427
269	6.84	11.75	8.02	1.41	2.32	2.36	2.46	2.10	0.0217	88,000	0.0210	89,200	541
270	7.45	12.60	8.75	1.27	2.58	2.82	3.14	2.38	0.0234	84,000	0.0215	87,300	638

APPENDIX E

TWO-PHASE DATA - VERTICAL TUBES

3/4" Tube No.3 Mixing Chamber

Test No.	Flow Pattern	t_w °F.	P_a psia.	W_f lbm/min.	W_g lbm/min.	X	P_B psig.	P_M psig.	P_T psig.	P_A psig.	$\bar{\alpha}$	$\frac{Q_g}{Q_g + Q_f}$	$\left(\frac{\bar{V}_g}{V_f}\right)$
272	Bubbly	47	14.80	217	0.067	0.00308	5.07	1.74	-1.58	1.74	0.200	0.179	0.87
273	Bubbly	47	14.80	207	0.116	0.000560	5.93	2.37	-1.32	2.34	0.286	0.277	0.95
274	Bubbly	47	14.80	195	0.210	0.00108	7.19	3.26	-0.88	3.21	0.391	0.412	1.09
275	Unsteady	47	14.80	188	0.296	0.00157	8.32	4.31	-0.38	4.14	0.465	0.493	1.12
276	Bubbly	48	14.82	282	0.294	0.00104	12.80	5.95	-2.44	5.57	0.376	0.375	1.00
277	Bubbly	48	14.82	268	0.361	0.00135	13.72	7.01	-1.74	6.50	0.414	0.425	1.05
278	Bubbly	48	14.82	274	0.418	0.00152	15.60	8.41	-1.17	7.80	0.432	0.442	1.04

Test No.	F_E lb_f	ΔP_T psi.	ΔP_f psi.	ΔP_e psi.	ΔP_m psi.	ΔP_{m_s} psi.	ΔP_{m_2} psi.	ΔP_{m_3} psi.	f_1	N_{Re_1}	f_2	N_{Re_2}	N_{Fr_m}
272	3.81	7.13	4.76	1.73	0.64	0.53	0.48	0.46	0.0198	80,000	0.0207	78,000	266
273	4.46	7.76	5.74	1.54	0.48	0.92	0.81	0.87	0.0234	76,500	0.0238	75,300	311
274	5.07	8.65	6.44	1.32	0.89	1.29	1.42	1.06	0.0253	72,000	0.0232	74,600	419
275	5.51	9.33	6.91	1.16	1.26	1.67	1.90	1.20	0.0256	69,400	0.0226	73,500	525
276	--	--	--	--	--	--	--	--	--	--	--	--	772
277	--	--	--	--	--	--	--	--	--	--	--	--	825
278	--	--	--	--	--	--	--	--	--	--	--	--	910

APPENDIX E

TWO-PHASE DATA - VERTICAL TUBES

3/4" Tube No.3 Mixing Chamber

Test No.	Flow Pattern	t_w $^oF.$	P_a psia.	W_f $\frac{lbm}{min.}$	W_g $\frac{lbm}{min.}$	X	P_B psig.	P_M psig.	P_T psig.	P_A psig.	$\bar{\alpha}$	$\frac{Q_g}{Q_g + Q_f}$	$\left(\frac{\overline{V_g}}{V_f}\right)$
279	Bubbly	48	14.82	248	0.584	0.00234	17.25	9.66	-0.09	9.12	0.505	0.536	1.13
280	Bubbly	48	14.82	233	0.297	0.00127	10.50	5.14	-0.35	5.11	0.414	0.429	1.06
281	Bubbly	48	14.82	227	0.361	0.00159	11.47	5.85	-0.84	5.58	0.441	0.478	1.15
282	Unsteady	48	14.82	217	0.418	0.00192	11.94	6.30	-0.33	6.05	0.483	0.520	1.16
283	Unsteady	48	14.82	210	0.464	0.00220	12.42	6.73	-0.12	6.44	0.505	0.549	1.19

Test No.	F_E lb_f	ΔP_T psi.	ΔP_f psi.	ΔP_e psi.	ΔP_m psi.	ΔP_{m_s} psi.	ΔP_{m_2} psi.	ΔP_{m_3} psi.	f_1	N_{Re_1}	f_2	N_{Re_2}	N_{Fr_m}
279	--	--	--	--	--	--	--	--	--	--	--	--	1082
280	--	--	--	--	--	--	--	--	--	--	--	--	630
281	--	--	--	--	--	--	--	--	--	--	--	--	719
282	--	--	--	--	--	--	--	--	--	--	--	--	772
283	--	--	--	--	--	--	--	--	--	--	--	--	825

APPENDIX E

TWO-PHASE DATA - VERTICAL TUBES

1/2" Tube No.3 Mixing Chamber

Test No.	Flow Pattern	t_w $^oF.$	P_a psia.	W_f $\frac{lbm}{min.}$	W_g $\frac{lbm}{min.}$	X	P_B psig.	P_M psig.	P_T psig.	P_A psig.	$\bar{\alpha}$	$\frac{Q_g}{Q_g + Q_f}$	$\left(\frac{\overline{V_g}}{V_f}\right)$
307	Bubbly	51	14.71	101.4	0.0986	0.000971	13.00	6.97	-0.35	6.65	0.335	0.348	1.07
309	Bubbly	51	14.71	49.8	0.0355	0.000714	5.17	2.97	0.76	2.97	0.278	0.322	1.24
310	Unsteady	51	14.71	49.4	0.0497	0.00101	5.41	3.07	0.71	3.06	0.344	0.402	1.29
311	Bubbly	51	14.71	50.1	0.0425	0.000848	5.31	3.05	0.73	3.03	0.314	0.363	1.24
312	Bubbly	51	14.71	51.6	0.0247	0.000478	5.00	2.89	0.76	2.88	0.212	0.242	1.20
315	Bubbly	51	14.81	104.2	0.0437	0.000419	10.05	4.93	-0.59	4.84	0.202	0.201	1.00
316	Bubbly	51	14.81	107.9	0.0712	0.000659	12.23	6.19	-0.67	5.99	0.265	0.272	1.04

Test No.	F_E lb_f	ΔP_T psi.	ΔP_f psi.	ΔP_e psi.	ΔP_m psi.	ΔP_{m_s} psi.	ΔP_{m_2} psi.	ΔP_{m_3} psi.	f_1	N_{Re_1}	f_2	N_{Re_2}	N_{Fr_m}
307	2.95	14.30	8.83	1.44	4.03	2.18	2.25	--	0.0183	59,700	0.0175	61,000	700
309	--	4.41	2.80	1.46	--	0.15	0.15	--	0.0282	29,300	0.0244	31,400	157
310	--	4.70	3.14	1.33	--	0.20	0.23	--	0.0292	29,100	0.0240	32,000	196
311	--	4.58	3.00	1.39	--	0.19	0.19	--	0.0282	29,500	0.0247	31,500	175
312	--	4.24	2.54	1.59	--	0.10	0.11	--	0.0258	30,400	0.0234	31,900	136
315	2.63	11.40	8.69	1.72	0.99	1.02	0.91	--	0.0204	61,500	0.0206	61,100	490
316	2.92	13.80	8.94	1.59	3.27	1.75	1.74	--	0.0181	63,500	0.0176	64,300	635

APPENDIX E

TWO-PHASE DATA - VERTICAL TUBES

1/2" Tube No.3 Mixing Chamber

Test No.	Flow Pattern	t_w $^oF.$	P_a psia.	W_f $\frac{lbm}{min.}$	W_g $\frac{lbm}{min.}$	X	P_B psig.	P_M psig.	P_T psig.	P_A psig.	$\bar{\alpha}$	$\frac{Q_g}{Q_g + Q_f}$	$\left(\frac{\overline{V_g}}{V_f}\right)$
317	Bubbly	51	14.81	100.2	0.1009	0.001002	13.05	6.85	-0.29	6.44	0.345	0.358	1.06
320	Bubbly	51	14.81	127.2	0.1158	0.000909	18.41	10.19	-1.03	9.43	0.327	0.306	0.91
321	Bubbly	51	14.81	79.9	0.0476	0.000596	8.09	4.26	0.18	4.19	0.251	0.272	1.11
322	Bubbly	51	14.81	76.1	0.0822	0.00108	9.13	4.96	0.27	4.84	0.369	0.394	1.11
323	Unsteady	51	14.81	72.6	0.1152	0.00159	9.86	5.50	0.38	5.31	0.453	0.483	1.13
324	Bubbly	51	14.80	144	0.0671	0.000466	17.34	8.74	-2.40	8.11	0.235	0.194	0.79
325	Bubbly	51	14.80	132	0.1141	0.000866	19.31	10.60	-1.14	9.85	0.322	0.291	0.87

Test No.	F_E lb_f	ΔP_T psi.	ΔP_f psi.	ΔP_e psi.	ΔP_m psi.	ΔP_{m_s} psi.	ΔP_{m_2} psi.	ΔP_{m_3} psi.	f_1	N_{Re_1}	f_2	N_{Re_2}	N_{Fr_m}
317	3.13	14.30	9.75	1.41	3.14	2.19	2.23	--	0.0203	59,000	0.0195	60,300	705
320	4.40	20.80	12.85	1.45	6.50	4.30	4.30	--	0.0171	75,000	0.0182	72,500	966
321	--	7.91	5.86	1.51	--	0.56	0.54	--	0.0237	47,000	0.0226	48,000	342
322	--	8.86	6.63	1.28	--	0.87	0.95	--	0.0248	44,900	0.0229	46,600	451
323	--	9.48	7.06	1.11	--	1.17	1.31	--	0.0252	42,800	0.0224	45,500	570
324	4.62	21.20	13.90	1.66	5.64	3.54	3.30	--	0.0165	84,600	0.0183	80,200	915
325	5.31	21.90	17.00	1.46	3.44	4.50	4.55	--	0.0212	77,800	0.0228	75,000	1015

APPENDIX F

SINGLE-PHASE TEST DATA - MOMENTUM FLUX

1" Tube

Test No.	Water Temp. $^{o}F.$	$\bar{V}_f$ ft/sec.	N_{Re_f}	M_f lb_f	F_5 lb_f	W_F lb_f	M_1 lb_f	C_1
23	62	17.4	123,000	3.27	3.24	0.13	3.37	0.97
24	62	19.5	138,000	4.11	4.07	0.13	4.20	0.98
25	62	22.7	161,000	5.56	5.57	0.13	5.70	0.98
26	61	18.7	130,000	3.78	3.70	0.13	3.83	0.99
27	64	17.5	127,000	3.31	3.24	0.13	3.37	0.98
28	62	15.0	106,000	2.43	2.50	0.13	2.63	0.92
29	64	13.2	92,500	1.89	1.91	0.13	2.04	0.93
30	64	10.3	72,000	1.14	1.10	0.13	1.23	0.93
31	65	21.0	155,000	4.77	4.73	0.13	4.86	0.98
32	64	19.4	141,000	4.07	4.13	0.13	4.26	0.96
33	64	15.4	118,000	2.56	2.56	0.13	2.69	0.95
34	64	11.2	81,500	1.36	1.35	0.13	1.48	0.92
35	65	20.1	149,000	4.37	4.40	0.13	4.53	0.97
36	65	15.2	113,000	2.52	2.54	0.13	2.67	0.94
37	65	11.4	84,000	1.42	1.41	0.13	1.54	0.92
38	61	19.4	135,000	4.07	4.09	0.13	4.22	0.96
39	61	15.2	106,000	2.52	2.56	0.13	2.69	0.94
40	61	11.8	82,000	1.51	1.52	0.13	1.65	0.92

APPENDIX G

TWO-PHASE DATA - MOMENTUM FLUX

No.3 Mixing Chamber

t_w = 62°F.

P_a = 14.55 psia.

ρ_g = 0.0753 $\frac{lbm}{ft^3}$

Test No.	Flow Pattern	W_f $\frac{lbm}{min.}$	W_g $\frac{lbm}{min.}$	X	Q_g $\frac{ft^3}{min.}$	Q_f $\frac{ft^3}{min.}$	$\frac{Q_g}{Q_g + Q_f}$	$\bar{\alpha}$	$\left(\frac{\overline{V_g}}{\overline{V_f}}\right)$	W_F lb_f	F_5 lb_f	C_2	C_3
38	Bubbly	367	0.0635	0.000173	0.844	5.90	0.125	0.140	0.88	0.11	4.11	0.93	0.95
39	Bubbly	357	0.141	0.000395	1.87	5.74	0.246	0.246	1.00	0.10	4.57	0.92	0.92
40	Bubbly	350	0.281	0.000803	3.74	5.62	0.399	0.360	1.18	0.08	5.28	0.97	0.91
41	Bubbly	340	0.435	0.00128	5.78	5.46	0.514	0.440	1.35	0.07	6.09	0.98	0.86
42	Bubbly	322	0.760	0.00235	10.10	5.17	0.662	0.570	1.47	0.05	7.11	1.09	0.86
43	Bubbly	314	0.960	0.00305	12.75	5.04	0.718	0.600	1.69	0.05	7.61	1.16	0.82
44	Bubbly	299	1.197	0.00398	15.90	4.80	0.768	0.650	1.78	0.04	8.10	1.21	0.80
45	Bubbly	300	0.0635	0.000212	0.844	4.81	0.149	0.165	0.88	0.11	2.82	0.92	0.93
46	Bubbly	293	0.142	0.000485	1.89	4.70	0.287	0.270	1.09	0.09	3.13	0.95	0.93
47	Bubbly	287	0.282	0.000983	3.74	4.61	0.448	0.385	1.30	0.08	3.70	1.01	0.90
48	Unsteady	273	0.436	0.00160	5.78	4.38	0.569	0.485	1.40	0.07	4.05	1.07	0.90
49	Unsteady	265	0.635	0.00238	8.44	4.25	0.665	0.570	1.50	0.06	4.63	1.14	0.89

APPENDIX G

TWO-PHASE DATA - MOMENTUM FLUX

No.3 Mixing Chamber

t_w = 64°F.

P_a = 14.70 psia.

ρ_g = 0.0759 $\frac{lbm}{ft^3}$

Test No.	Flow Pattern	W_f $\frac{lbm}{min.}$	W_g $\frac{lbm}{min.}$	X	Q_g $\frac{ft^3}{min.}$	Q_f $\frac{ft^3}{min.}$	$\frac{Q_g}{Q_g + Q_f}$	$\bar{\alpha}$	$\left(\frac{\overline{V_g}}{\overline{V_f}}\right)$	W_F lb_f	F_5 lb_f	C_2	C_3
50	Bubbly	265	0.0640	0.000241	0.844	4.25	0.166	0.185	0.87	0.10	2.26	0.91	0.93
51	Bubbly	266	0.1426	0.000536	1.88	4.27	0.306	0.290	1.07	0.09	2.52	1.00	0.97
52	Unsteady	253	0.283	0.00112	3.73	4.06	0.479	0.405	1.35	0.08	3.11	0.98	0.86
53	Unsteady	241	0.518	0.00214	6.83	3.87	0.638	0.535	1.53	0.06	3.68	1.10	0.85
54	Bubbly	205	0.0640	0.000312	0.844	3.29	0.204	0.210	0.97	0.10	1.41	0.89	0.90
55	Bubbly	200	0.142	0.000710	1.87	3.22	0.368	0.335	1.16	0.09	1.61	0.95	0.91
56	Unsteady	189	0.282	0.00149	3.72	3.04	0.550	0.460	1.44	0.07	1.89	1.09	0.87
57	Bubbly	413	0.0641	0.000155	0.846	6.63	0.113	0.128	0.87	0.11	5.16	0.93	0.94
58	Bubbly	414	0.1426	0.000344	1.88	6.64	0.221	0.225	0.97	0.10	5.98	0.92	0.92
59	Bubbly	405	0.283	0.000700	3.73	6.50	0.364	0.335	1.14	0.09	6.96	0.93	0.89
60	Bubbly	378	0.621	0.00164	8.19	6.07	0.574	0.510	1.27	0.06	8.54	1.00	0.87
61	Bubbly	366	0.860	0.00234	11.33	5.87	0.660	0.575	1.43	0.05	9.41	1.06	0.85
62	Bubbly	354	1.205	0.00340	15.90	5.69	0.737	0.640	1.57	0.05	10.60	1.14	0.84

APPENDIX G

TWO-PHASE DATA - MOMENTUM FLUX

No.5 Mixing Chamber

t_w = 64°F.

P_a = 14.55 psia.

ρ_g = 0.0750 $\frac{lbm}{ft^3}$

Test No.	Flow Pattern	W_f $\frac{lbm}{min.}$	W_g $\frac{lbm}{min.}$	X	Q_g $\frac{ft^3}{min.}$	Q_f $\frac{ft^3}{min.}$	$\frac{Q_g}{Q_g + Q_f}$	$\bar{\alpha}$	$\left(\frac{\bar{V}_g}{\bar{V}_f}\right)$	W_F lb_f	F_5 lb_f	C_2	C_3
63	Bubbly	380	0.145	0.000382	1.93	6.10	0.240	0.240	1.00	0.10	5.06	0.94	0.94
64	Bubbly	346	0.450	0.00130	6.00	5.56	0.520	0.460	1.27	0.07	6.30	1.00	0.89
65	Unsteady	330	0.775	0.00234	10.33	5.30	0.661	0.560	1.53	0.06	7.45	1.09	0.84
66	Unsteady	307	1.228	0.00398	16.36	4.94	0.768	0.650	1.78	0.04	8.48	1.22	0.81
67	Bubbly	309	0.0918	0.000297	1.22	4.97	0.197	0.205	0.96	0.10	3.15	0.94	0.94
68	Bubbly	296	0.289	0.000976	3.86	4.75	0.448	0.395	1.24	0.08	3.98	1.00	0.91
69	Unsteady	286	0.445	0.00156	5.94	4.60	0.563	0.480	1.40	0.07	4.68	1.01	0.85
70	Unsteady	279	0.644	0.00230	8.59	4.48	0.657	0.560	1.51	0.06	5.22	1.10	0.86
71	Bubbly	226	0.0921	0.000407	1.23	3.63	0.253	0.253	1.01	0.10	1.74	0.95	0.95
72	Bubbly	223	0.172	0.000771	2.29	3.58	0.390	0.340	1.23	0.08	2.06	0.97	0.90
73	Unsteady	218	0.250	0.00115	3.33	3.50	0.488	0.415	1.34	0.07	2.26	1.01	0.89
74	Unsteady	214	0.356	0.00166	4.75	3.44	0.580	0.500	1.38	0.06	2.56	1.06	0.89

APPENDIX G

TWO-PHASE DATA - MOMENTUM FLUX

No.1 Mixing Chamber

t_w = 64°F.

P_a = 14.80 psia

ρ_g = 0.0764 $\frac{lbm}{ft^3}$

Test No.	Flow Pattern	W_f $\frac{lbm}{min.}$	W_g $\frac{lbm}{min.}$	X	Q_g $\frac{ft^3}{min.}$	Q_f $\frac{ft^3}{min.}$	$\frac{Q_g}{Q_g + Q_f}$	$\bar{\alpha}$	$\left(\frac{\overline{V_g}}{\overline{V_f}}\right)$	W_F lb_f	F_5 lb_f	C_2	C_3
75	Bubbly	394	0.093	0.000236	1.22	6.33	0.162	0.180	0.88	0.10	5.22	0.89	0.91
76	Bubbly	367	0.358	0.000976	4.69	5.89	0.444	0.400	1.20	0.07	6.37	0.96	0.86
77	Bubbly	358	0.784	0.00218	10.25	5.75	0.641	0.550	1.57	0.06	7.71	1.17	0.87
78	Bubbly	319	1.264	0.00396	16.60	5.12	0.765	0.650	1.74	0.04	9.24	1.19	0.80
79	Bubbly	316	0.0927	0.000294	1.21	5.07	0.193	0.200	0.96	0.10	3.33	0.92	0.93
80	Bubbly	303	0.292	0.000964	3.83	4.87	0.440	0.390	1.23	0.08	4.20	0.98	0.90
81	Unsteady	292	0.454	0.00155	5.95	4.69	0.559	0.485	1.34	0.07	4.78	1.02	0.87
82	Unsteady	290	0.650	0.00224	8.52	4.66	0.646	0.545	1.52	0.06	5.55	1.08	0.85
83	Bubbly	232	0.0658	0.000284	0.86	3.72	0.188	0.200	0.93	0.10	1.76	0.90	0.92
84	Unsteady	223	0.173	0.000775	2.26	3.58	0.387	0.340	1.23	0.08	2.04	0.97	0.91
85	Unsteady	220	0.252	0.00114	3.30	3.54	0.483	0.415	1.32	0.07	2.33	1.00	0.88
86	Unsteady	217	0.357	0.00165	4.68	3.48	0.574	0.495	1.37	0.06	2.61	1.06	0.89

APPENDIX G

TWO-PHASE DATA - MOMENTUM FLUX

No.4 Mixing Chamber

t_w = 61°F.

P_a = 14.65 psia

ρ_g = 0.0759 $\frac{lbm}{ft^3}$

Test No.	Flow Pattern	W_f $\frac{lbm}{min.}$	W_g $\frac{lbm}{min.}$	X	Q_g $\frac{ft^3}{min.}$	Q_f $\frac{ft^3}{min.}$	$\frac{Q_g}{Q_g + Q_f}$	$\bar{\alpha}$	$\left(\frac{\overline{V_g}}{\overline{V_f}}\right)$	W_F lb_f	F_5 lb_f	C_2	C_3
87	Bubbly	391	0.0658	0.000168	0.868	6.28	0.121	0.140	0.85	0.11	4.57	0.95	0.97
88	Bubbly	334	0.780	0.00233	10.3	5.36	0.656	0.580	1.39	0.05	7.89	1.05	0.86
89	Bubbly	315	1.230	0.00389	16.2	5.06	0.760	0.650	1.73	0.04	8.97	1.18	0.81
90	Bubbly	308	0.0922	0.000299	1.22	4.95	0.198	0.198	1.00	0.10	3.11	0.94	0.97
91	Bubbly	290	0.290	0.00100	3.82	4.66	0.450	0.400	1.24	0.08	3.89	0.98	0.90
92	Unsteady	280	0.445	0.00159	5.87	4.50	0.567	0.480	1.42	0.07	4.42	1.02	0.86
93	Unsteady	284	0.646	0.00237	8.52	4.56	0.652	0.550	1.53	0.06	5.33	1.10	0.85
94	Bubbly	241	0.0657	0.000272	0.868	3.87	0.183	0.200	0.90	0.10	1.92	0.90	0.92
95	Unsteady	235	0.146	0.000621	1.93	3.78	0.338	0.310	1.13	0.09	2.17	0.94	0.91
96	Unsteady	232	0.252	0.00109	3.32	3.72	0.472	0.395	1.37	0.08	2.50	1.00	0.88
97	Unsteady	226	0.358	0.00158	4.72	3.63	0.566	0.480	1.41	0.07	2.73	1.07	0.90

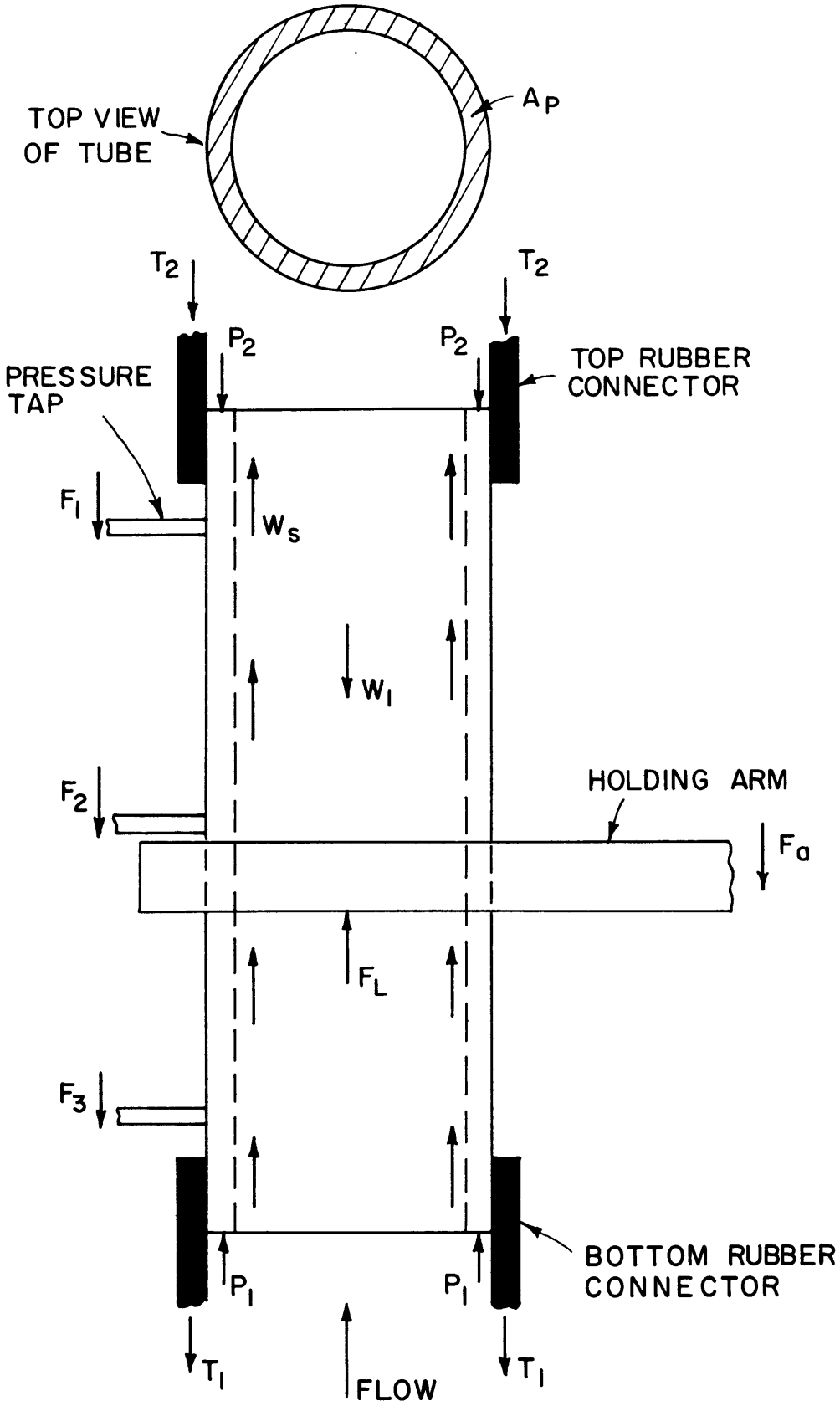

FIGURE 1 FREE BODY DIAGRAM OF VERTICAL TUBE

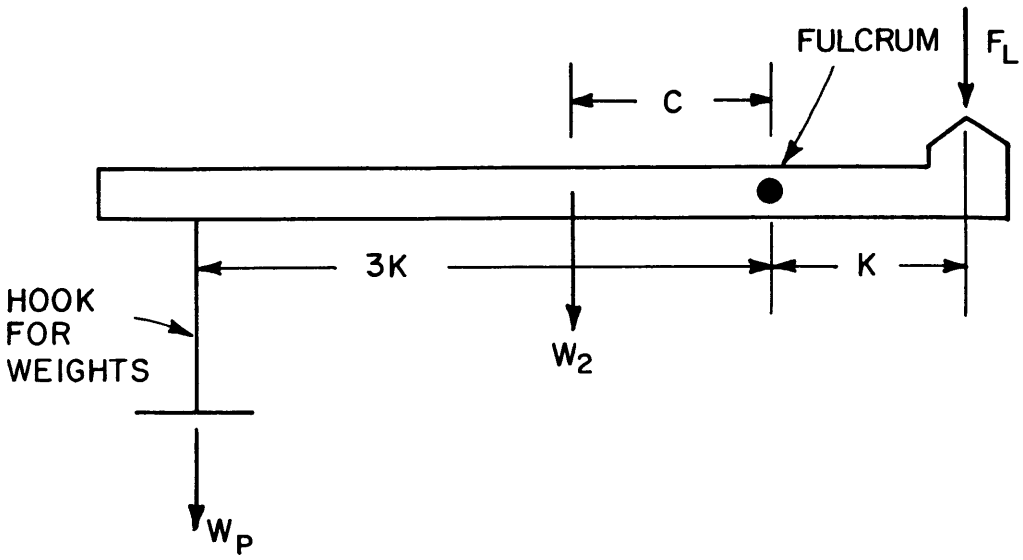

FIGURE 2 FREE BODY DIAGRAM OF LEVER

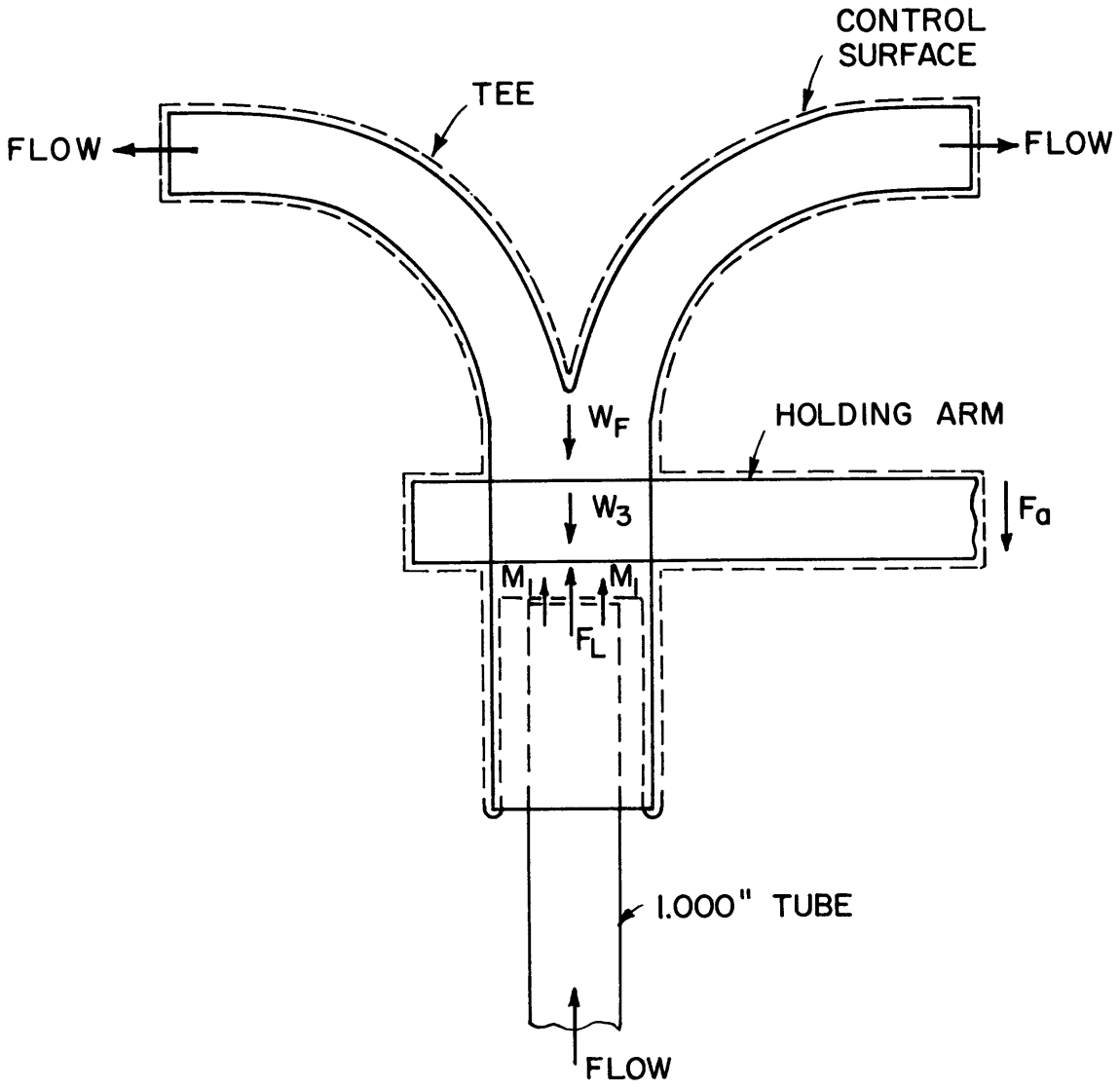

FIGURE 3 CONTROL VOLUME FOR MOMENTUM FLUX ANALYSIS

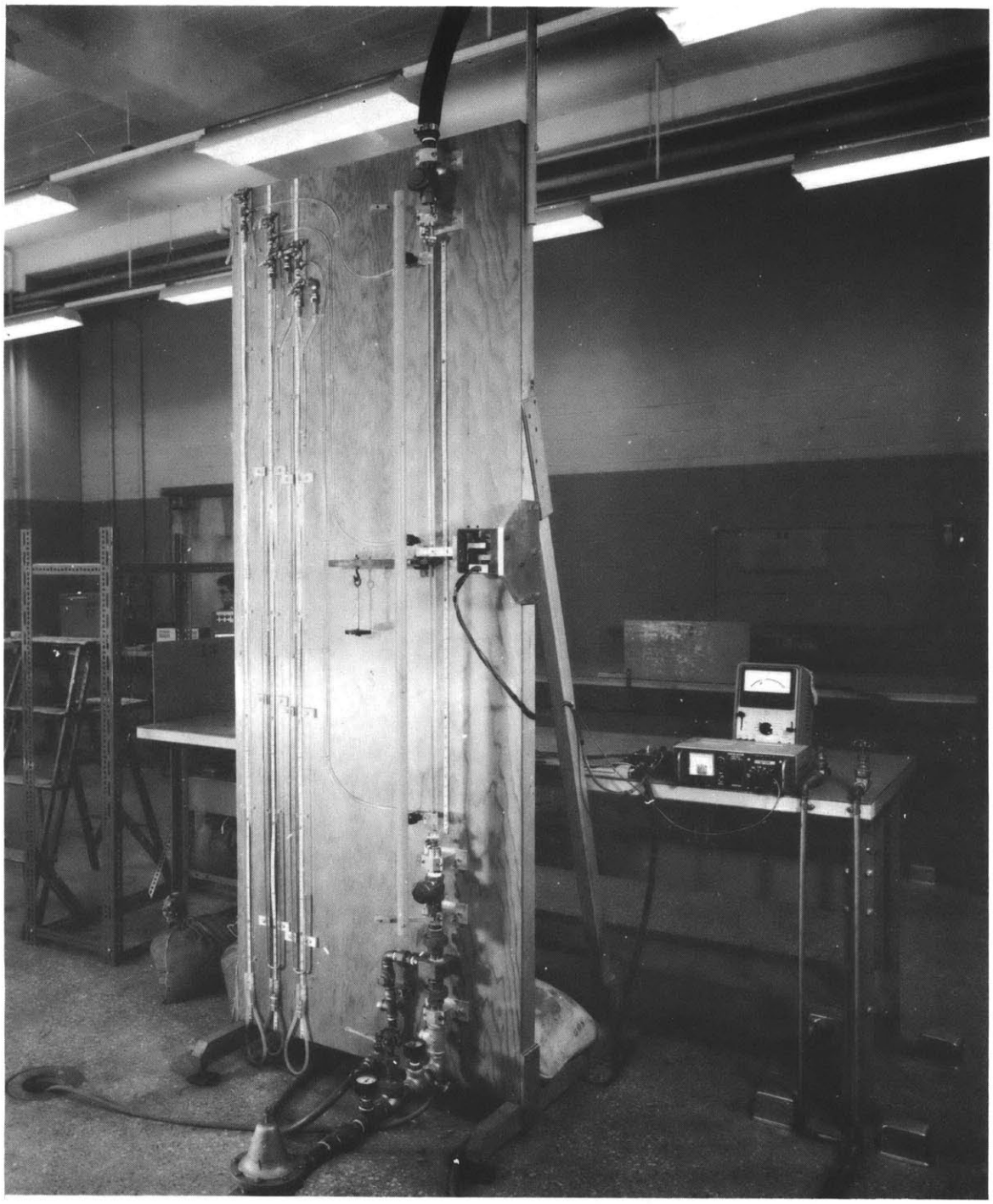

FIGURE 4 PHOTOGRAPH OF VERTICAL TUBE APPARATUS

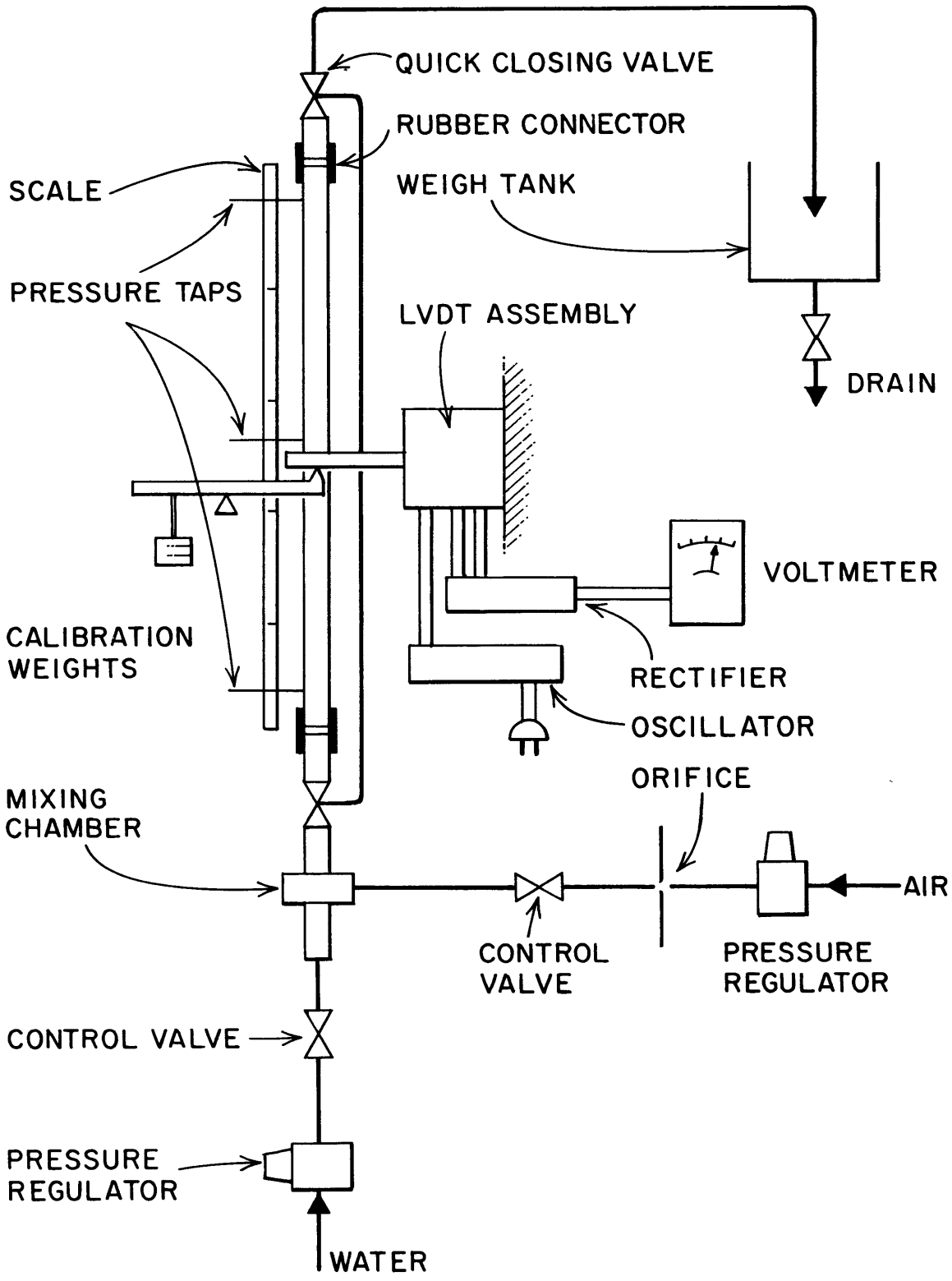

FIGURE 5 SCHEMATIC DIAGRAM OF VERTICAL TUBE APPARATUS

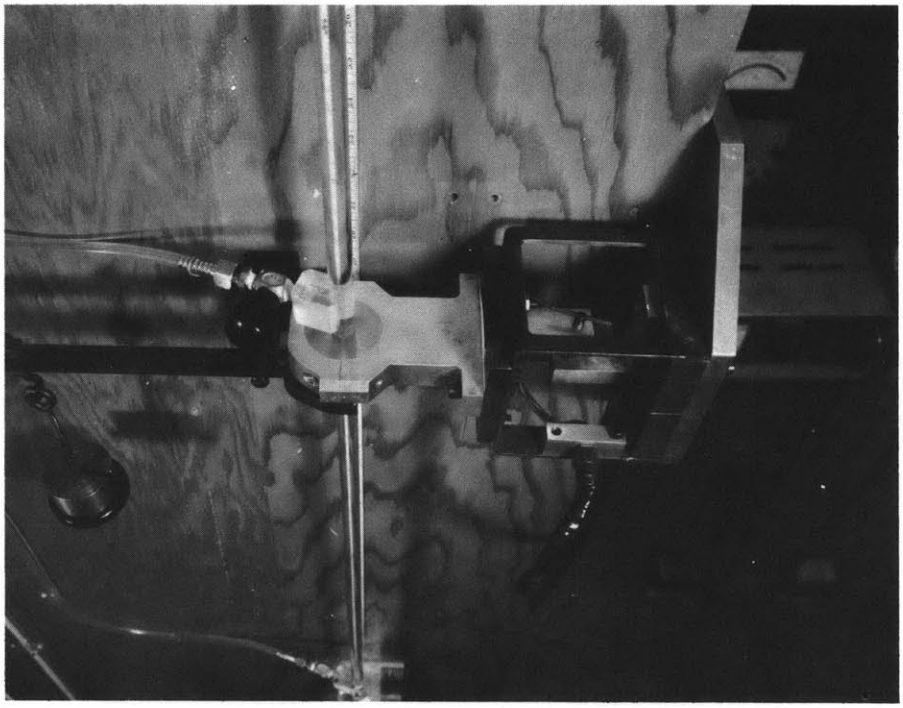

FIGURE 6 TOP VIEW OF LVDT APPARATUS

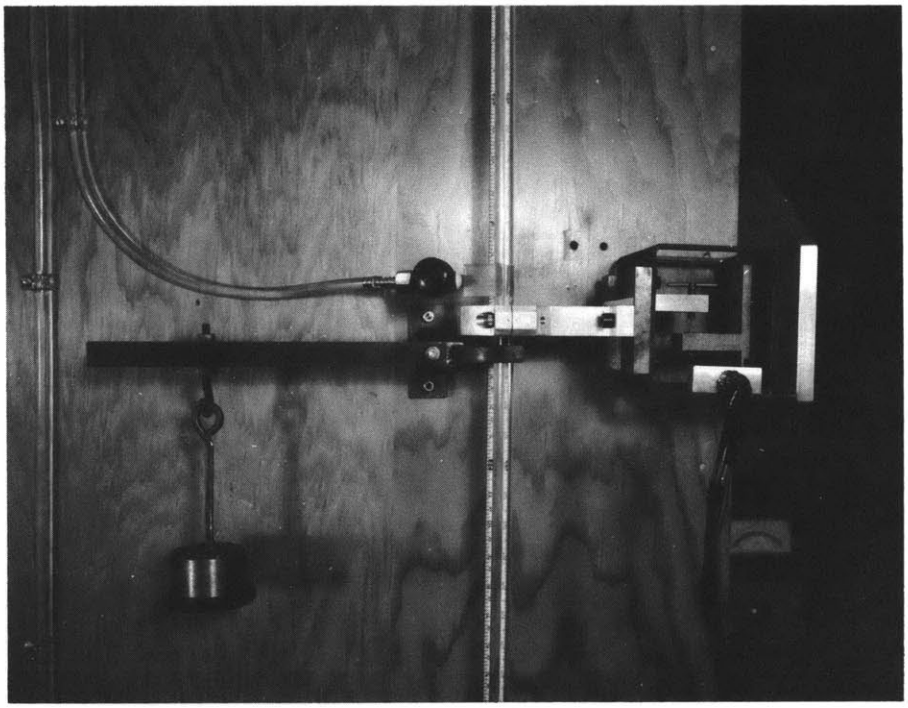

FIGURE 7 SIDE VIEW OF LVDT APPARATUS

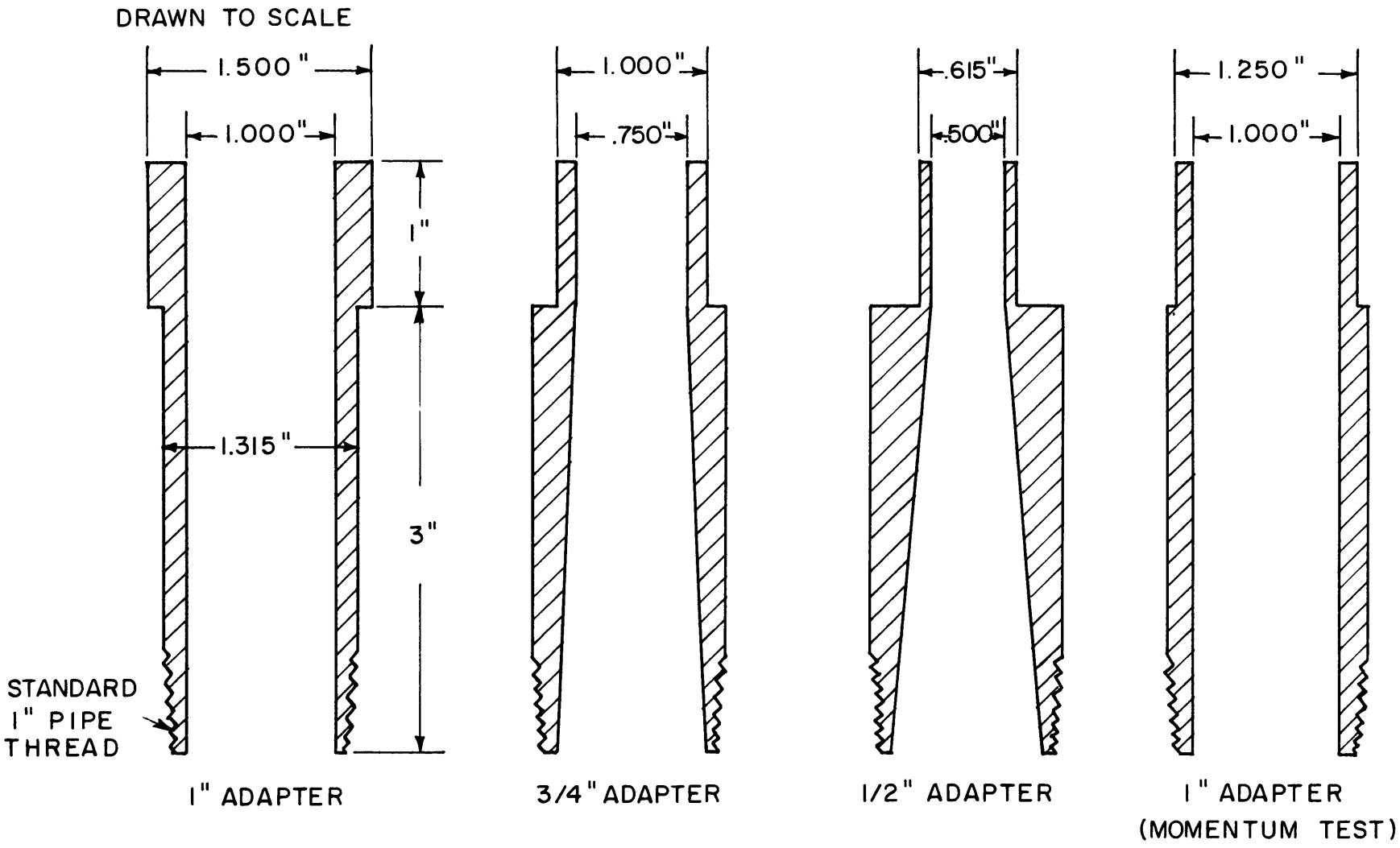

FIGURE 8 CROSS-SECTIONAL VIEW OF VALVE-TUBE ADAPTERS

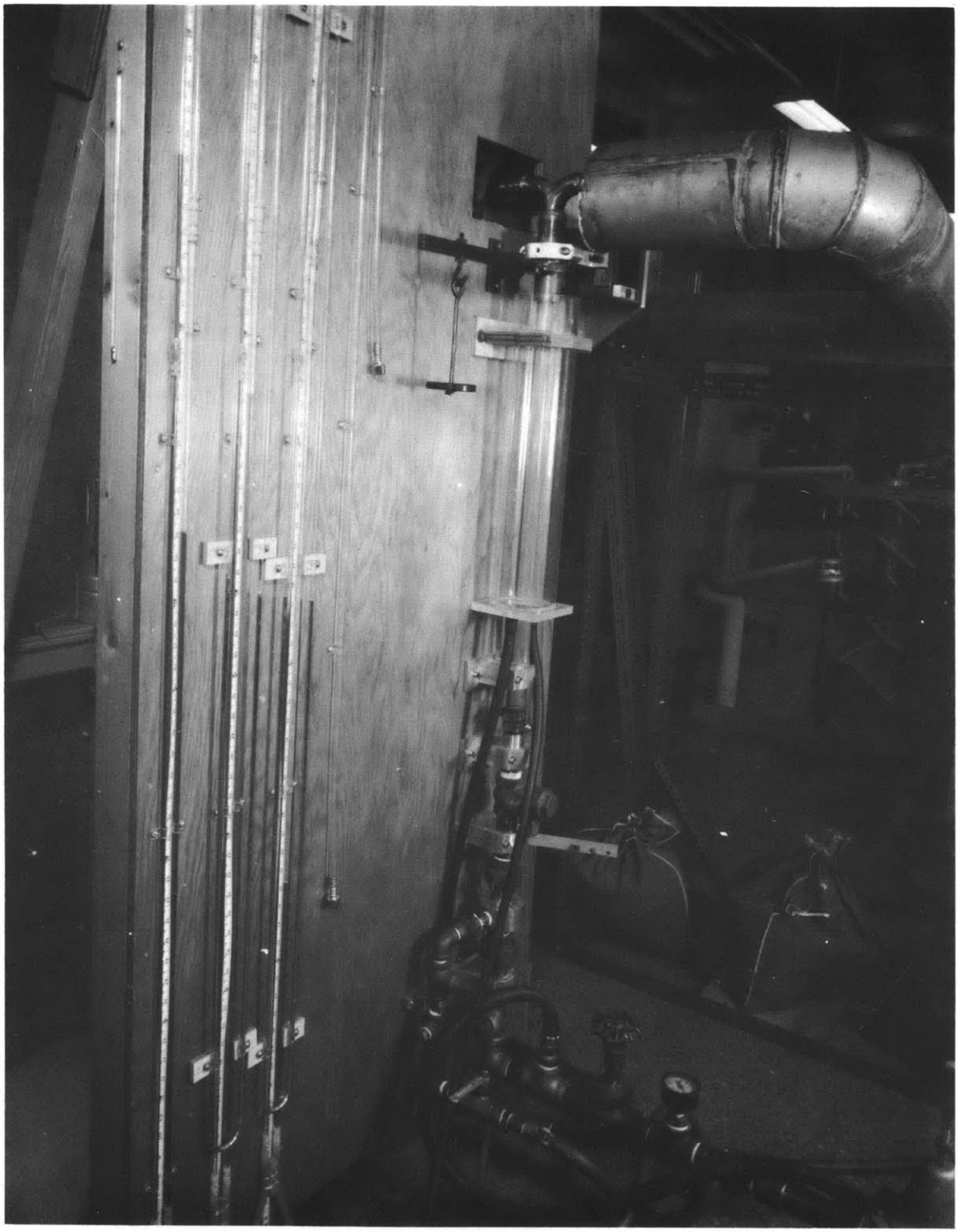

FIGURE 9 PHOTOGRAPH OF MOMENTUM MEASURING APPARATUS

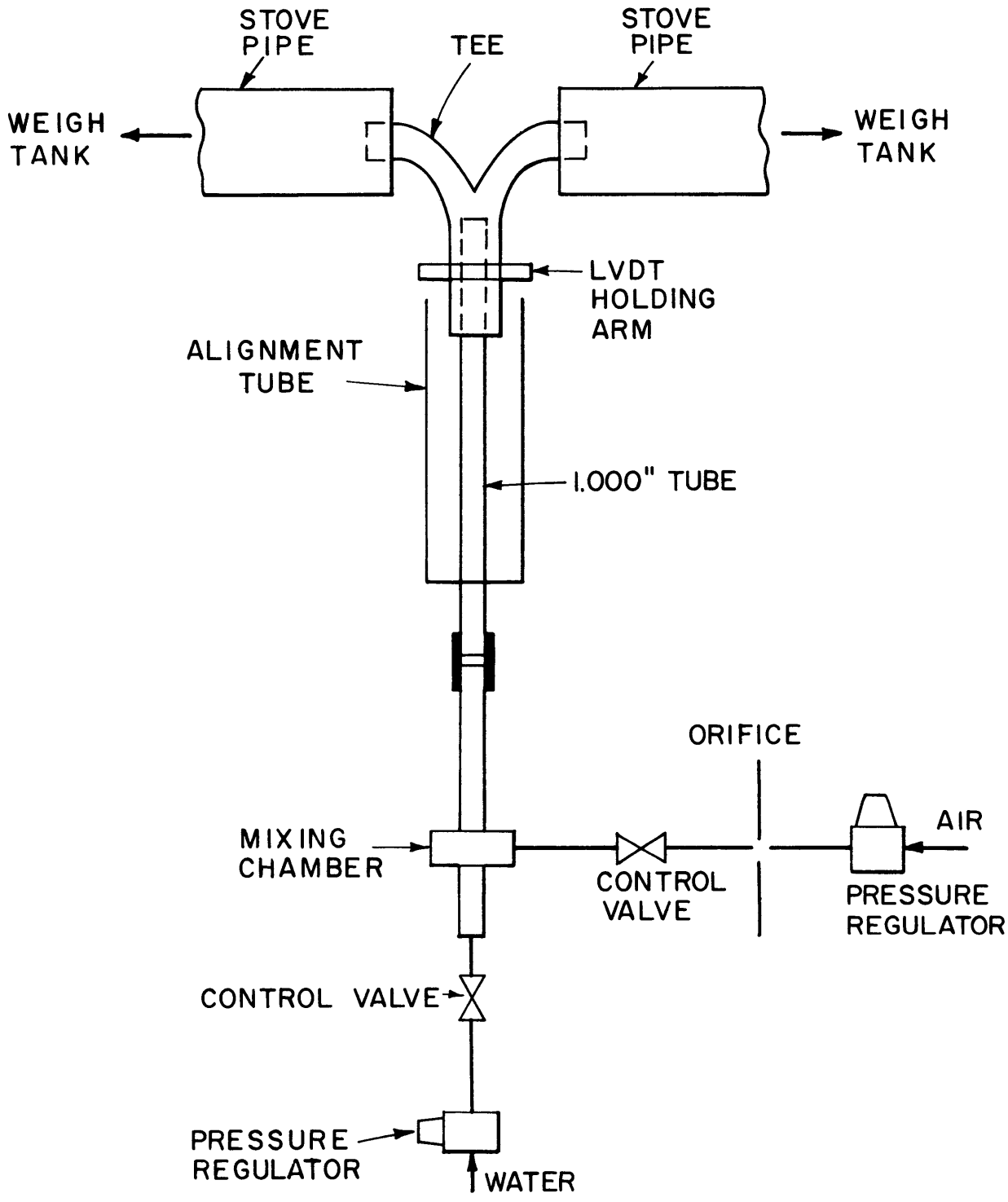

FIGURE 10 SCHEMATIC DIAGRAM OF MOMENTUM MEASURING APPARATUS

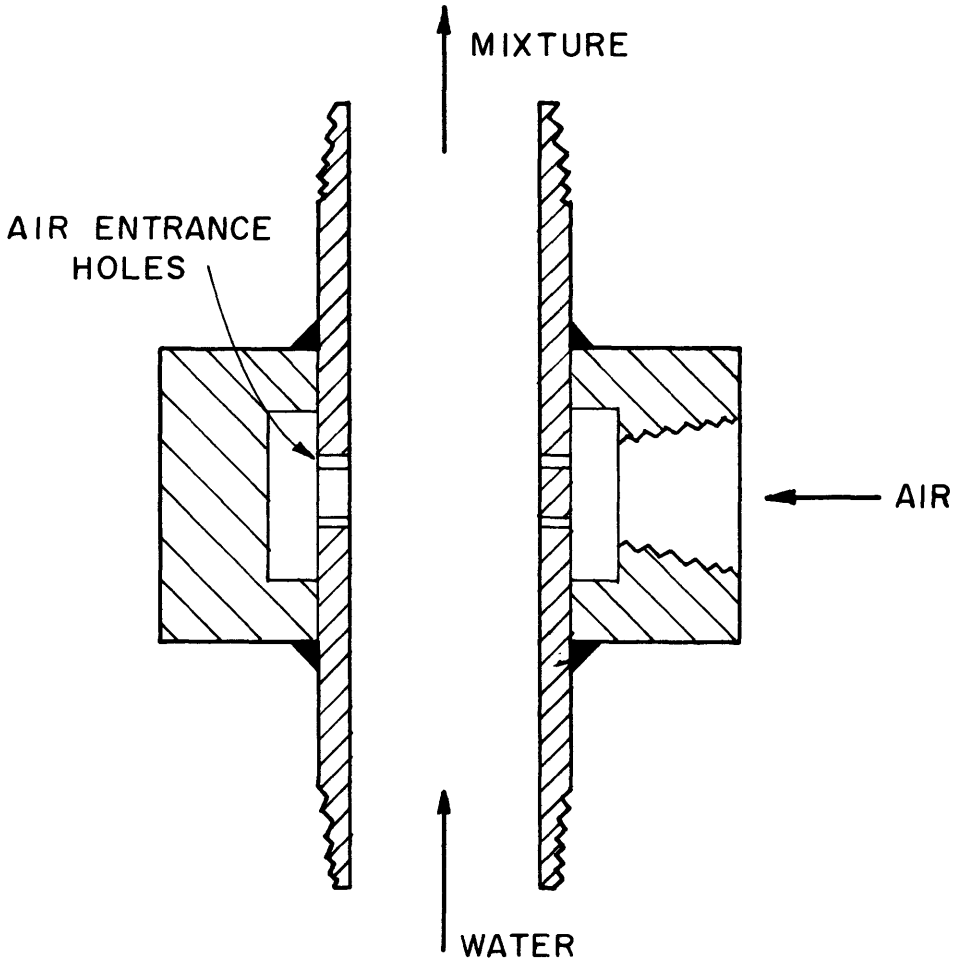

FIGURE II CROSS-SECTIONAL VIEW OF MIXING CHAMBER

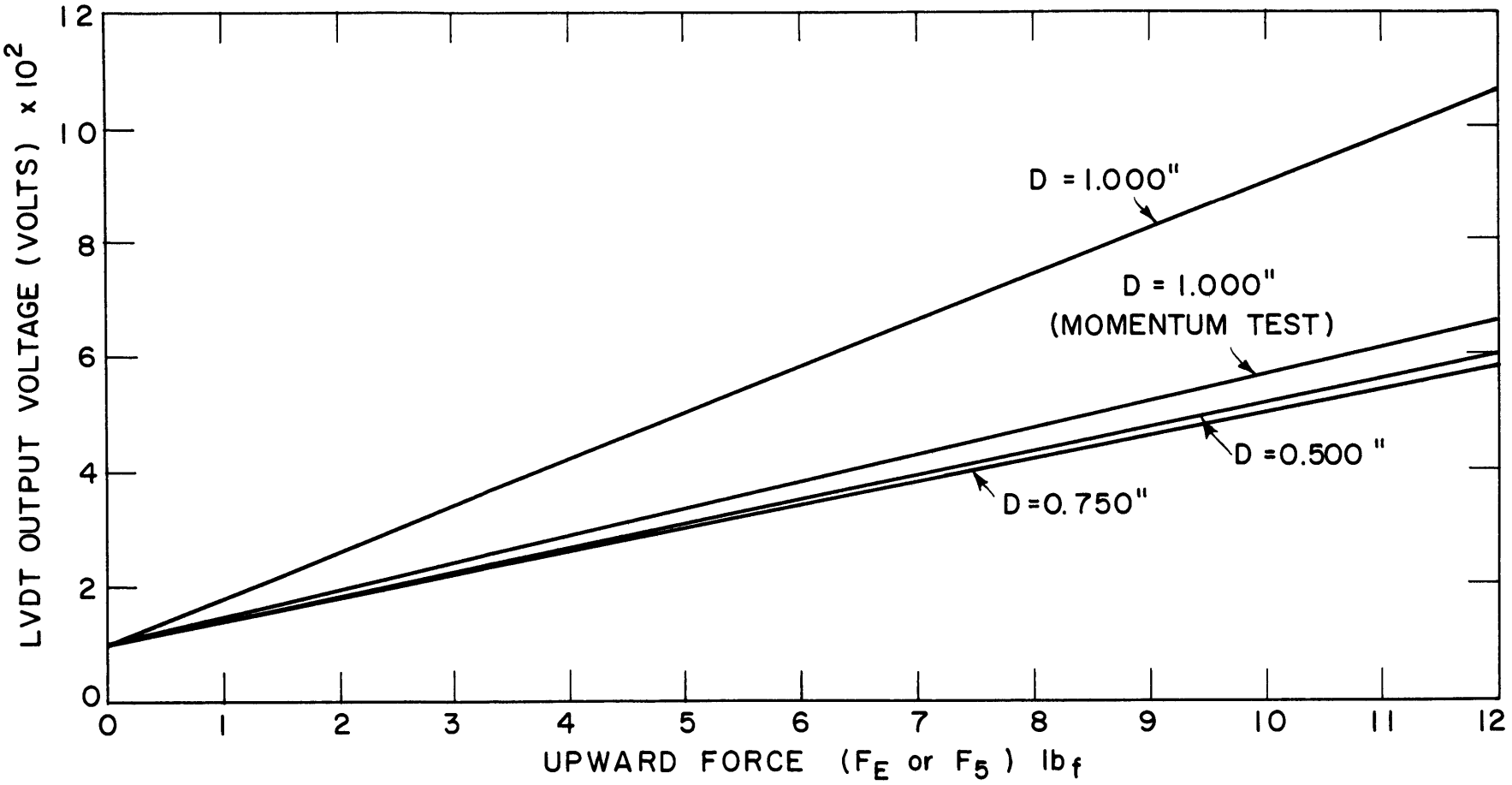

FIGURE 12 LVDT CALIBRATION PLOTS

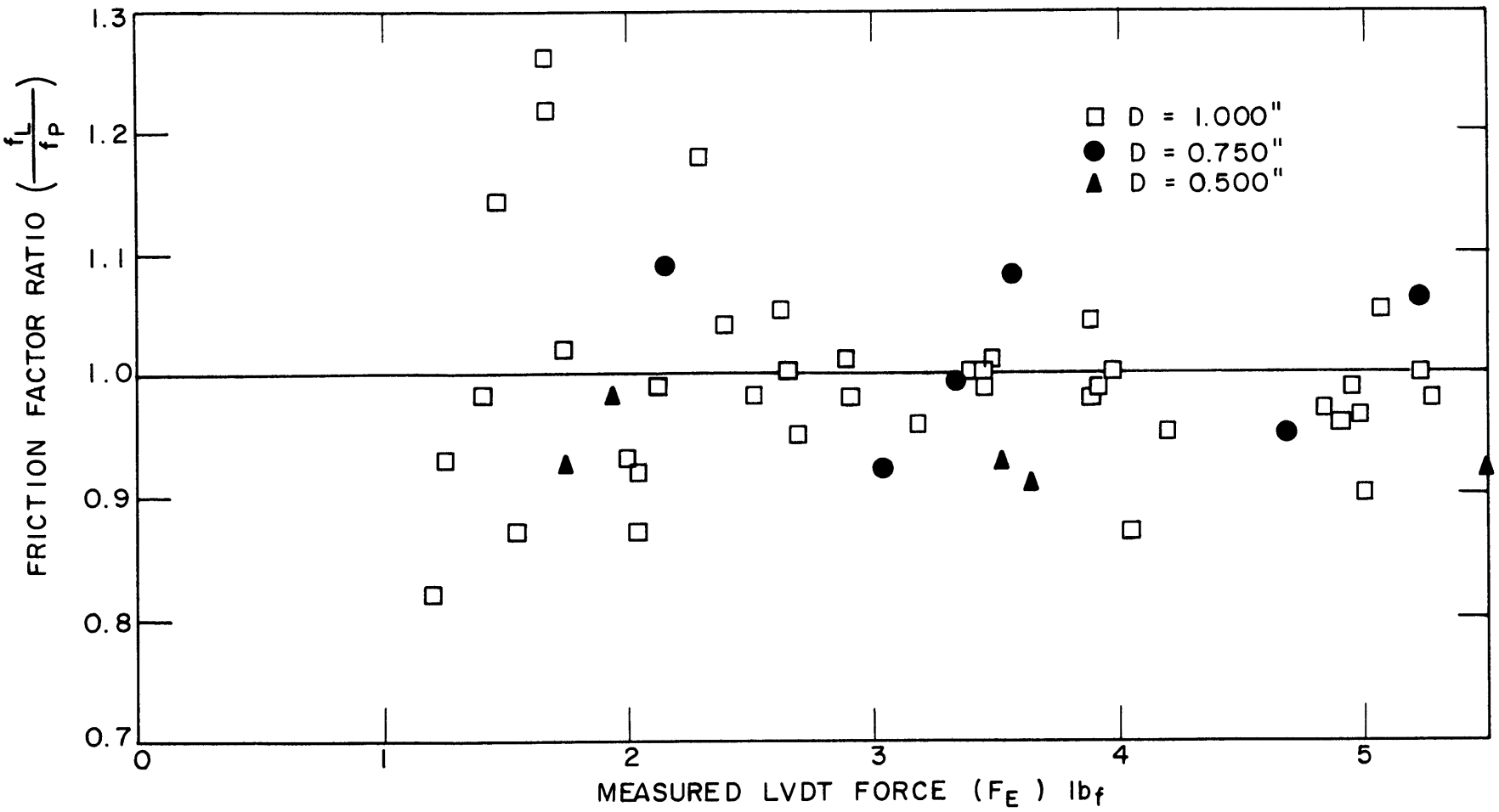

FIGURE 13 COMPARISON OF SINGLE-PHASE FRICTION FACTORS

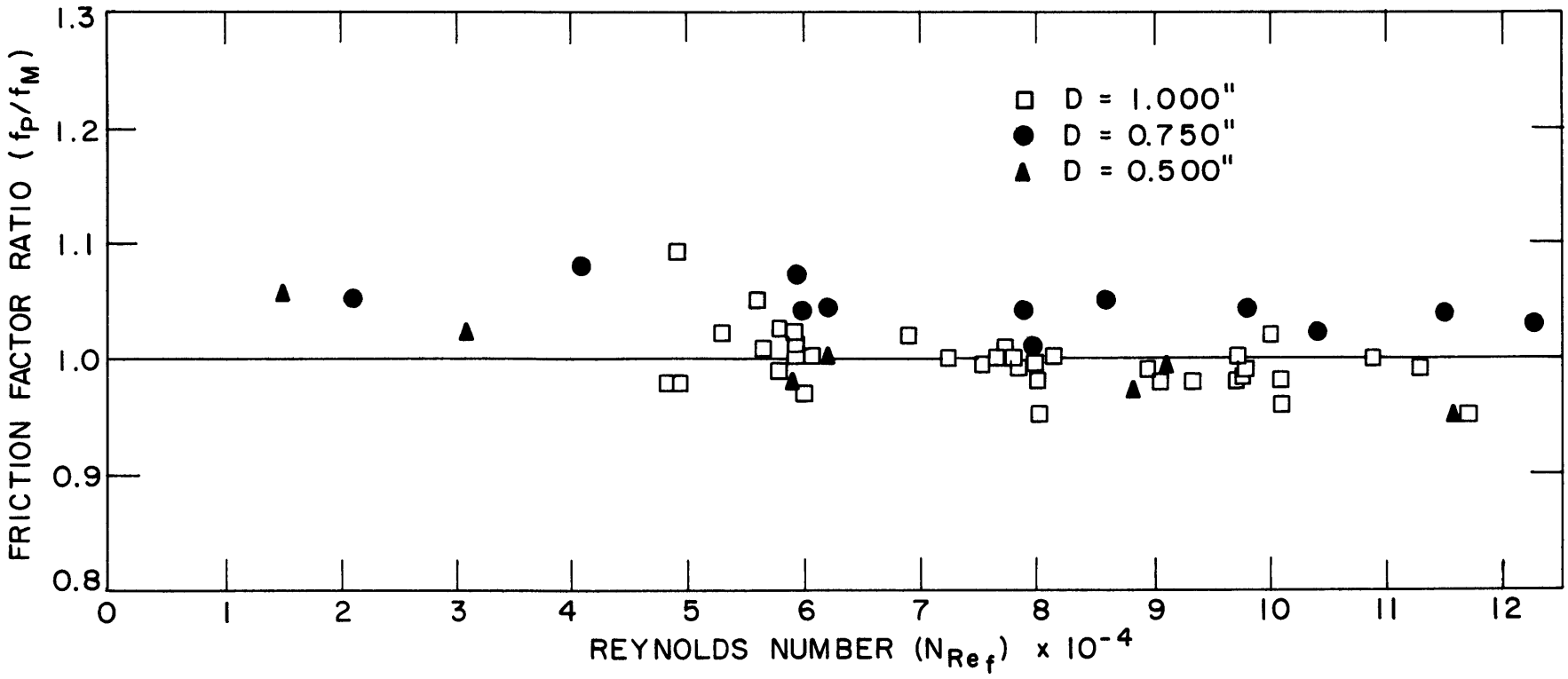

FIGURE 14 COMPARISON OF SINGLE-PHASE FRICTION FACTORS

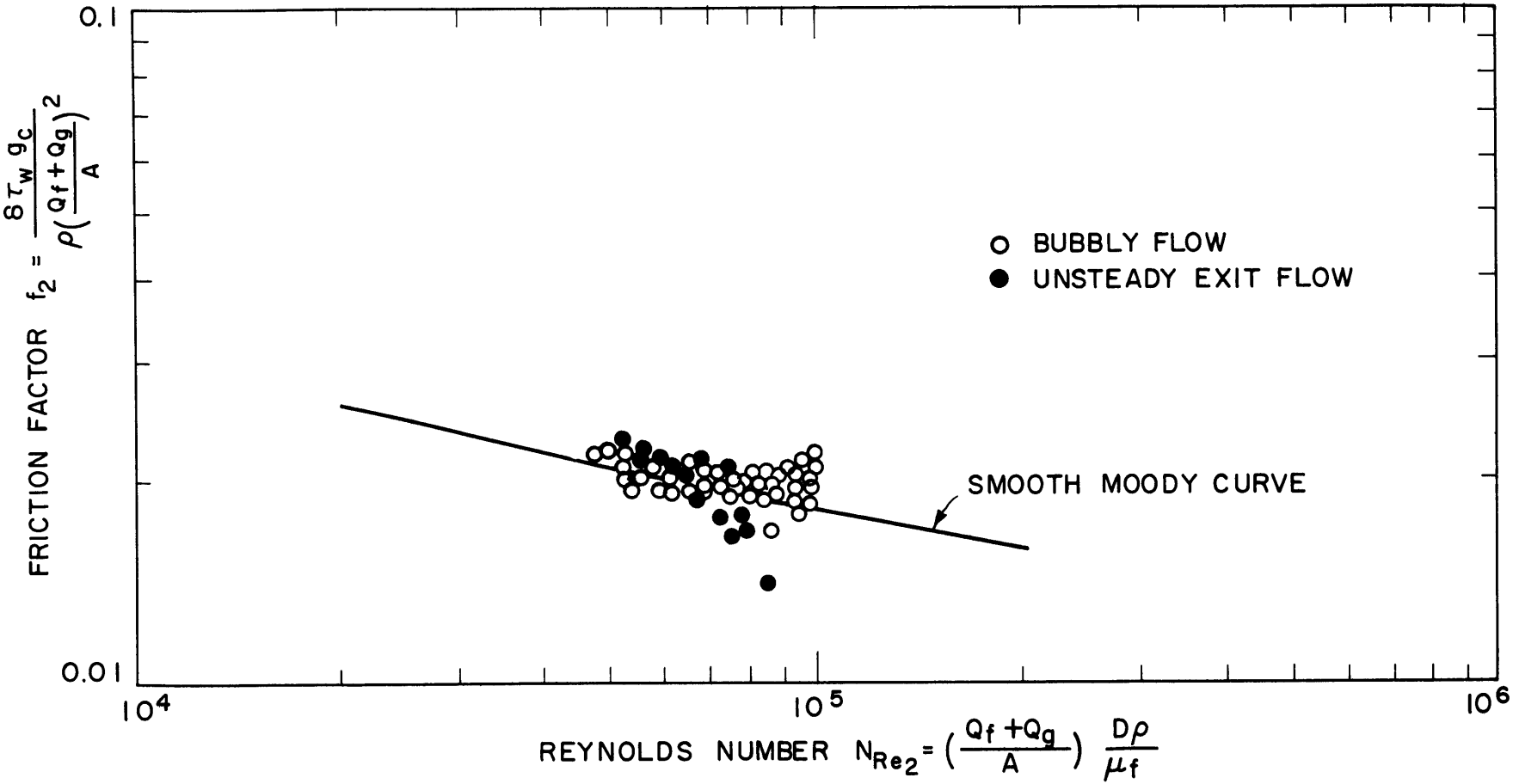

FIGURE 15 FRICTION FACTOR CORRELATION FOR 1.000" TUBE WITH NO. 3 MIXING CHAMBER

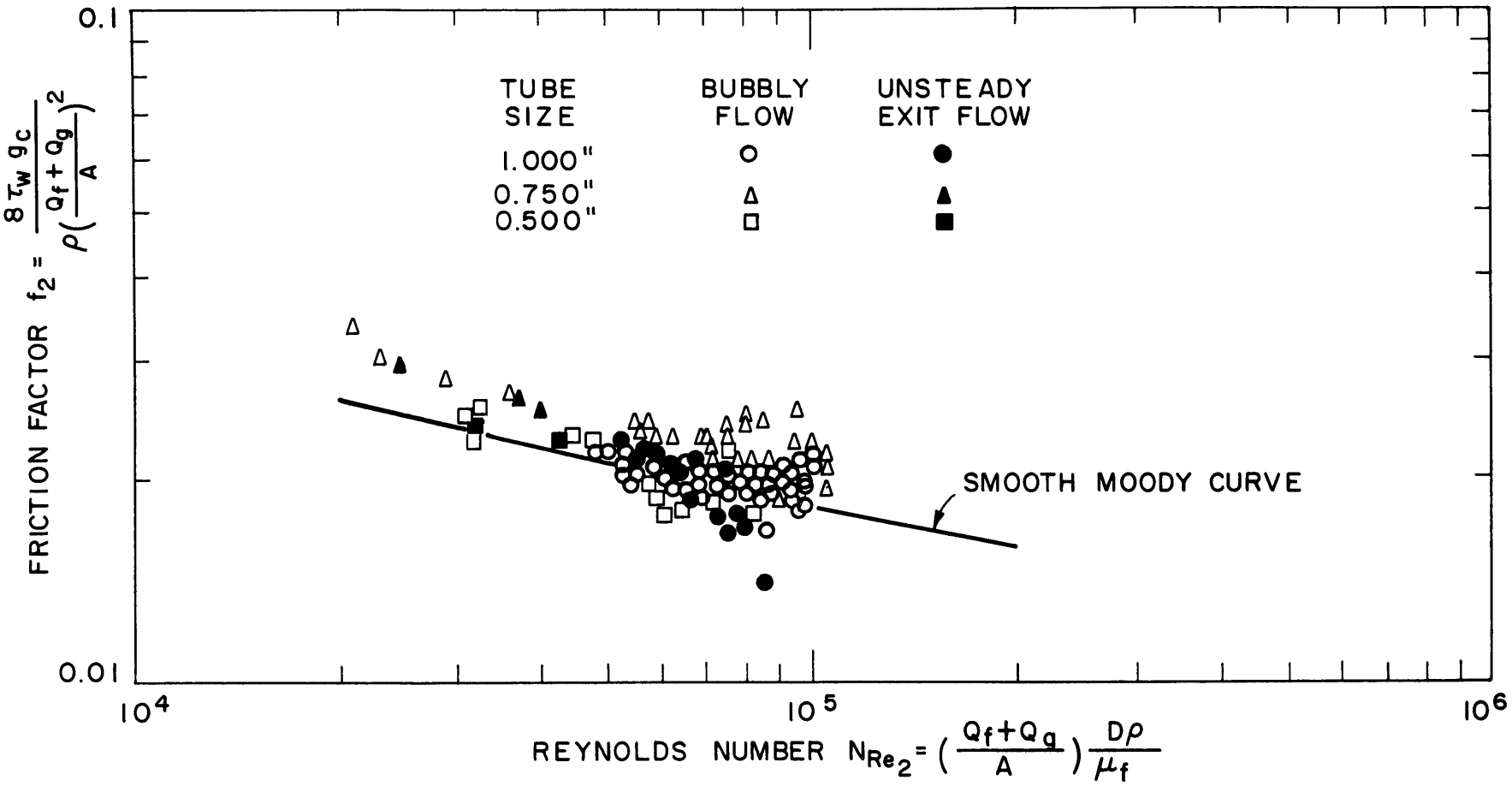

FIGURE 16 FRICTION FACTOR CORRELATION FOR ALL DATA POINTS WITH NO. 3 MIXING CHAMBER

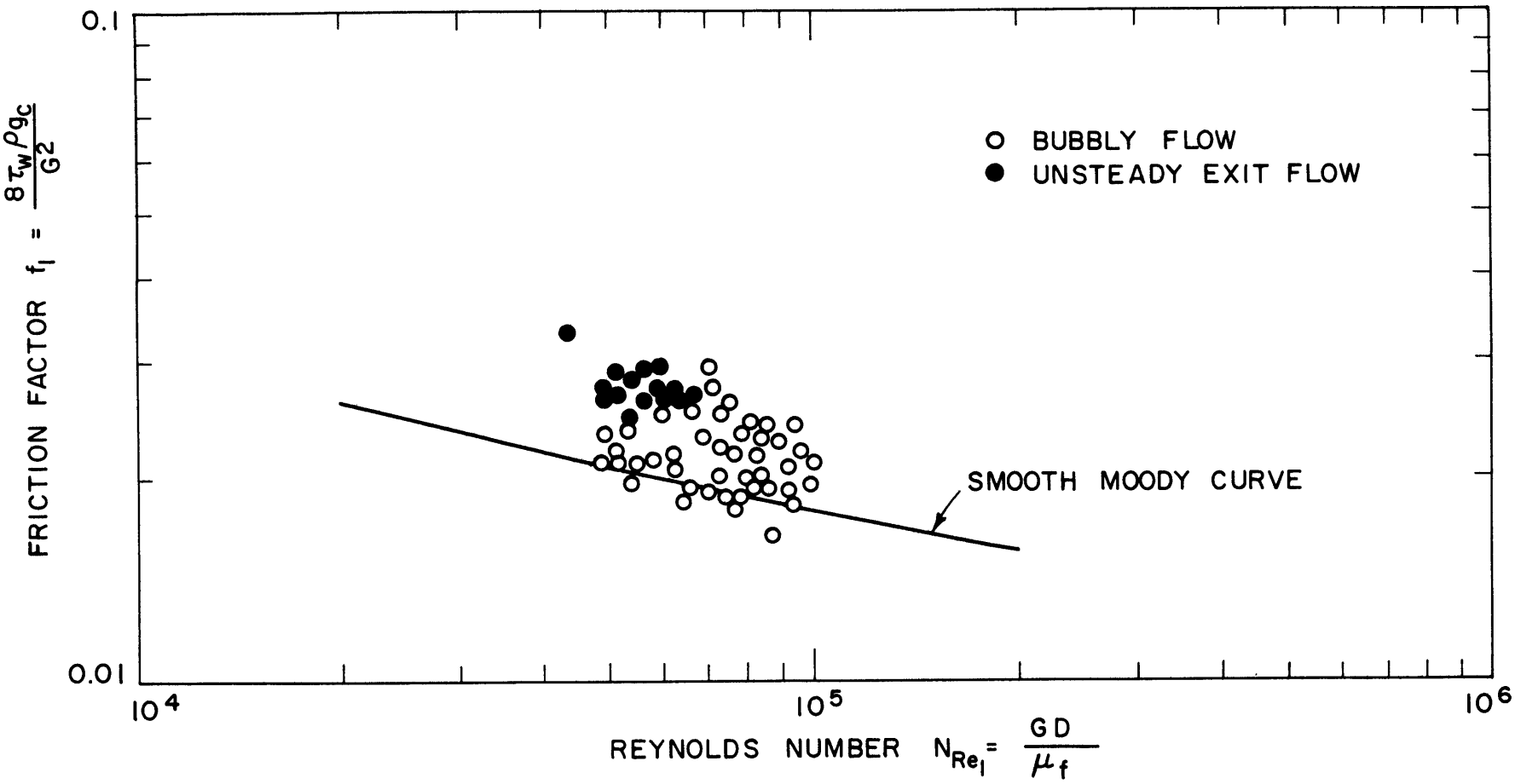

FIGURE 17 FRICTION FACTOR CORRELATION FOR 1.000" TUBE WITH NO. 3 MIXING CHAMBER

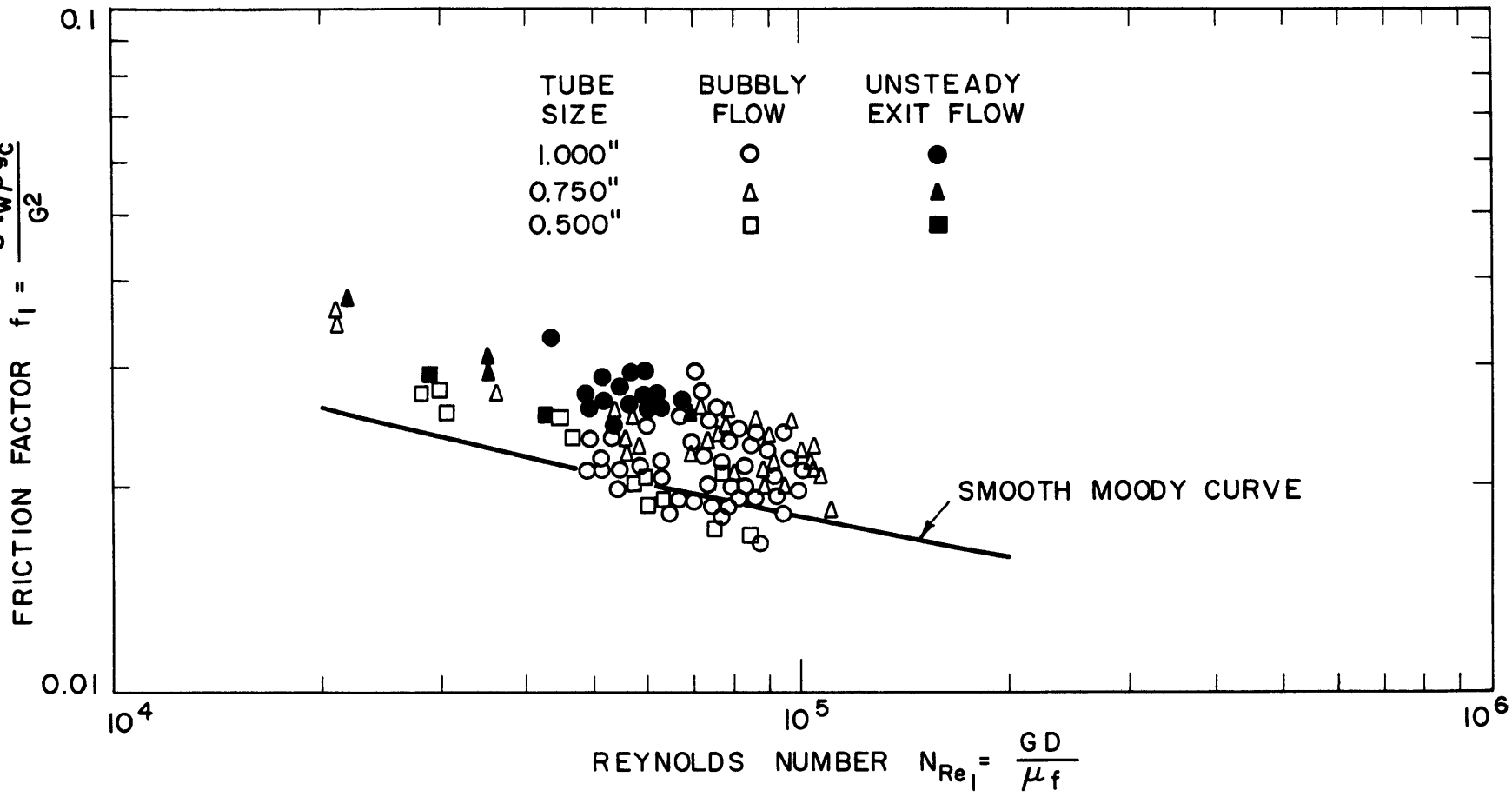

FIGURE 18 FRICTION FACTOR CORRELATION FOR ALL DATA POINTS WITH NO. 3 MIXING CHAMBER

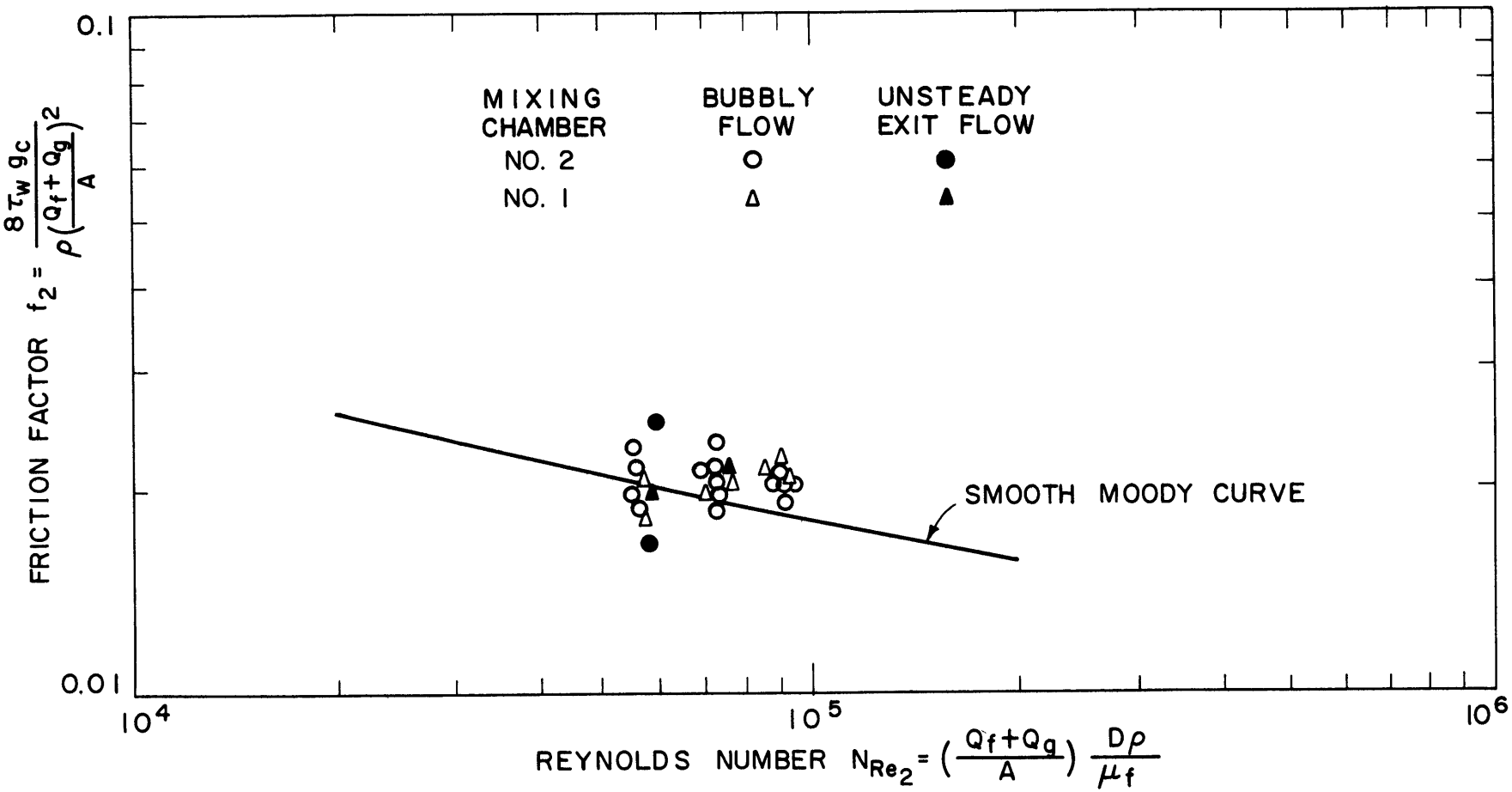

FIGURE 19 FRICTION FACTOR CORRELATION FOR 1.000" TUBE WITH DIFFERENT MIXING CHAMBERS

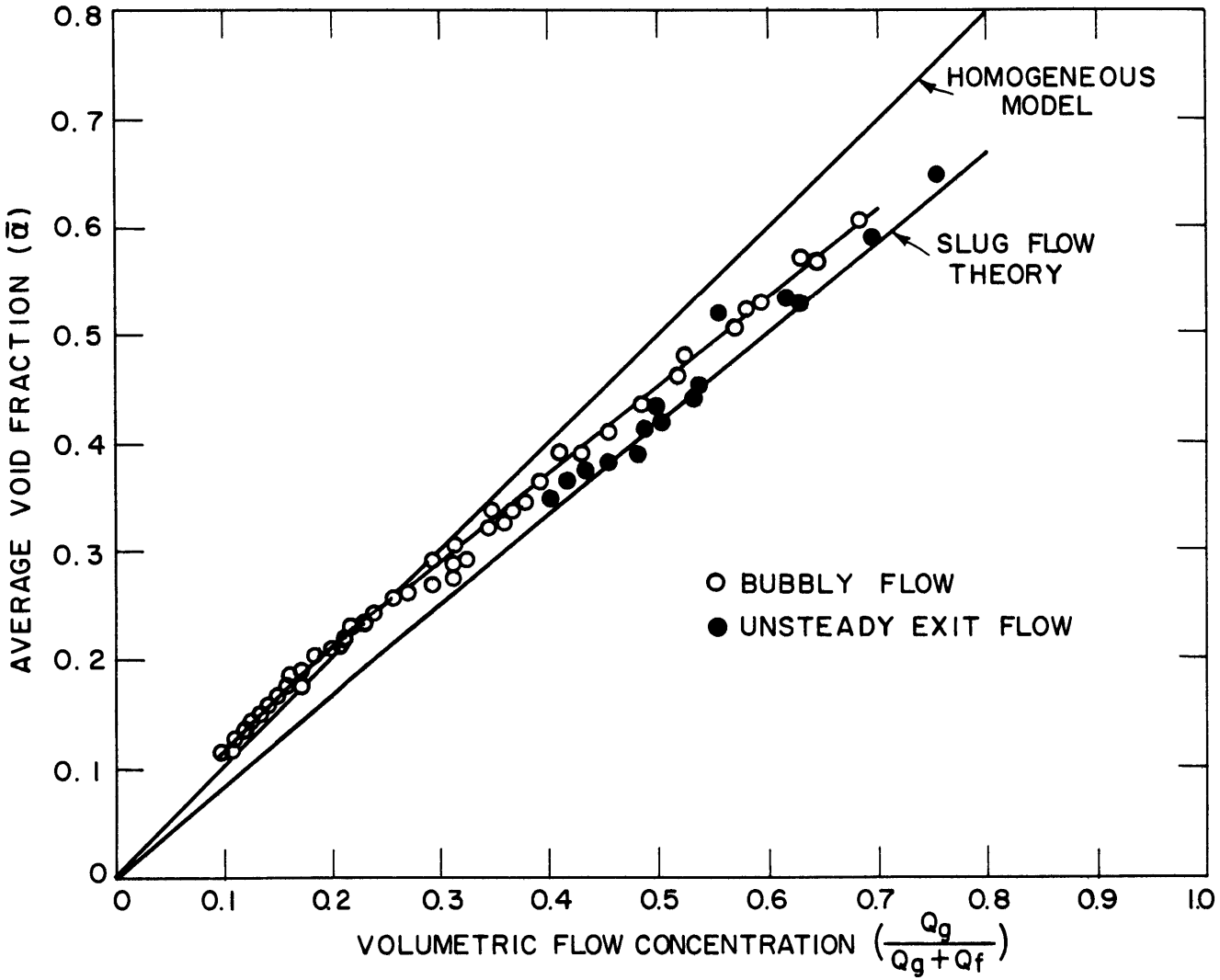

FIGURE 20 VOID FRACTION CORRELATION FOR 1.000" TUBE WITH NO. 3 MIXING CHAMBER

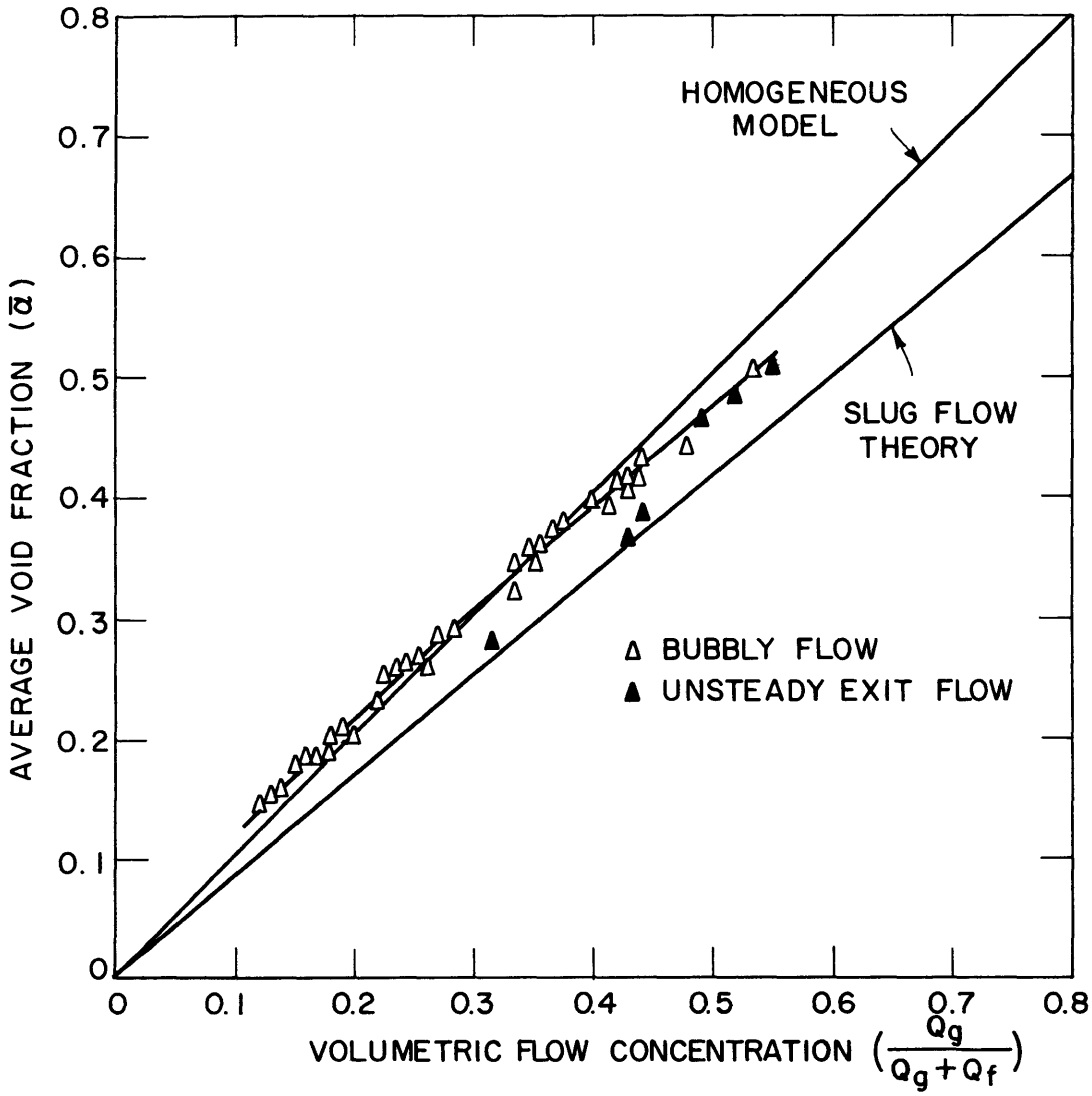

FIGURE 21 VOID FRACTION CORRELATION FOR 0.750" TUBE WITH NO. 3 MIXING CHAMBER

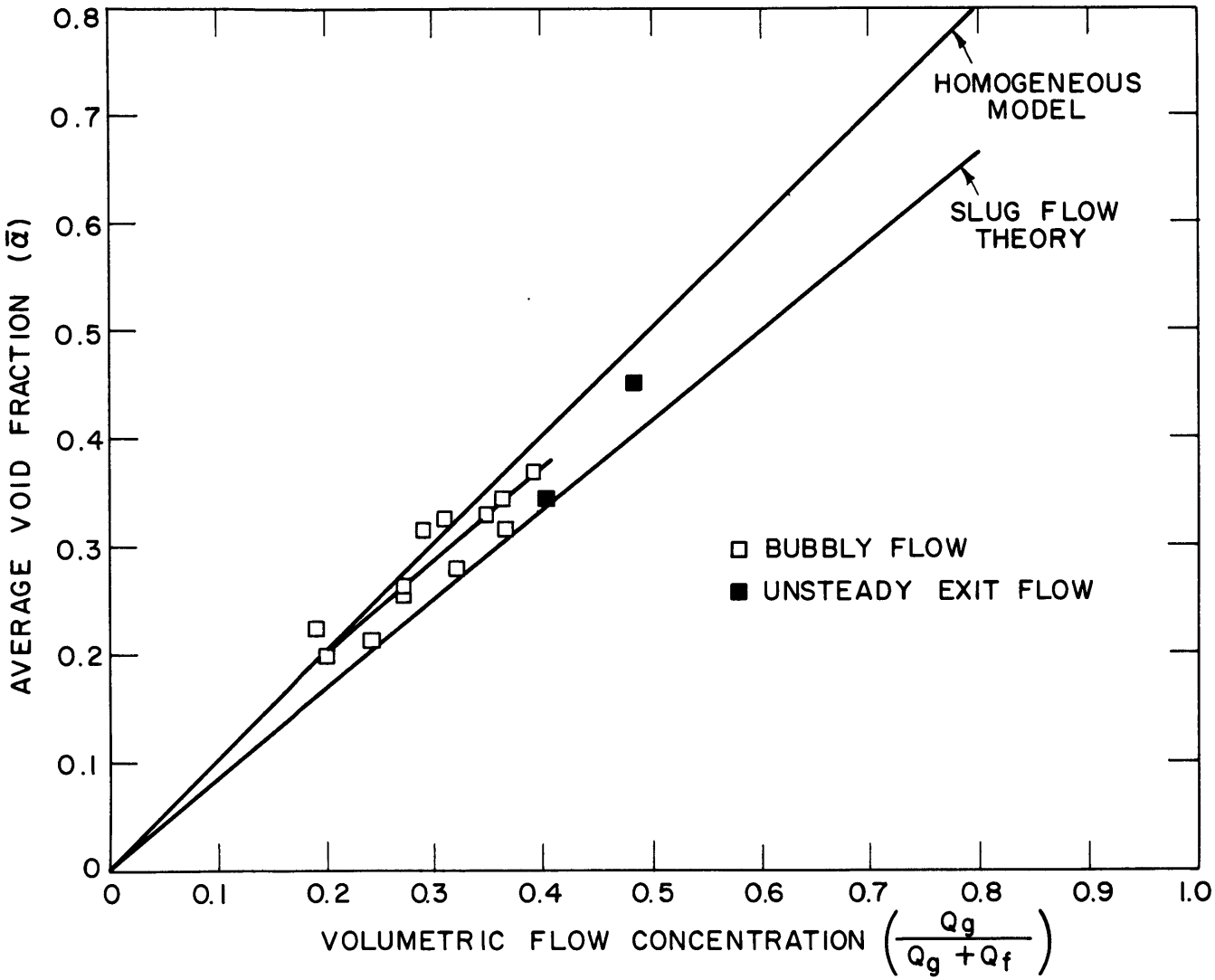

FIGURE 22 VOID FRACTION CORRELATION FOR 0.500" TUBE WITH NO. 3 MIXING CHAMBER

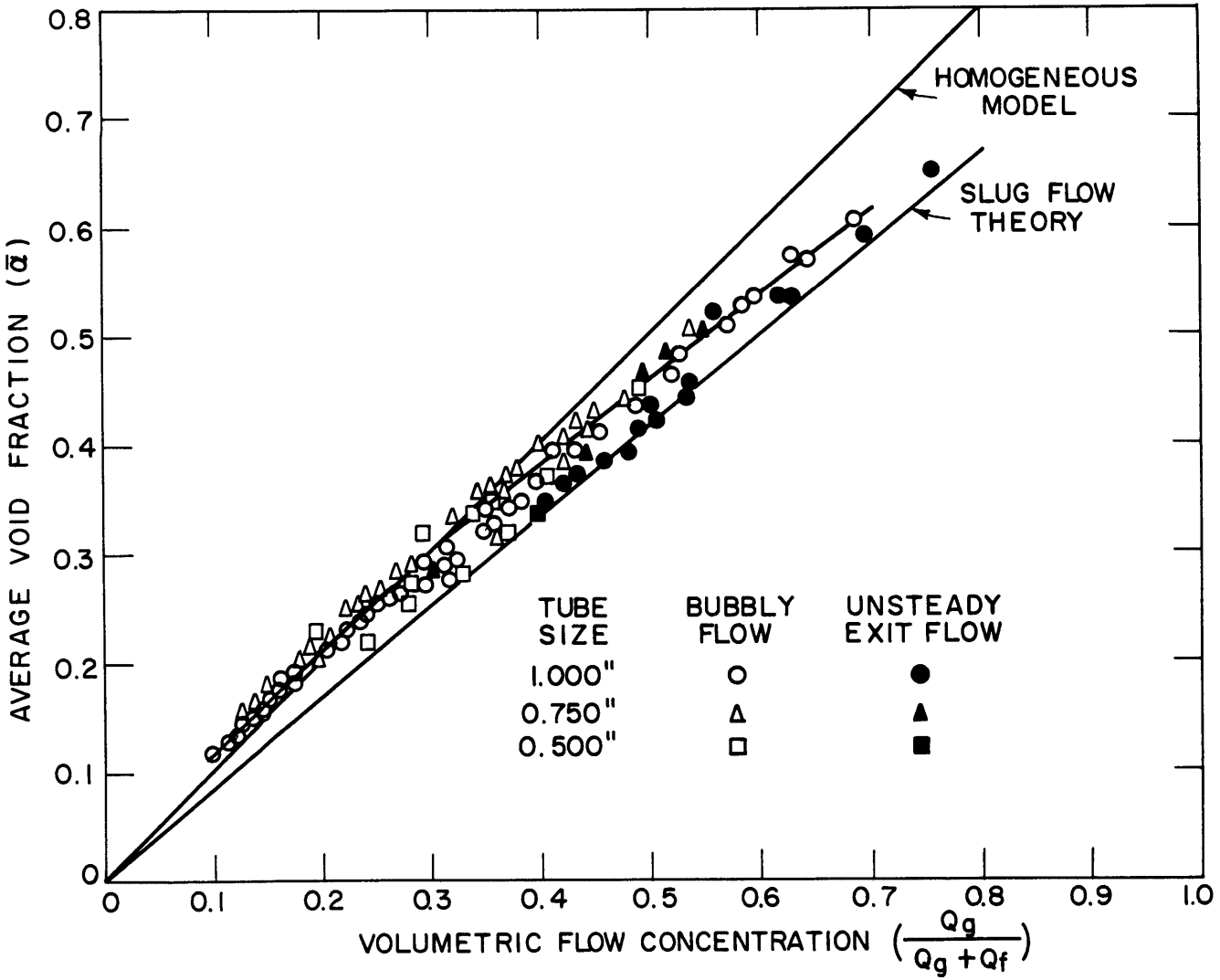

FIGURE 23 VOID FRACTION CORRELATION FOR ALL DATA POINTS WITH NO 3 MIXING CHAMBER

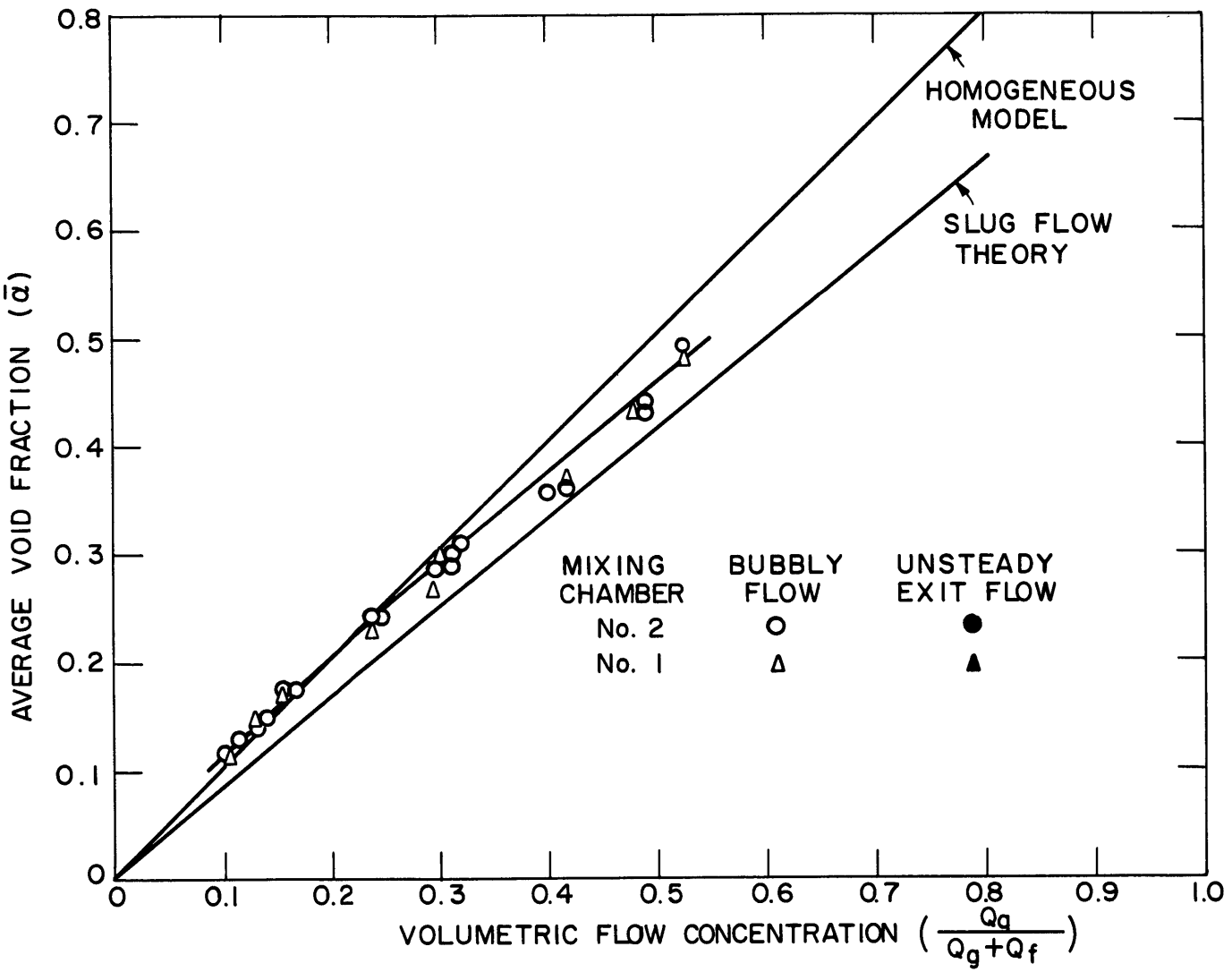

FIGURE 24 VOID FRACTION CORRELATION FOR 1.000" TUBE WITH DIFFERENT MIXING CHAMBERS

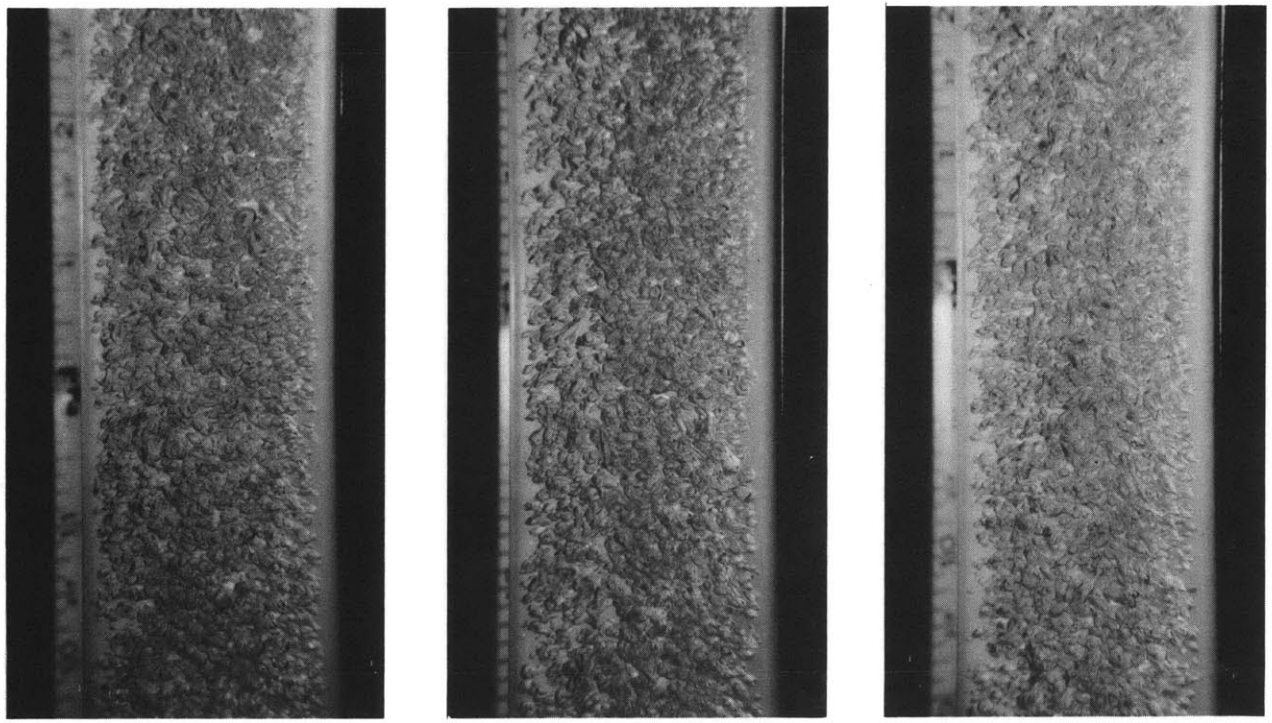

$\alpha = 0.17$

$\bar{V}_g = 12.6$ ft/sec

$\bar{V}_f = 14.2$ ft/sec

$\left(\overline{\frac{V_g}{V_f}}\right) = 0.89$

TEST 102-1 TEST 102-2 TEST 102-3

FIGURE 25 PHOTOGRAPHS OF BUBBLY FLOW PATTERN

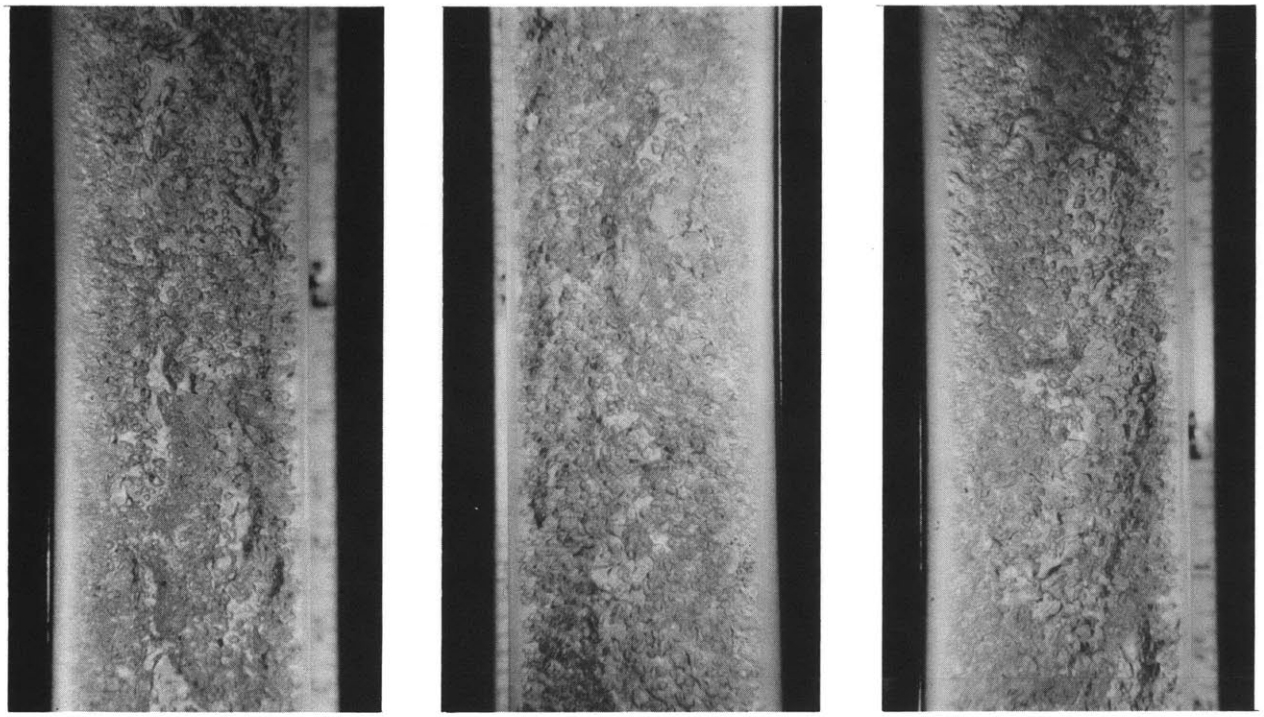

$\alpha = 0.37$

$\bar{V}_g = 21.0$ ft/sec

$\bar{V}_f = 17.1$ ft/sec

$\overline{\left(\frac{V_g}{V_f}\right)} = 1.23$

TEST 104-1 TEST 104-2 TEST 104-3

FIGURE 26 PHOTOGRAPHS OF UNSTEADY FLOW PATTERN

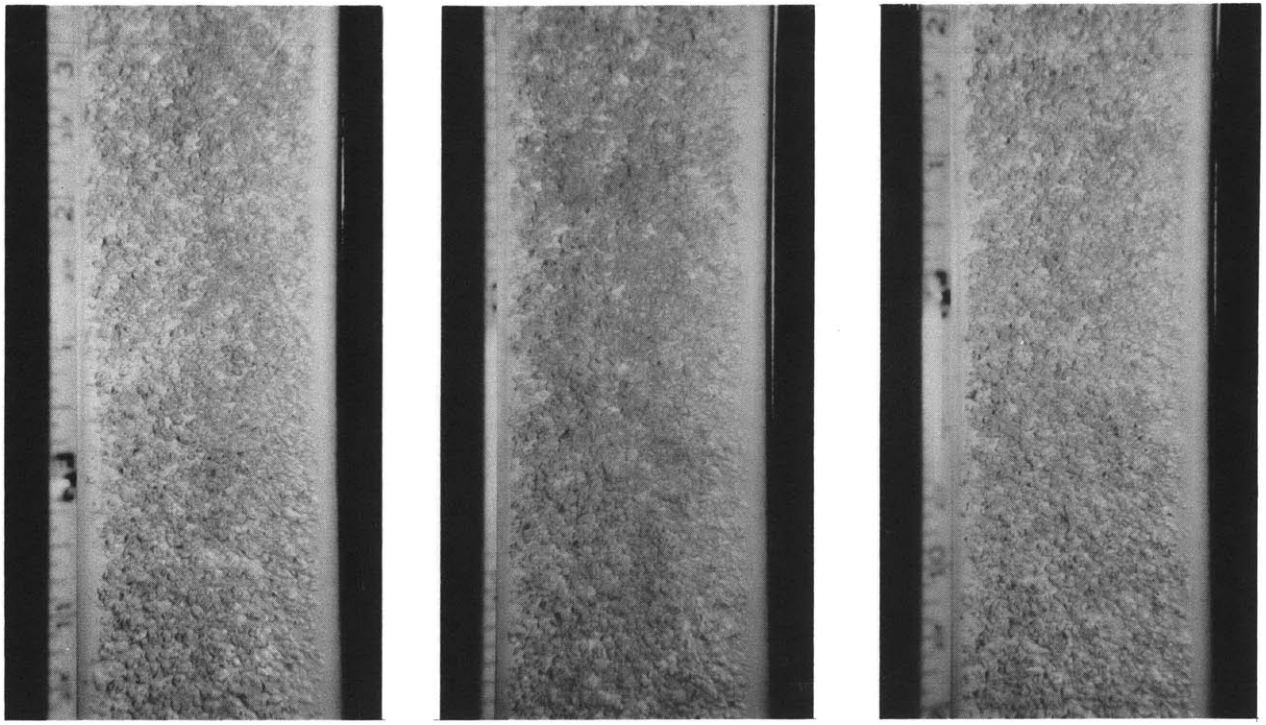

α = 0.11

$\bar{V}_g$ = 19.0 ft/sec

$\bar{V}_f$ = 21.7 ft/sec

$\left(\frac{\overline{V_g}}{V_f}\right)$ = 0.88

TEST 136-1 TEST 136-2 TEST 136-3

FIGURE 27 PHOTOGRAPHS OF BUBBLY FLOW PATTERN

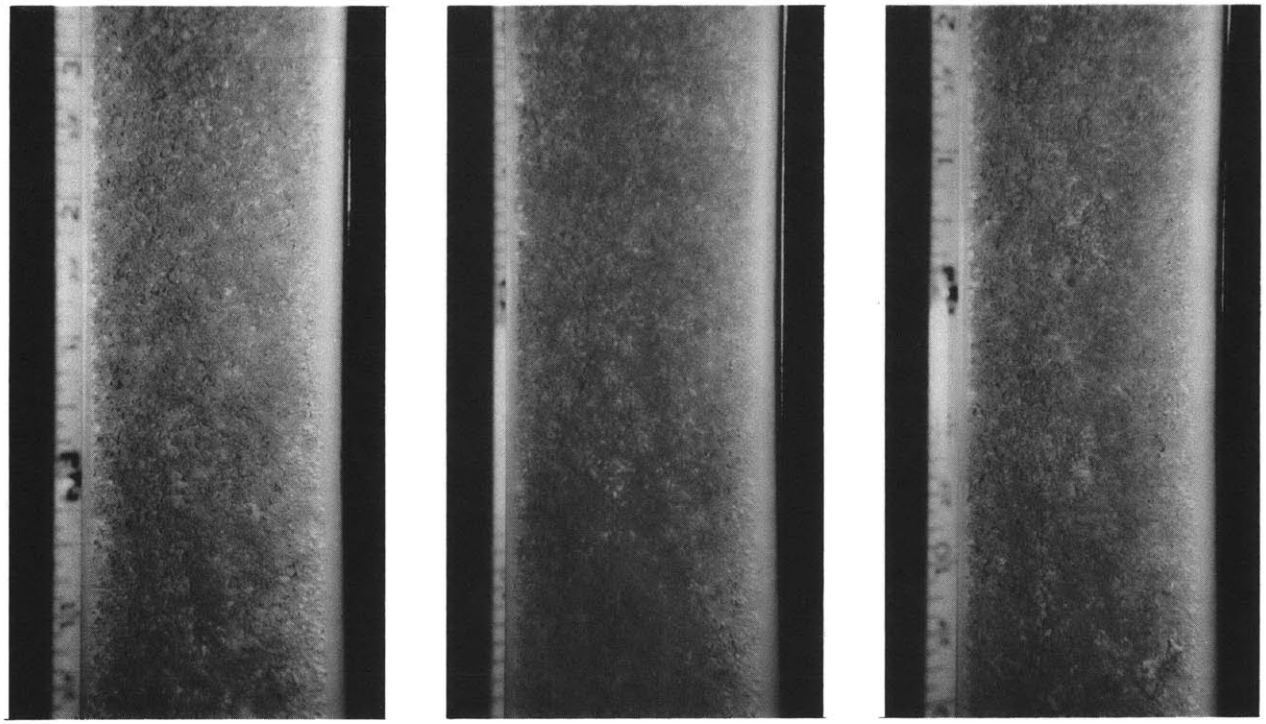

$\alpha = 0.30$

$\overline{V_g} = 27.8$ ft/sec

$\overline{V_f} = 26.7$ ft/sec

$\overline{\left(\frac{V_g}{V_f}\right)} = 1.04$

TEST 138-1 TEST 138-2 TEST 138-3

FIGURE 28 PHOTOGRAPHS OF BUBBLY FLOW PATTERN

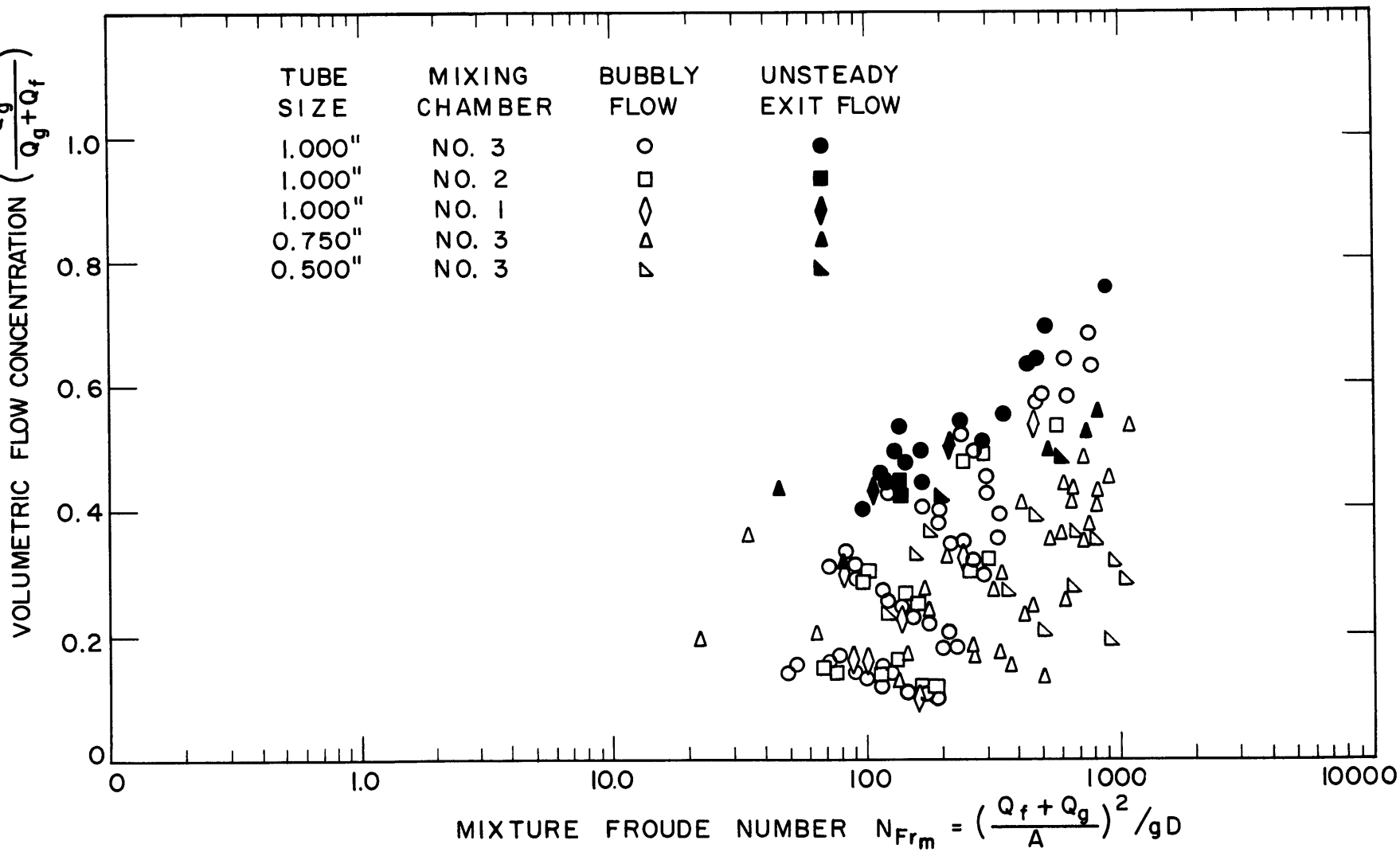

FIGURE 29 FLOW REGIME MAP FOR VERTICAL TUBE DATA

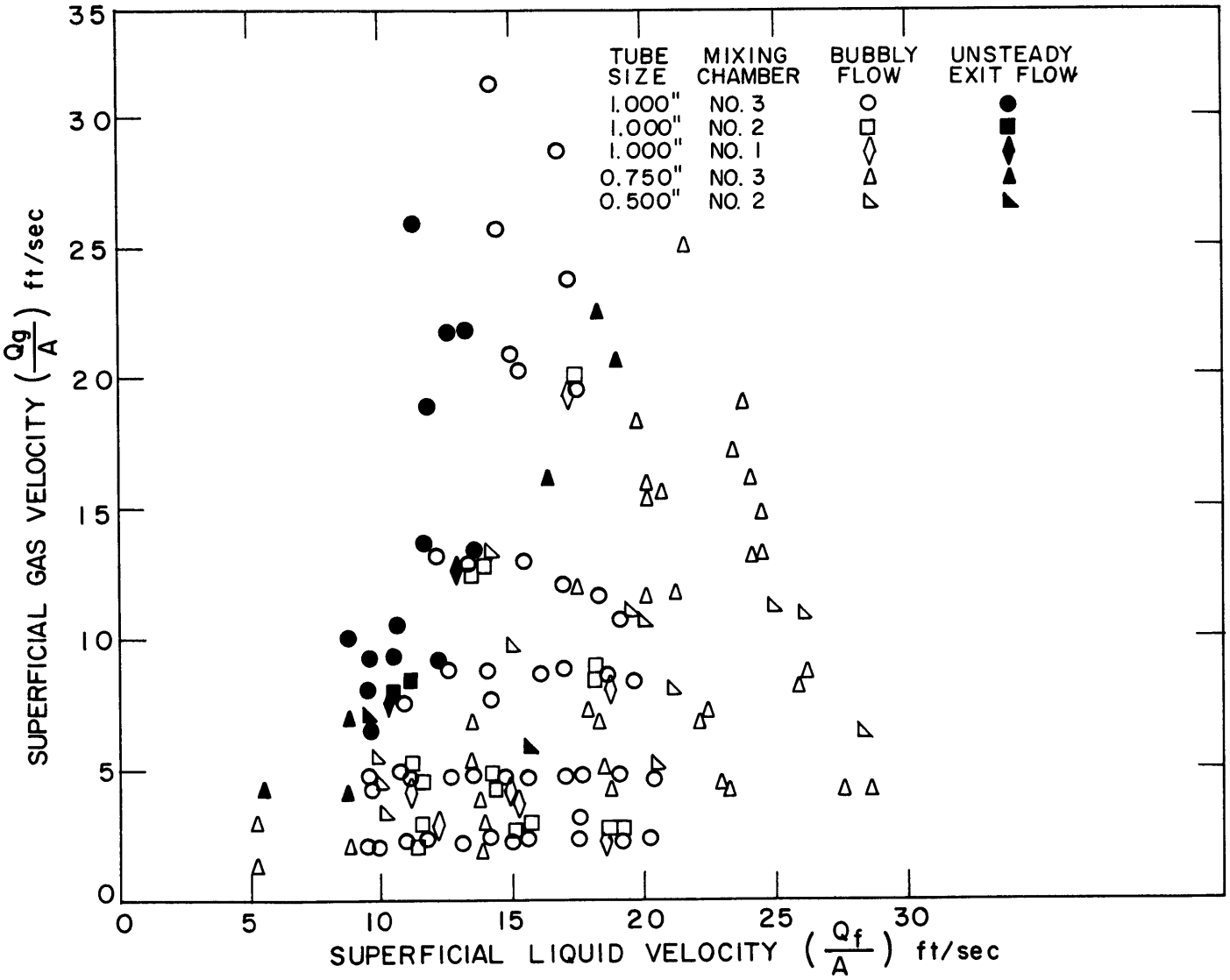

FIGURE 30 FLOW REGIME MAP FOR VERTICAL TUBE DATA

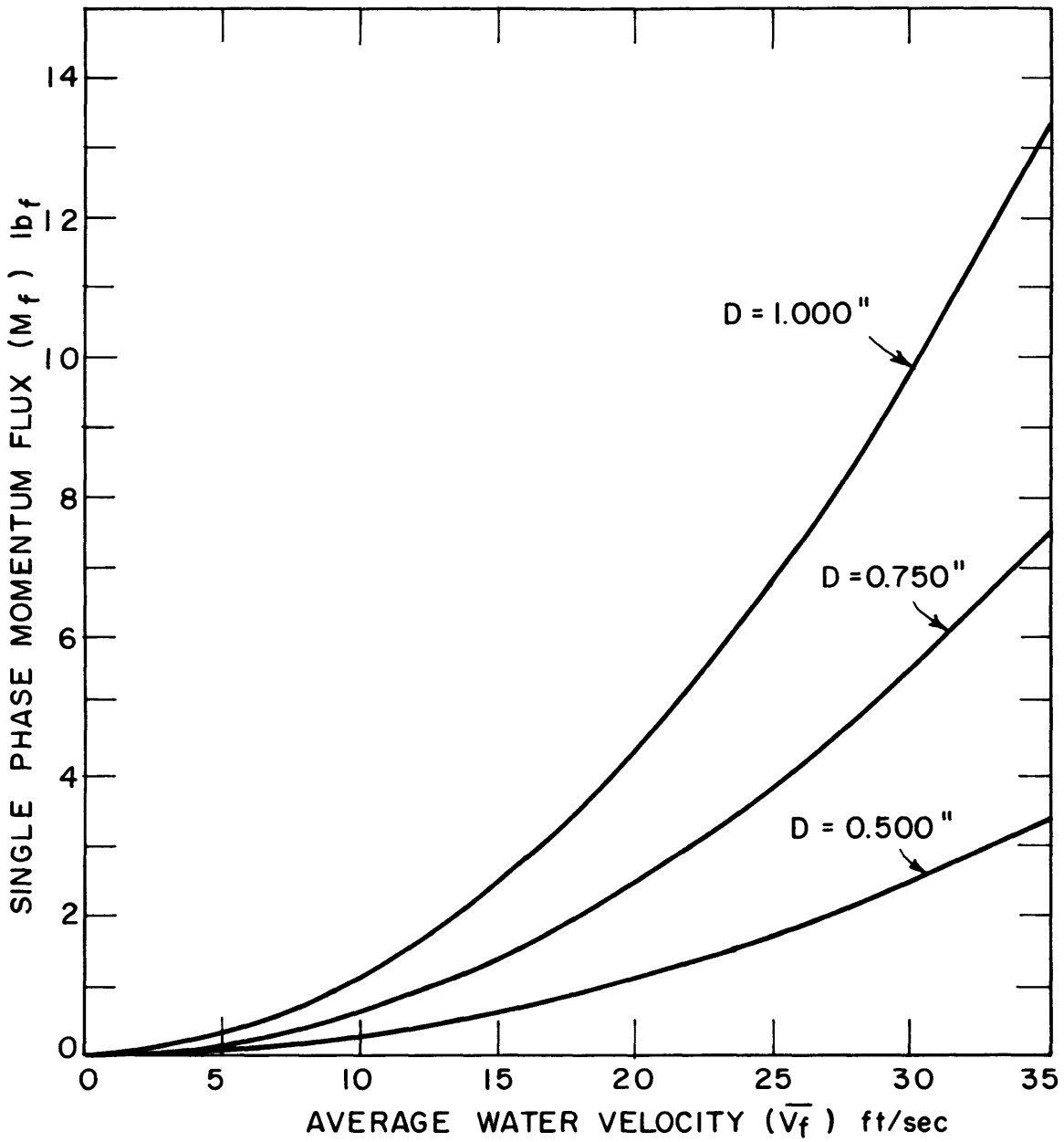

FIGURE 31 SINGLE PHASE MOMENTUM FLUX

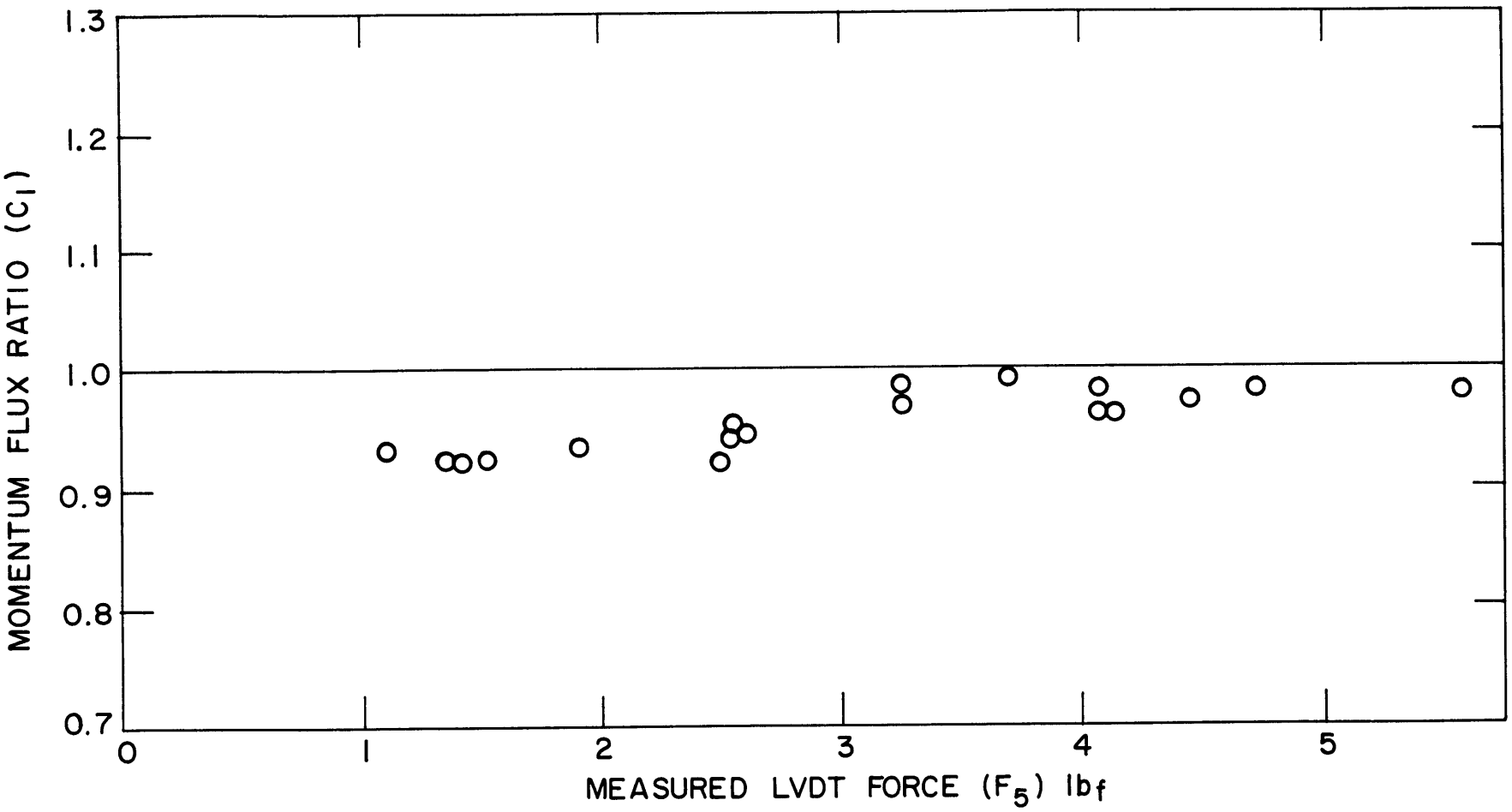

FIGURE 32 COMPARISON OF SINGLE PHASE PREDICTED AND MEASURED MOMENTUM FLUX

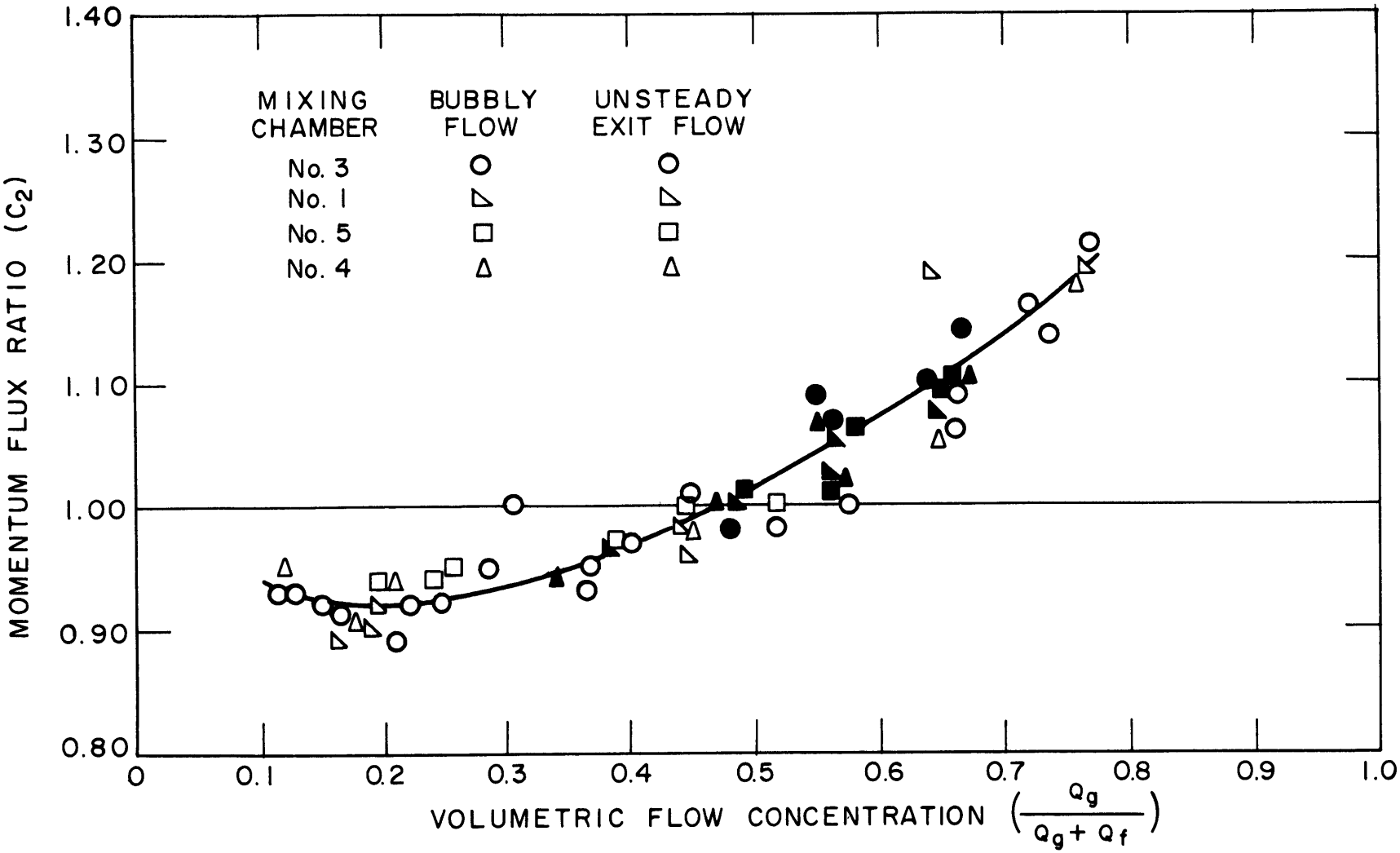

FIGURE 33 COMPARISON OF HOMOGENEOUS MODEL AND MEASURED MOMENTUM FLUX

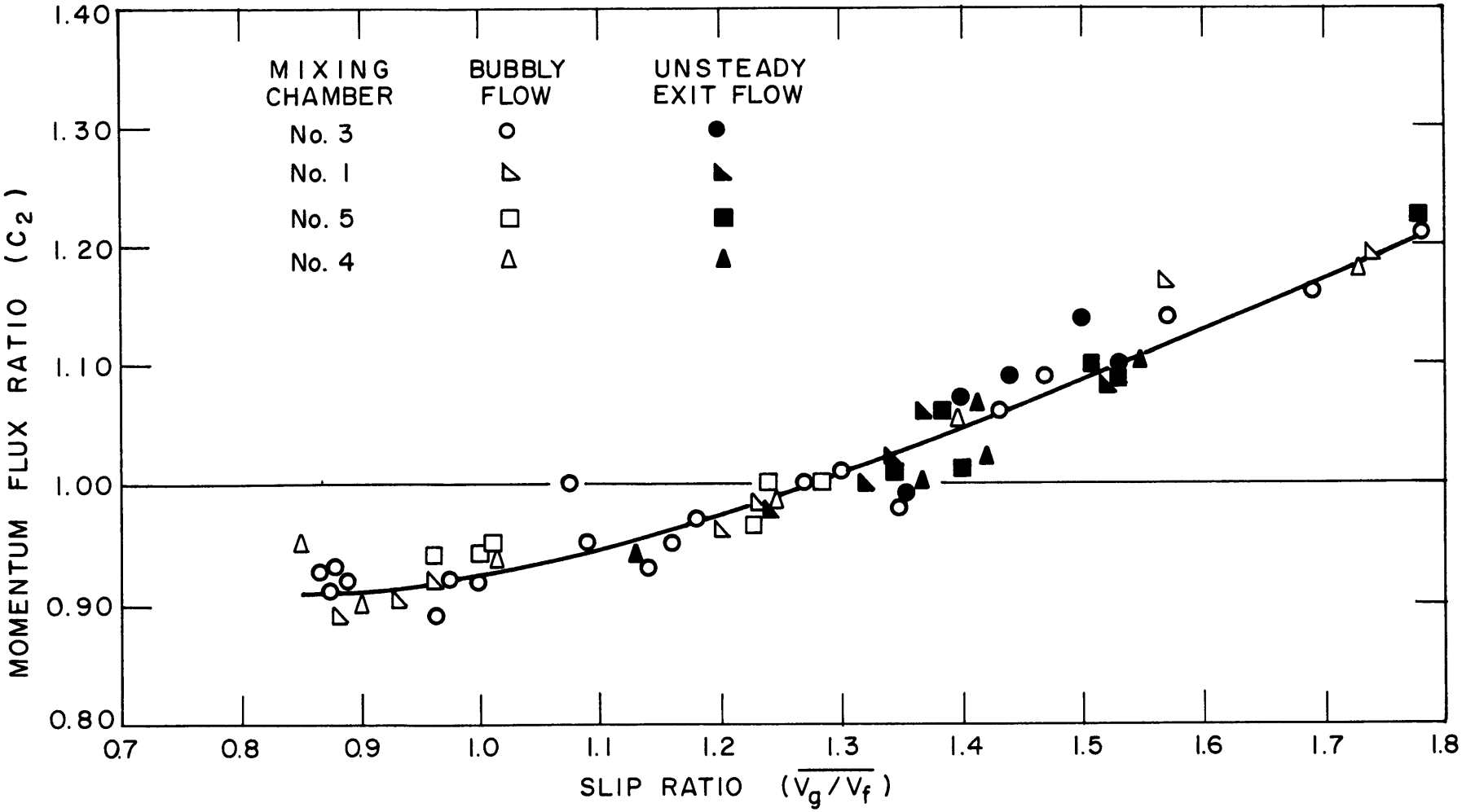

FIGURE 34 COMPARISON OF HOMOGENEOUS MODEL AND MEASURED MOMENTUM FLUX

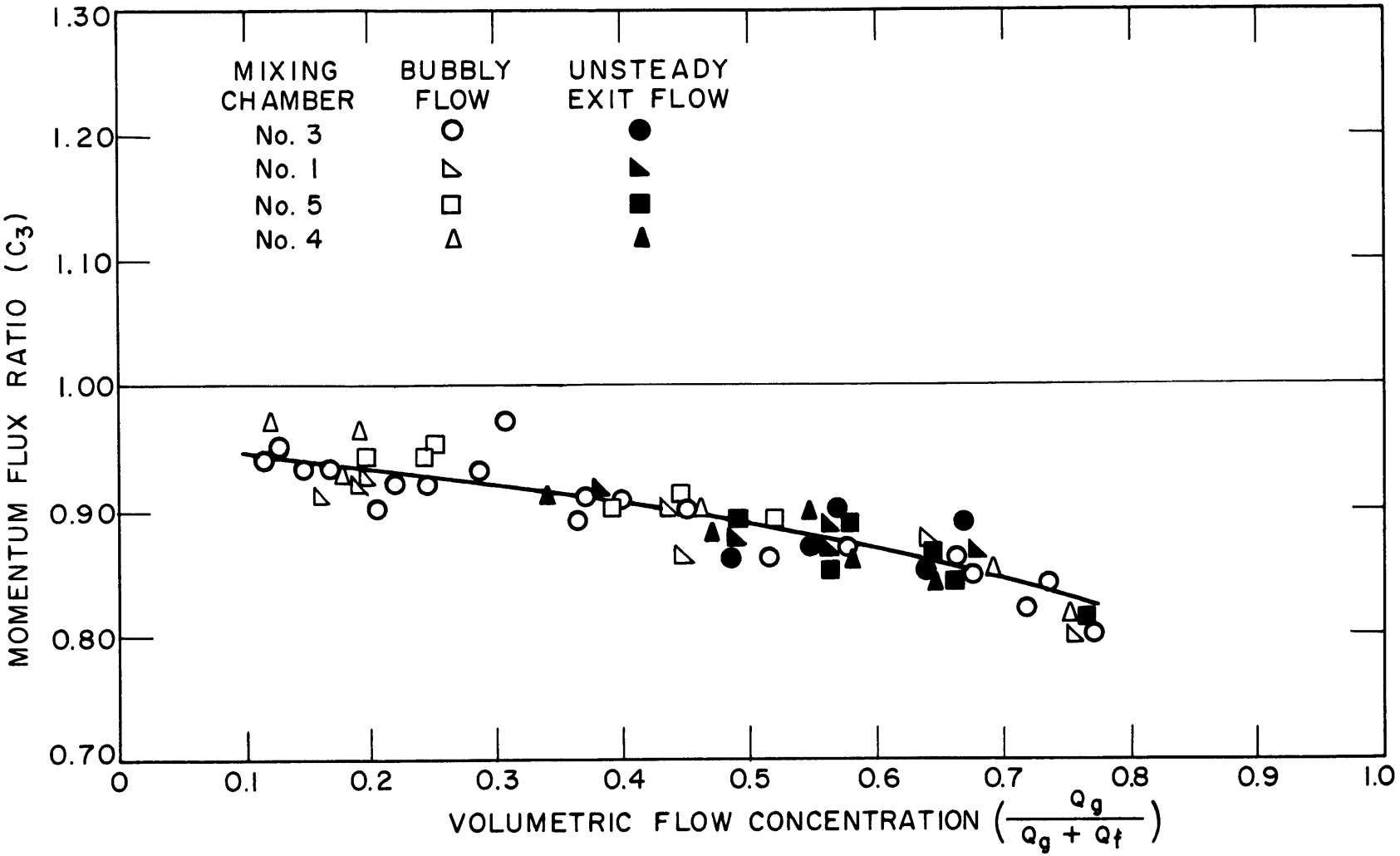

FIGURE 35 COMPARISON OF SEPARATED MODEL AND MEASURED MOMENTUM FLUX

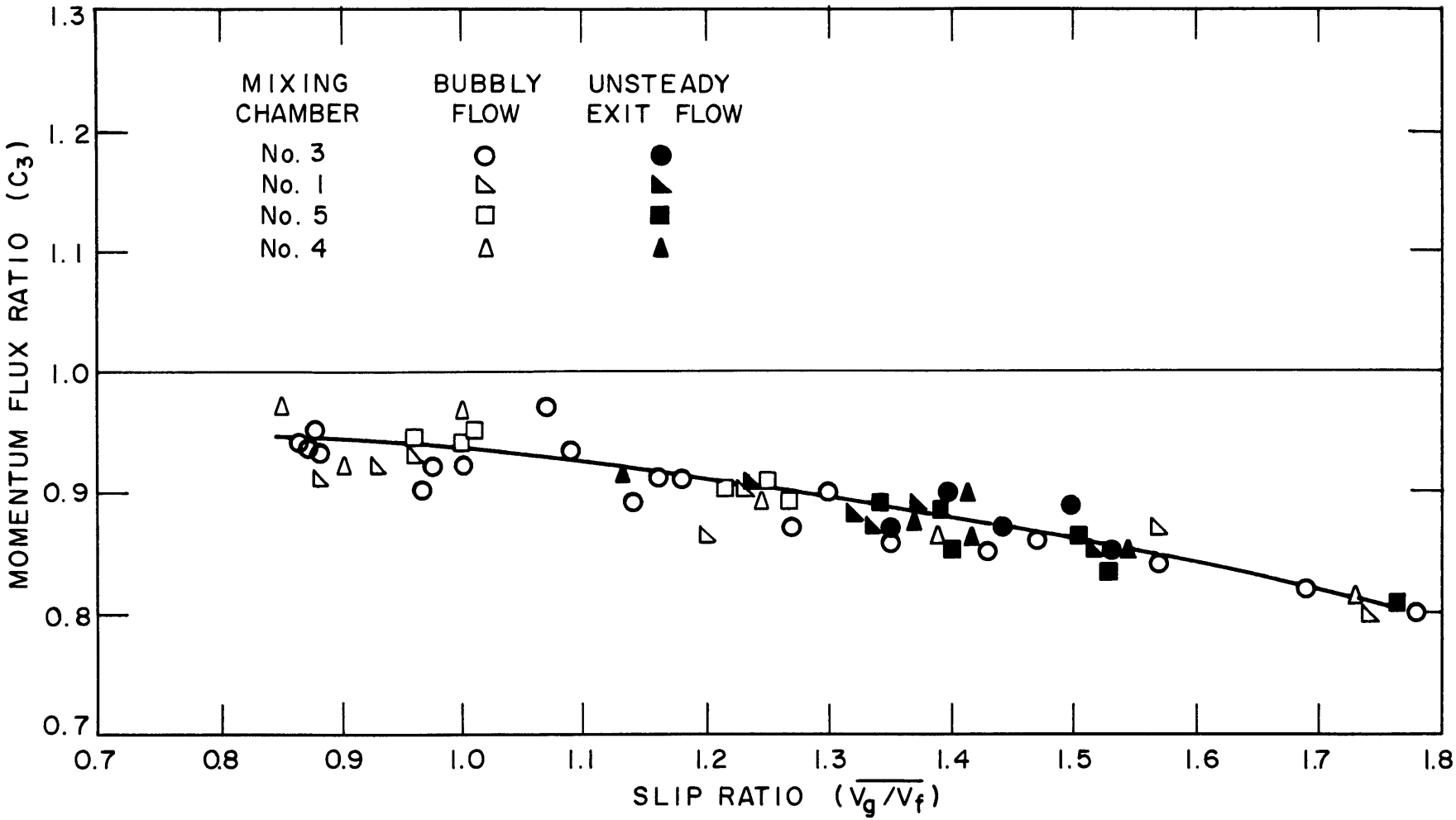

FIGURE 36 COMPARISON OF SEPARATED MODEL AND MEASURED MOMENTUM FLUX

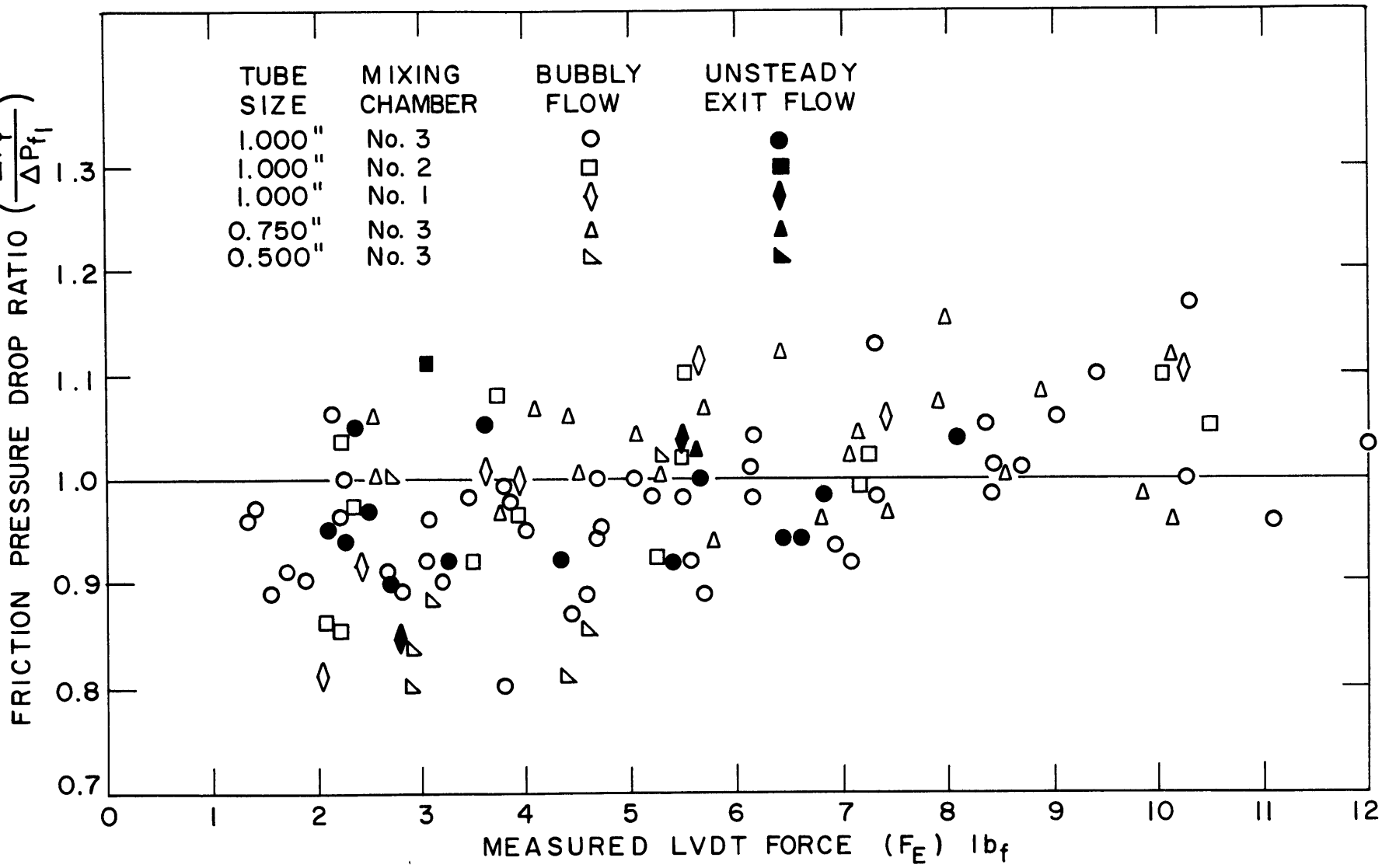

FIGURE 37 COMPARISON OF FRICTION PRESSURE DROPS

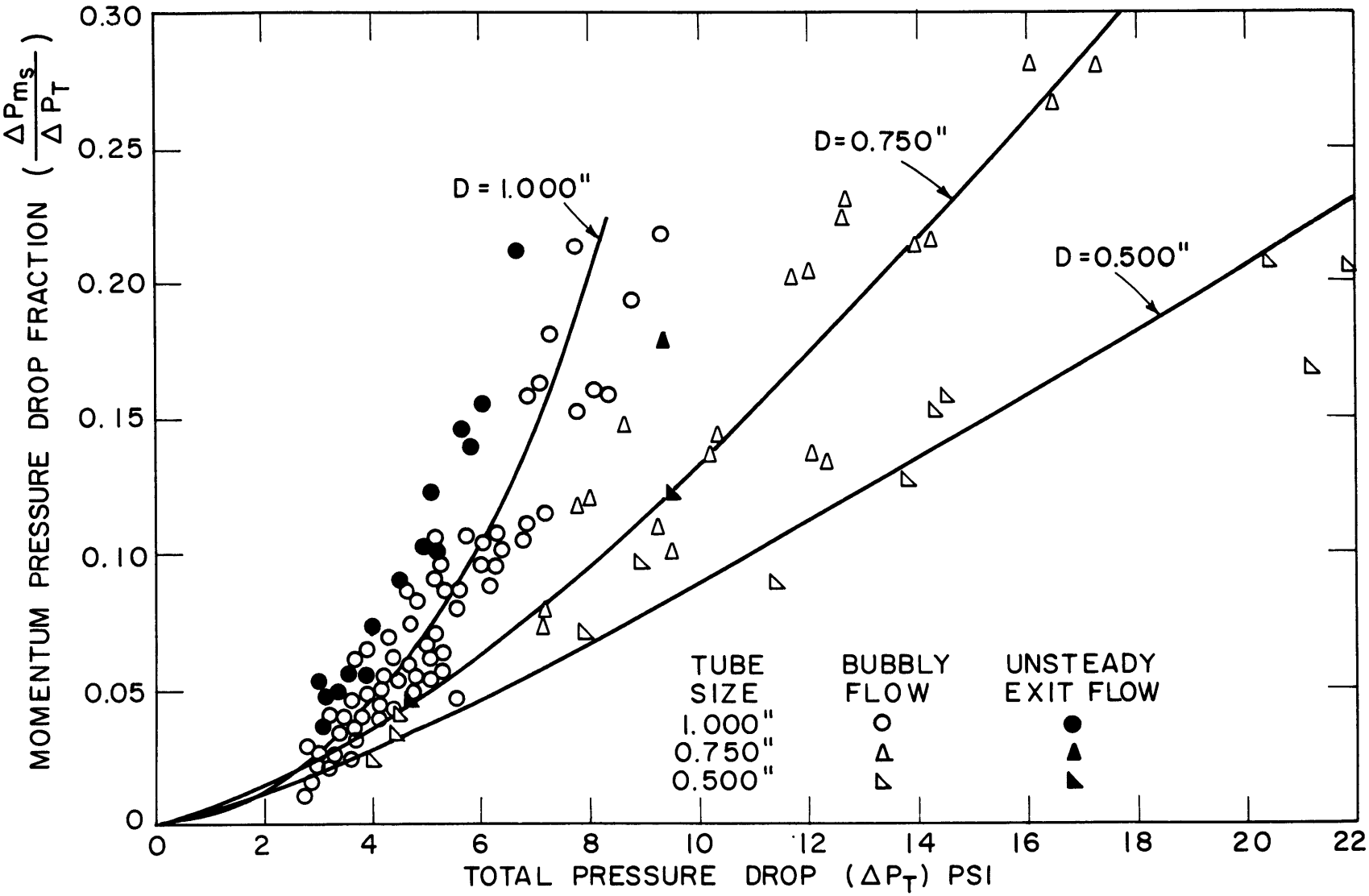

FIGURE 38 MAGNITUDE OF MOMENTUM PRESSURE DROP

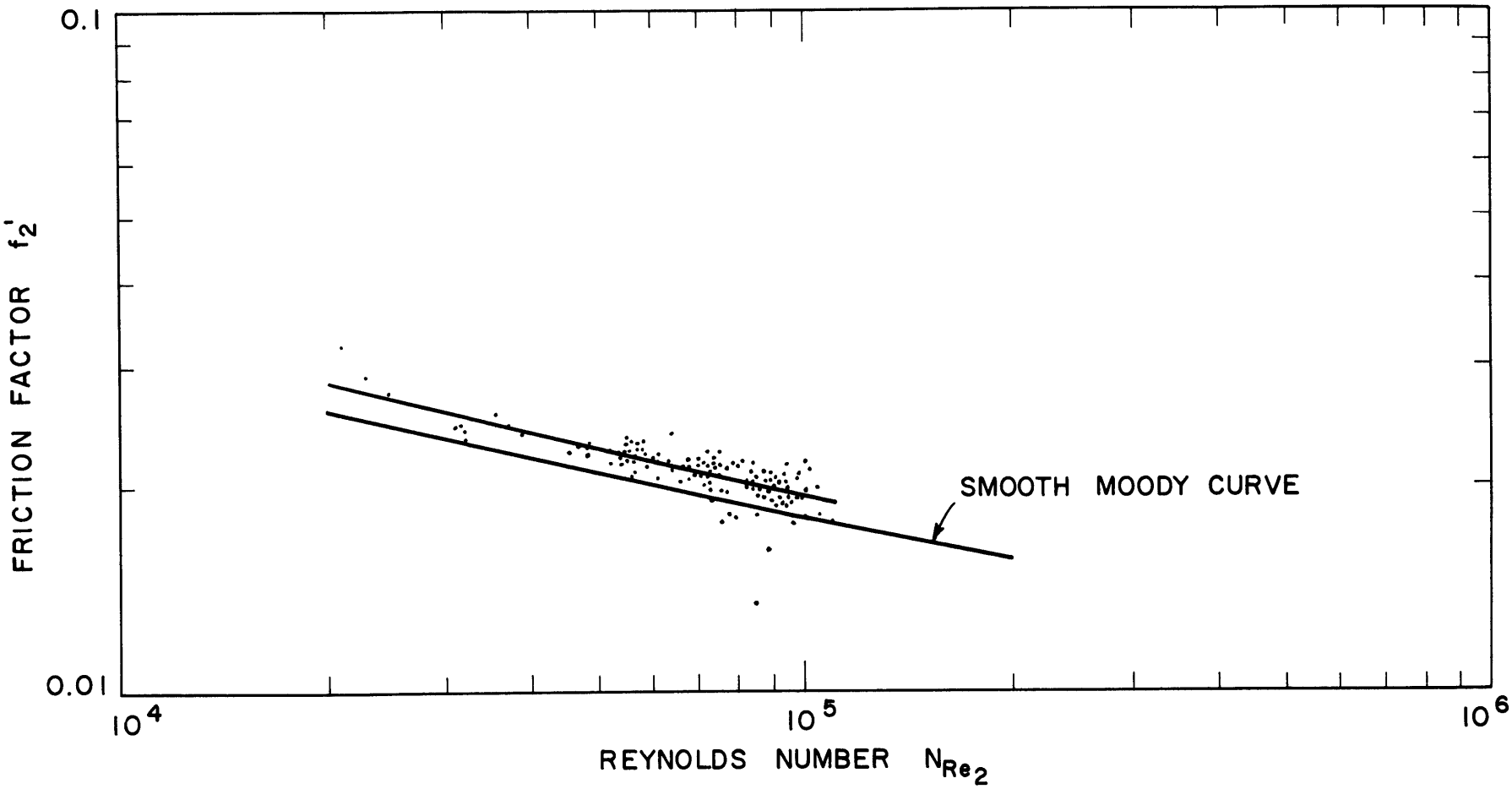

FIGURE 39 FRICTION FACTOR CORRELATION FOR ALL DATA POINTS

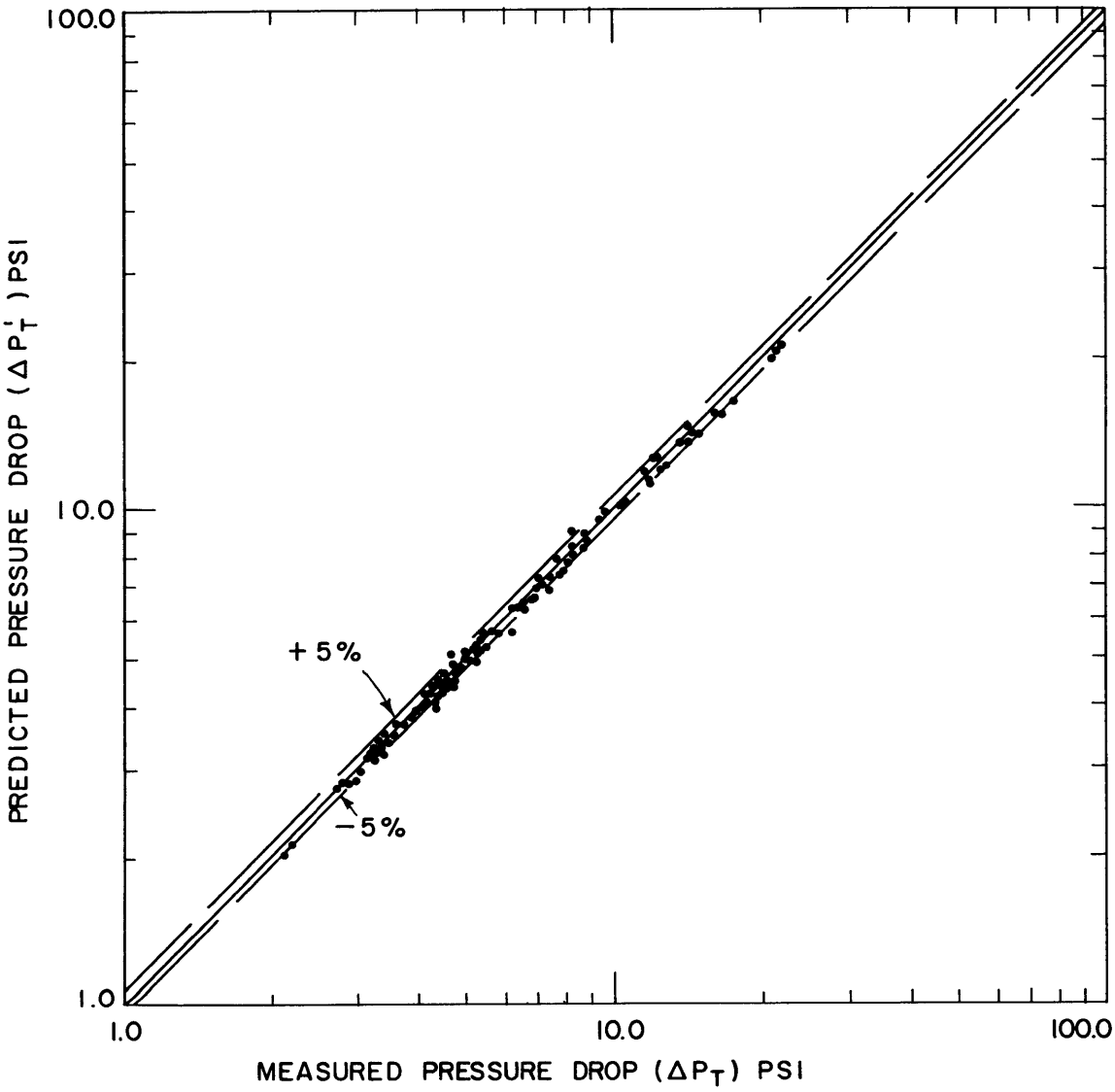

FIGURE 40 COMPARISON OF PREDICTED AND MEASURED TOTAL PRESSURE DROP FOR ALL BUBBLY DATA POINTS

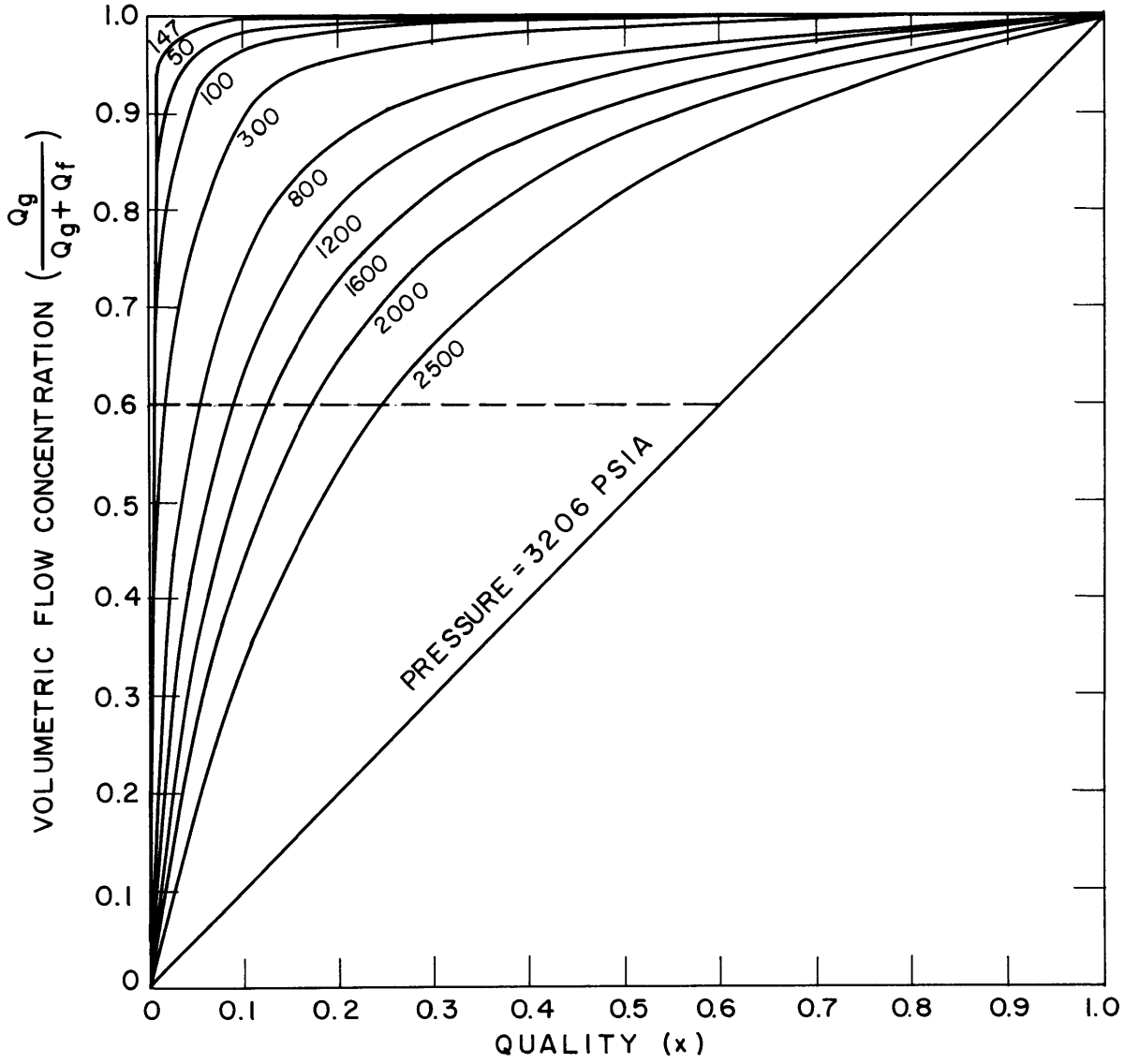

FIGURE 41 RELATIONSHIP OF FLOWING VOLUME TO WEIGHT QUALITY FOR STEAM-WATER MIXTURES